CANADA

DEPARTMENT OF
ENERGY, MINES AND RESOURCES
MINES BRANCH

OTTAWA

ANALYSIS OF ROCK SLOPES USING THE FINITE ELEMENT METHOD

Y. S. YU AND D. F. COATES

MINING RESEARCH CENTRE

OCTOBER 1970

Research Report R 229

Price $1.25

Available by mail from Information Canada and
at the following Canadian Government bookshops

HALIFAX
1735 Barrington Street

MONTREAL
Æterna-Vie Building, 1182 St. Catherine St. West

OTTAWA
Daly Building, Corner Mackenzie and Rideau

TORONTO
221 Yonge Street

WINNIPEG
Mall Center Bldg., 499 Portage Avenue

VANCOUVER
657 Granville Street

or through your bookseller

Price $1.25 Catalogue No. M38-1/229

Price subject to change without notice

Information Canada
Ottawa, 1971

Mines Branch Research Report R 229

ANALYSIS OF ROCK SLOPES, USING THE FINITE ELEMENT METHOD

by

Y. S. Yu* and D. F. Coates**

- - -

SUMMARY

Studies have been conducted on the deformation and stress patterns around typical rock slopes, taking into account slope angle, slope shape, gravity and/or tectonic stress field, by using the finite element method. These two-dimensional studies have been supplemented by three-dimensional axisymmetric investigations.

Initial studies verified the compatibility of the finite element technique with results obtained from photoelastic experiments. A total of 45 loading conditions were examined. Comparison of results between the two-dimensional plane strain and the three-dimensional axisymmetric case indicates that the two solutions produced almost the same results in a gravity stress field. However, the results differ increasingly with an increase in the residual horizontal stresses; e.g., the tangential stresses near the toe in plane strain could be 56 and 100 per cent higher as compared with that of axisymmetric geometry and loading for K=1 and 3 respectively.

For both solutions of plane strain and axisymmetric geometry, the excavation displacements at the crest are approximately proportional to the factor K as well as to the slope angle. Also, the largest principal stress induced near the toe is proportional to the factor K but not to the slope angle where it exceeds 60^{o}; in other words, the rate of increase of stress near the toe decreases when the slope angle is increased from 60^{o} to 90^{o}.

Tensions seem to occur along the slope face under some loading conditions and definitely do occur in axisymmetric models when loaded with a high uniaxial horizontal stress.

Analyses based on Mohr's strength theory indicate that if failure occurred, it would be initiated at some distance behind the toe, although this depends on loading conditions.

---

* Research Scientist, ** Head, Mining Research Centre, Mines Branch, Department of Energy, Mines and Resources, Ottawa, Canada.

Direction des mines
Rapport de recherches R 229

ÉTUDE ANALYTIQUE DES TALUS ROCHEUX PAR LA MÉTHODE DES ÉLÉMENTS FINIS

par

Y.S. Yu* et D.F. Coates**

RÉSUMÉ

Les auteurs ont étudié les configurations de déformations et de contraintes autour de talus rocheux type, en faisant intervenir l'angle de pente, la forme du talus, la gravité et (ou) le champ de contraintes tectoniques, par la méthode des éléments finis. A ces études en deux dimensions sont venues s'ajouter des recherches sur des systèmes tridimensionnels possédant un axe de symétrie.

Les premières études ont confirmé la compatibilité de la technique des éléments finis avec les résultats des expériences de photo-élasticimétrie. Les auteurs ont étudié, au total, 45 conditions de charge. La comparaison des résultats obtenus dans le cas d'une répartition plane des tensions sur modèle à deux dimensions et dans le cas d'un modèle tridimensionnel possédant un axe de symétrie, montre que les deux approches ont apporté des résultats presque identiques dans le cas d'un champ de contraintes gravitationnelles. Cependant, les résultats diffèrent d'autant plus que les contraintes résiduelles horizontales sont plus importantes; par exemple, les contraintes tangentielles à proximité du pied du talus, dans le cas d'une répartition plane des tensions, pouvaient être supérieures de 56 et de 100 pour cent à celles correspondant à une géométrie et à une charge présentant un axe de symétrie, pour K=1 et K=3 respectivement.

Dans les deux cas de répartition plane des tensions et de géométrie présentant un axe de symétrie, les déplacements à la crête du talus et dus à l'excavation sont approximativement proportionnels au facteur K et à l'angle de pente. Egalement, la plus grande contrainte principale induite près du pied du talus est proportionnelle au facteur K, mais non à l'angle de pente si celui-ci dépasse 60°; autrement dit, le taux d'accroissement de la contrainte près du pied du talus diminue lorsque l'angle de pente augmente de 60° à 90°.

Il semble que des tensions existent le long de la face du talus sous certaines conditions de charge et ces tensions existent certainement dans les modèles possédant une axe de symétrie, s'ils sont soumis à de fortes contraintes horizontales et parallèles.

---

* Chercheur scientifique, ** Chef du Centre de recherche sur les techniques minières, Direction des mines, ministère de l'Énergie, des Mines et des Ressources, Ottawa, Canada.

Des analyses basées sur la théorie des contraintes de Mohr montrent que, si une fracture se produisait, elle prendrait naissance à une certaine distance derrière le pied du talus, encore que ceci dépende des conditions de charge.

CONTENTS

(Concluded -

(Contents, concluded)

FIGURES

(Cont'd -

FIGURES (Continued)

(Cont'd -

FIGURES (Continued)

(Concluded -

FIGURES (Concluded)

TABLES

1. INTRODUCTION

A vigorous effort is presently under way around the world to place the design of rock slopes on a rational basis. Therefore, a knowledge of stress distributions in and under slopes is a fundamental requirement for any mechanistic understanding of rock slope behaviour. An accurate evaluation of stresses and displacements around excavations in rock is a difficult task, particularly for the geometries of rock slopes, if the rock mass in which the slope is to be cut is not homogeneous, isotropic, and elastic.

Rock slope research arises primarily in Canada from the need for more information on the stability of the walls in large open-pit mines. During the last decade the mineral production from open-pit mines in Canada has significantly increased, so that now this method accounts for approximately 60% of the total ore mined. In turn, this had led to a great increase in the volume of waste excavations. At present, the selection of pit slope angles is, however, still largely a matter of experience and engineering judgement. Thus, much thought is being given to the considerable economic benefit which would result if pit slope angles could be made steeper by even two or three degrees. Alternatively, the same economic benefit might be also achieved by changing the slope so that the volume of waste excavation would be reduced, i.e., using possibly a convex, parabolic outline of slope instead of a constant slope.

It is generally recognized that slope stability depends, primarily, on how the rock behaves under a stress sytem caused by the excavations. In general, the design of an open-pit mine should be such that the slopes are steep enough to result in economical mining and flat enough to ensure safety of the miners and of the equipment in the pit. Research work is still required to provide the necessary scientific information and to show its method of application to the design of optimum pit slopes.

In view of the importance of this matter to the Canadian mining industry, the Mining Research Centre of the Mines Branch has been conducting research to gain some knowledge and a better understanding of the factors governing the stability of pit slopes. It started with an attempt to solve the differential equations applicable to the slope geometry in plane strain conditions. However, it soon became apparent that, even with recent developments in modern mathematics, no simple solution of this problem would be obtained. Alternate techniques were examined. On the one hand, it was decided to initiate some experimental work on deformable models, to obtain experimentally some useful data. On the other hand, numerical approximation techniques were examined, one of which, the finite element method, looked very promising.

The finite element technique was developed for the design of irregular structures in both aeronautical and civil engineering (1, 2). It seems to be an extremely precise and flexible tool for problems in complex-shaped continua. With this method, the inclusion of anisotropic properties does not unduly complicate the problem. In addition, arbitrary loading functions can be readily analysed. Initial studies have verified the compatibility of the numerical simulation technique with results obtained from photoelastic experiments (3). An extensive study regarding the deformation and stress patterns has been conducted taking into account slope angles (30°, 45°, 60°, and 90°), slope shape, and tectonic stress fields. These two-dimensional studies have been supplemented by a three-dimensional investigation of slopes with slope angles

of 30^{o}, 60^{o}, and 90^{o}, under gravitational and tectonic stresses.

2. STRESS ANALYSIS TECHNIQUES FOR EXCAVATED ROCK SLOPES

Although many elastic prototypes can be used to provide useful information for structures with geometries and loadings that can be approximated by these solutions, there are many practical cases of irregular geometries, non-uniform material and non-uniform loadings, such as rock slopes, that cannot be solved by the theory of elasticity.

In the past decade, stress investigations of rock slopes have largely been performed by experimental techniques such as photoelastic and geomechanical modelling. With these laboratory techniques the making of satisfactory models for effective simulation takes up much time and normally can be performed only by specially trained and highly skilled personnel. With the photoelastic method, for example, possible error could arise from inaccurate loading, conversion of isochromatic fringes to principal stresses, temperature sensitivity, inelastic behaviour of the model material, non-simulation of Poisson's ratio, and body weight. Similarly, with geomechanical models, major problems are associated with obtaining accurate model materials and simulating actual loading. As a result, there has been continual need for more flexible and precise tools.

With the advent of the high-speed digital computers and of complex-shaped aerospace structures, the finite element method was devised to handle the cases that could not be solved in the classical manner (4, 5).

2.1 The Finite Element Method

The basic concept of the finite element method is the idealization of the actual continuum as an assemblage of a finite number of discrete structural elements, interconnected at a finite number of nodes at which some fictitious forces, representative of the distributed stresses acting on the element boundary, are introduced.

The finite elements are formed by figuratively cutting the original continuum into a number of appropriately shaped pieces, each element retaining properties of the original material. In the analysis, these assumed structural elements are equivalent to the components of an ordinary framed structure. Thus, the analytic process consists merely of the normal operations of satisfying compatibility and equilibrium conditions at nodal points, using any standard structural analysis procedure. In practice, the displacement formulation has been found most convenient and is generally used.

Several types of elements may be used in the representation of a structure. In the plane stress or plane strain analysis, either triangular or quadrilateral elements can be used. In the finite element approximation of axisymmetric solids, the continuous structure is replaced by a system of axisymmetric elements which are interconnected at circumferential nodes or nodal circles. Mathematically, it is two-dimensional in nature, but the triangular or quadrilateral element of plane stress or strain analysis becomes the cross section of these ring elements.

An example of a 60^{o} slope mesh is illustrated in Figure 1(b). The coordinate system is labeled r, z, and t, as shown in Figure 1(a), so that the same subscripts can be used for both plane strain and axisymmetric analysis. Figure 1(b) represents schematically the finite element model that was used to determine the stress and displacement around the 60^{o} slope.

The slope, as shown in Figure 1(b), is divided into a finite number of elements connected at their nodal points. Either quadrilateral or triangular elements can be used. However, the quadrilateral elements, if used, were subdivided automatically into four triangles within the computer program. On the basis of an assumed variation of displacements within an element (e.g. linear), together with stress-strain characteristic of this element material, the stiffness of each nodal point of each element is computed. For each nodal point in the system, two equilibrium equations may be written expressing the nodal points force in terms of the nodal-point displacement and stiffness. These equations are then solved for the unknown displacements. With the displacements of all nodal points known, strains and stresses within each element are then computed. The basis and derivation of the mathematical formulation have been described in great detail (4, 5, 6).

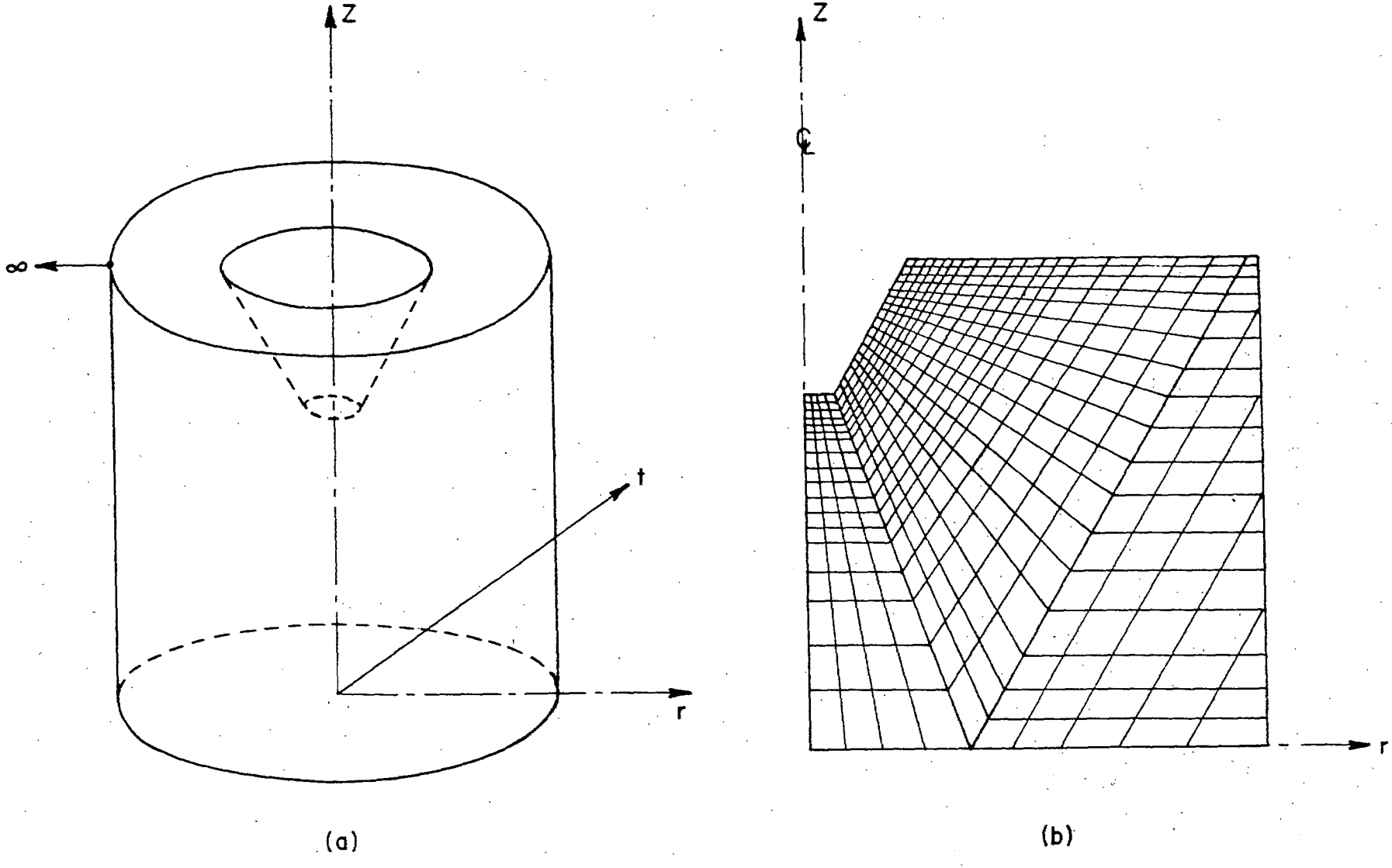

Figure 1. The geometry of the slope studies: (a) definition of axes, (b) finite element model.

2.2 Initial State of Stress

The state of stress in the undisturbed rock consists of the vertical initial stress S_v and the horizontal initial stress S_x. Vertical stress existing in the medium in the undisturbed state is due to gravity and, in a uniform medium, will vary linearly with depth. The horizontal component of stress is due partly to gravity and Poisson's effect, but can be due to the residual stress arising from the geological history of the medium. No matter what its cause, the horizontal component is always expressed as the vertical stress times a factor, i.e., $S_x = KS_v$.

2.2.1 Constrained Lateral Stress:

The concept of constrained lateral stress has enjoyed considerable popularity. If, during the loading history of the rock, the lateral displacement is rigidly constrained, then the horizontal stress will be a fraction of the vertical stress as shown in Figure 2 (a).

2.2.2 Constant Lateral Pressure:

Another type of tectonic stress which might be considered is a constant horizontal stress. This would be applicable when the tectonic stress, S_t, is several times the overburden stress, a case that has been verified by measurements in several instances (7). The initial stress state has the form as shown in Figure 2(a).

2.3 Excavation Displacement by the Finite Element Technique

Excavation displacement is defined as the movement of the rock mass induced by excavation. It is an important aspect in examining the ground reaction to the removal of pit material. In order to determine the excavation displacement, the initial state of the displacement, i.e. the elastic displacement of the model without excavation, must be known. This can be easily accomplished by the following approach: The mathematical model is first loaded with its field stress (gravity and/or tectonic stress) without the excavation; the tectonic stress, if any, is assumed uniformly distributed across the depth; the resulting displacements are then used as the initial conditions for the model with the desired excavations. Then the excavation displacements can be obtained by subtracting the initial displacements at each node from the final displacements of model with the excavations, as shown in Figure 2(b).

The second approach is to apply changes in stress, ΔS, to the excavation boundary as illustrated in Figure 2(c). Application of changes in stress (ΔS) which are equal to the initial stresses (So) but opposite in sign, results in a stress-free condition along the excavated boundary. The applied change in stress is resisted by the remaining rock, and induced displacements, strain, and stress changes in the rock may be calculated by the finite element analysis. The state of stress subsequent to excavation is determined by adding the stress changes at any location to the initial stress values for that location. It should be mentioned that the initial horizontal and vertical stresses S_h and S_v are not calculated by the conventional formulae ($S_v = -\gamma h$, and $S_h = KS_v$), because the topography may be irregular and the material heterogeneously distributed. Instead, it is generated by the finite element method, using the model without excavations and taking account of the inhomogeneous materials. Comparison of these two approaches for homogeneous, regular models yields the same result.

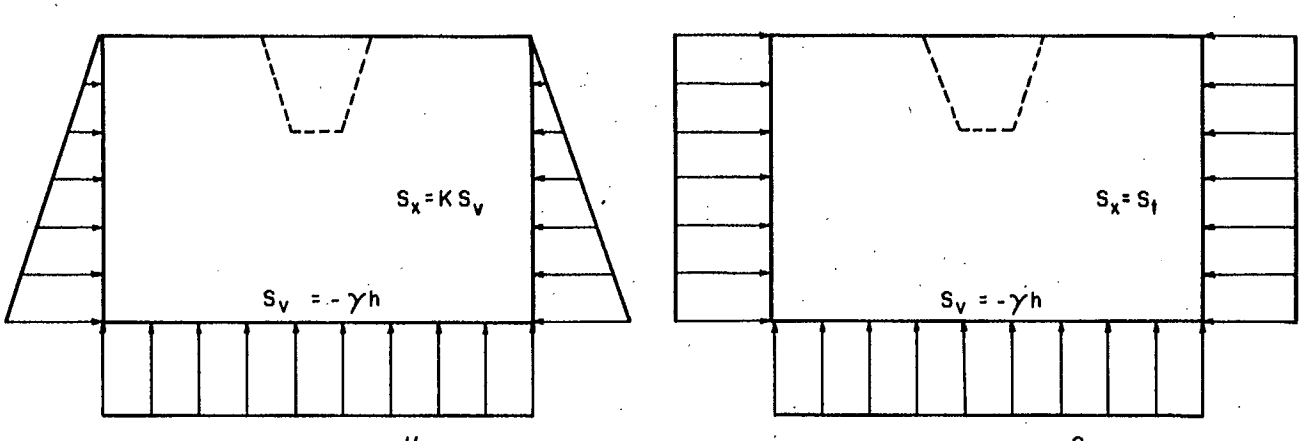

(a) Initial state of stress

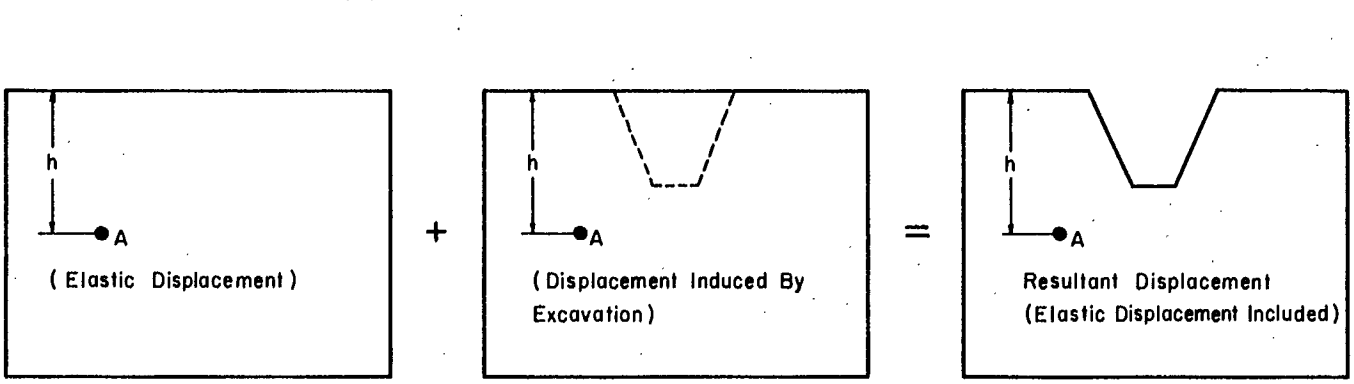

$$\left\{\begin{matrix}\delta_{xi} + \delta_{xe} = \delta_{xr} \\ \delta_{yi} + \delta_{ye} = \delta_{yr}\end{matrix}\right\} \quad \text{or} \quad \left\{\begin{matrix}\delta_{xe} = \delta_{xr} - \delta_{xi} \\ \delta_{ye} = \delta_{yr} - \delta_{yi}\end{matrix}\right\}$$

(b) Determination of excavation displacement - first approach

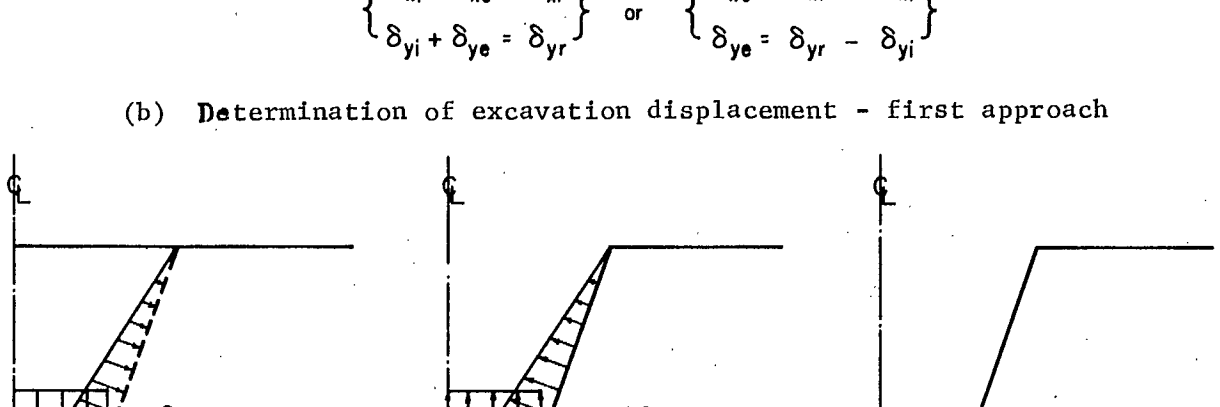

(c) Determination of excavation displacement - second approach

Figure 2. Analysis of stress in an excavated rock slope.

2.4 Finite Element Computer Programs

Two computer programs have been used for this analytical work. The original finite element programs, developed by Wilson (4) and Dunham and Nickell (5), have since been modified for simulating excavation sequence to obtain excavation displacements. The results obtained from the two individual programs have been checked, each against the other (10).

Supplementary computer programs have been developed to interpret the massive output of the finite element analysis. With the use of a computerized plotter, the results can be displayed in several different ways. These include principal stress plots (direction, magnitude, and their numerical values) and displacement plots (direction and magnitude).

3. RESULTS OF ANALYSIS OF ROCK SLOPES

In this section, the analytical results for elastic analysis of rock slopes are given. In these analyses, the influence of initial stress conditions, the influence of slope angles, the influence of slope geometries, and the influence of three-dimensional effects on the stress distributions are all evaluated.

The stress distributions within several slope models for a variety of loading conditions, in either two-dimensional or three-dimensional axisymmetry, were determined using the finite element technique. A summary of loading conditions is included in Table 1.

3.1 Comparison between Finite Element Method and Photoelasticity

The photoelastic procedure using a highly deformable material has been previously dexcribed (8). The photoelastic models were made from Mirelite with a fringe value of 0.312 psi. Figure 3 shows the photoelastic model with the testing frame. The geometry was 25.75 in. x 11.50 in. x 2.00 in. It contained an opening to simulate an open-pit mine with a slope angle of 60^{o}. The bottom width of this opening was 2.25 in. and the slope height was 4.25 in.

A finite element model was also constructed. The slope was also cut at 60^{o}, and approximately the same ratio of slope height to the bottom width was maintained. But the overall dimensions of the mathematical model were much larger than those of the photoelastic one. It was judged that the mathematical-model dimensions should be at least four times the size of opening so that the end effect would be minimized. Because of symmetry, only half of the pit was considered. The physical properties of the model were more or less arbitrarily assumed; the elastic modulus E and the density γ were taken as 7.03×10^{5} kg/cm^{2} (10×10^{6} psi) and 2.7 gm/cm^{3} (168 lb/ft^{3}), respectively. Poisson's ratio of 0.47 was used to simulate the photoelastic model.

The results determined from the finite element method and the photoelastic model, both being subjected to a gravity loading only, are shown in Figures 4a and 4b.

Figure 4a shows the variations of vertical stress with depth along a vertical section away from the cut. For both methods, the stresses seem to be in very good agreement with the calculated values. For the finite element solution, relatively larger errors were introduced at the boundaries. The vertical stresses at bottom boundary are approximately 7% and 6% lower than the calculated values respectively for the solutions by the finite element and by photoelasticity, which are probably less than the degrees of accuracy of the models.

TABLE 1. Summary of Loading Conditions for Slope Model Study

CASE	Slope Configuration		Geometry and Loading		
			Two-dimensional	Three-dimensional	
			Plane Strain*	Axisymmetric Loading	Non-axisymmetric Loading
1 2 3	60°		K = 1/3, gravity only K = 1, P_r = 81 K = 3, P_r = 243		
4 5 6	45°		K = 1/3, gravity only K = 1, P_r = 81 K = 3, P_r = 243		
7 8 9	30°		K = 1/3, gravity only K = 1, P_r = 81 K = 3, P_r = 243		
10 11 12	90°		K = 1/3, gravity only K = 1, P_r = 81 K = 3, P_r = 243		
13 14 15	Parabola-shaped Slopes	No. 1	K = 1/3, gravity only K = 1, P_r = 81 K = 3, P_r = 243		
16 17 18		No. 2	K = 1/3, gravity only K = 1, P_r = 81 K = 3, P_r = 243		
19 20 21		No. 3	K = 1/3, gravity only K = 1, P_r = 81 K = 3, P_r = 243		
22 23 24		No. 4	K = 1/3, gravity only K = 1, P_r = 81 K = 3, P_r = 243		

* Stress units are : kg/cm^2.

Continued -

Table 1 - Cont'd.

CASE	Slope Configuration		Geometry and Loading		
			Two-dimensional	Three-dimensional	
			Plane Strain	Axisymmetric Loading	Non-axisymmetric Loading
25 26 27	Parabola-shaped Slopes	No. 5 No. 5	K = 1/3, gravity only K = 1, P_r = 81 K = 3, P_r = 243		
28 29 30	Parabola-shaped Slopes	No. 6	K = 1/3, gravity only K = 1, P_r = 81 K = 3, P_r = 243		
31 32 33	30°			K = 1/3, gravity only K = 1, $P_r = P_t$ = 81 K = 3, $P_r = P_t$ = 243	
34 35 36	60°			K = 1/3, gravity only K = 1, $P_r = P_t$ = 81 K = 3, $P_r = P_t$ = 243	
37 38 39 40 41 42	60°				K = 1/3, P_r = 27, P_t = 0 K = 1/3, P_r = 0, P_t = 27 K = 1, P_r = 81, P_t = 0 K = 1, P_r = 0, P_t = 81 K = 3, P_r = 243, P_t = 0 K = 3, P_r = 0, P_t = 243
43 44 45	90°			K = 1/3, gravity only K = 1, $P_r = P_t$ = 81 K = 3, $P_r = P_t$ = 243	

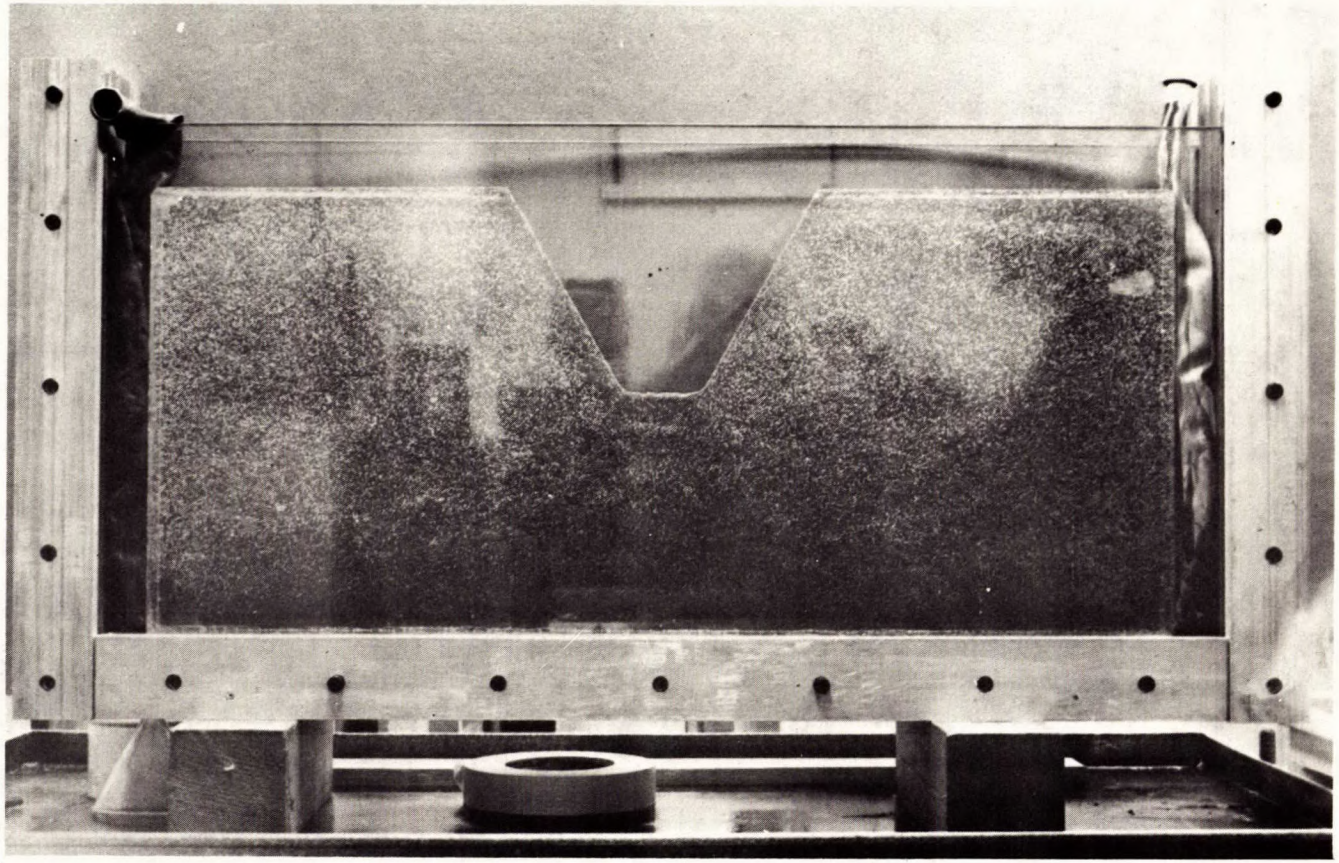

Figure 3. Photoelastic model with testing frame.

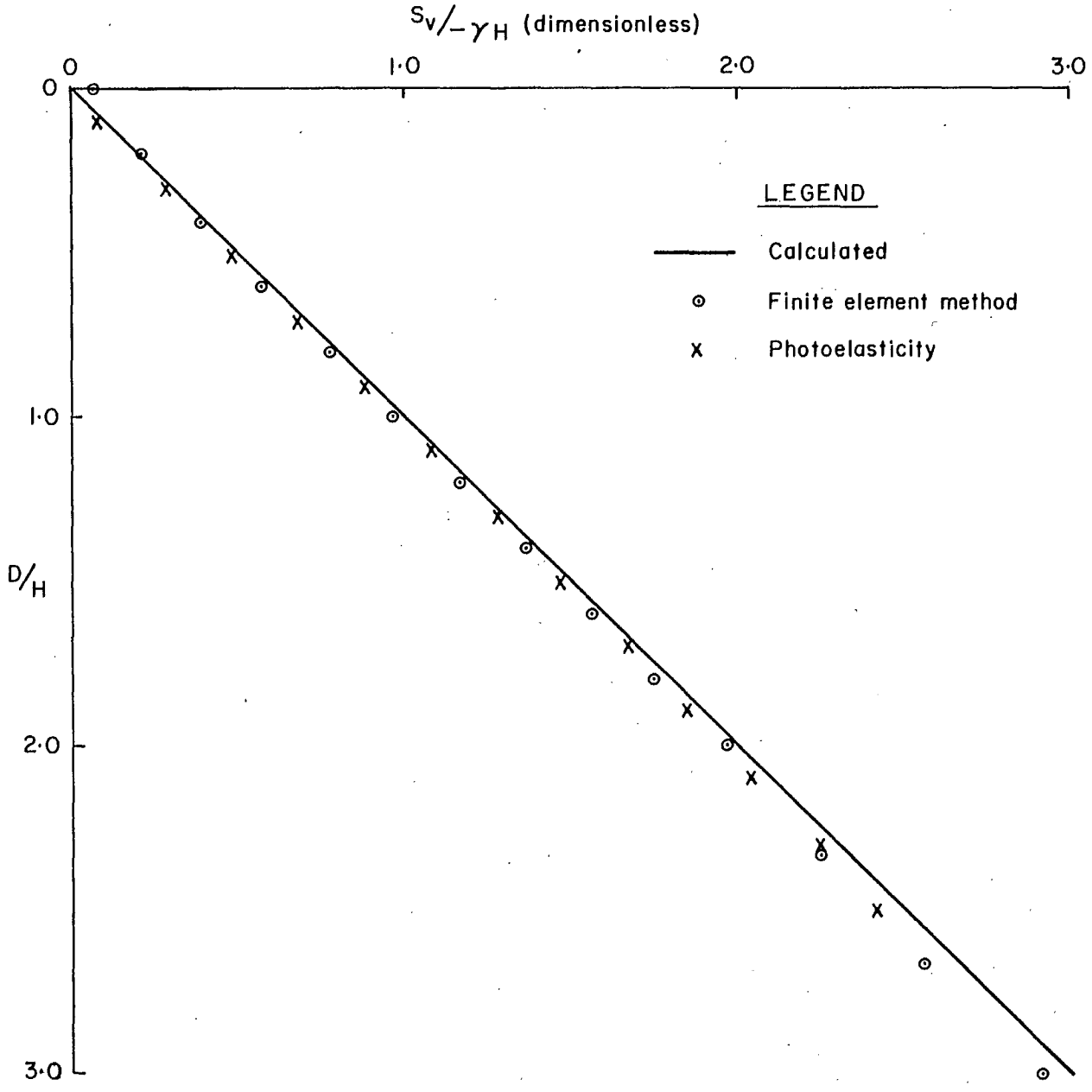

Figure 4a. Comparison of stress variations along a vertical section away from the excavation, determined by photoelasticity and by finite element method.

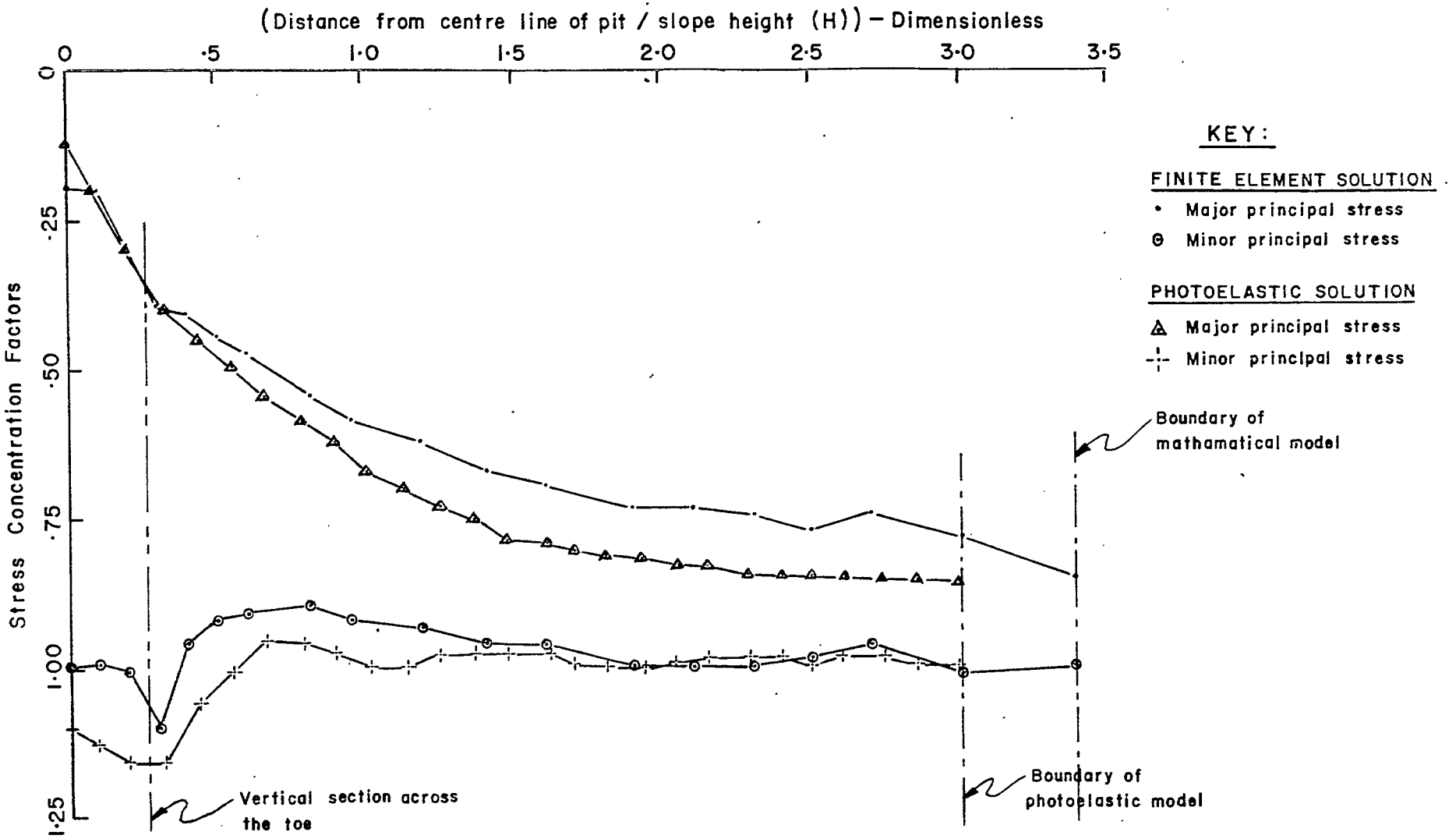

Figure 4b. Comparison of principal stresses along a horizontal section at a distance of 0.1H below the pit bottom, determined by photoelasticity and by finite element method.

As expected, larger stress concentrations occur around the toe area. A maximum stress concentration of 1.5 near the toe was obtained by the finite element method, as compared to that of 1.6 by photoelasticity. The difference is only 7%. The stress concentration factors of major and minor principal stresses are plotted along a horizontal section at a distance of 0.1H below the pit bottom as shown in Figure 4b. Again, the results indicate that the agreement between the solutions is good.

The photoelastic model work cannot determine the displacements in the model, so that no comparison can be made between the displacements resulting from a slope cut by the two different techniques.

Although the two different approaches produced similar results, the finite element method is more flexible and economical than the photoelastic technique and it is completely general with respect to geometry and material properties. Therefore, all subsequent work was carried out using the finite element method.

3.2 The Influence of Residual Horizontal Stress on Slope Stability

Residual stresses, parallel to the earth's surface, will be different in different locations around the world. Vertical stresses existing in the medium in the undisturbed state are due to gravity and, in a uniform medium, will vary linearly with depth. The horizontal component of stress is due partly to gravity and Poisson's effect but can also be due to the residual stress arising from tectonic origin. No matter what its cause, it is usual to relate the horizontal component of stress to the vertical component.

Two types of lateral stress have been considered in this primary study. First is "constrained lateral stresses", i.e., during the loading history of the rock, if the lateral displacement is constrained, then a horizontal stress of $\frac{\mu}{1-\mu}$ times the vertical stress will be developed where μ is Poisson's ratio. In other words, the horizontal stress is developed by Poisson's effect only; the factor K has the value of $\frac{\mu}{1-\mu}$.

The second type of lateral stress is "constant lateral pressure". It is assumed a constant horizontal stress exists across the depth. This would be a close approximation when the tectonic stress is several times the gravity stress at a depth, a case that has been verified by measurements in several instances. In this case, the factor K will be defined as the ratio of the horizontal tectonic stress to the vertical gravity stress at the toe of the pit.

Now, when an open pit is cut in either a homogeneous or an anisotropic rock formation which is subjected to a form of regional horizontal stress, the stress and displacement patterns are altered in the vicinity of the cuts. The resulting changes will depend on the geometry of the pit and the magnitude of the horizontal stresses. It is believed that the presence of regional tectonic stress will affect the stability of rock slopes; therefore, some knowledge of these effects will be beneficial for rational design of any open-pit mine.

A finite element model was constructed. The slope was cut at 60^{o} with a depth of 300 metres (900 ft). The field stress condition consisted of vertical gravitational stresses arising from an average density of 2.7 gm/cm^3 (168 lb/ft^3) and a variety of uniform (constant) horizontal stresses, S_h. The ore and wall rocks were assumed to be perfectly elastic with deformation properties of E = 7.03 kg/cm^2 (10 x 10^6 psi) and μ = 0.2.

In order to study the influence of the Poisson's ratio, μ, on the stress and deformation pattern, μ values varying between 0 and 0.47 were examined under the loading of gravity only.

3.2.1 Stresses

Under gravitational loading with different Poisson's ratios, the stress distributions are essentially identical although the magnitudes of horizontal components are larger for higher μ values. In Figure 5, the final principal stress directions are indicated by the orientations of the crossed lines; the shorter of the two lines indicates the direction of the major principal stress (compression negative). It may be noted that the principal stress trajectories vary significantly with the magnitude of the residual horizontal stress (Figures 5 and 6). The principal stress directions are either approximately parallel or perpendicular to the surfaces, the pit walls, and the crest. This would be expected since these faces are principal planes.

It is clear that the introduction of the horizontal tectonic stress to a gravity-loaded rock mass containing an open-pit mine, produces results which differ considerably from that of an open-pit mine which is subjected to gravity stress only. The stresses in the vicinity of the opening are significantly increased, as shown in Figure 6. Figure 7 shows that the average tangential stress near the toe is proportional to the factor K. Figure 8 shows the horizontal stresses acting near the ground surface. For increasing K values, the horizontal stresses gradually approach the field stress. Perhaps it is important to point out that tensions have not been developed along the ground surface.

3.2.2 Excavation Displacements

The displacement of the slope face and the crest of slope varies to a considerable degree with the value of K. When the value of K equals or is less than 1, the crest is displaced upwards. Figure 9 shows excavation displacements for K = 1/3. There are two effects which affect the crest displacement. The first is the relief of the vertical stress by removing the pit material, which will cause upward displacement; the second is the relief of horizontal stress which causes horizontal, inward movement together with some downward movement due to Poisson's effect. As shown in Figure 9 for μ = 0 (K = 0), there is no relief of horizontal stress during excavation and therefore there is no tendency for inward displacement of the slope face; however, Poisson's effect associated with release of vertical stress produces some outward movement at the crest.

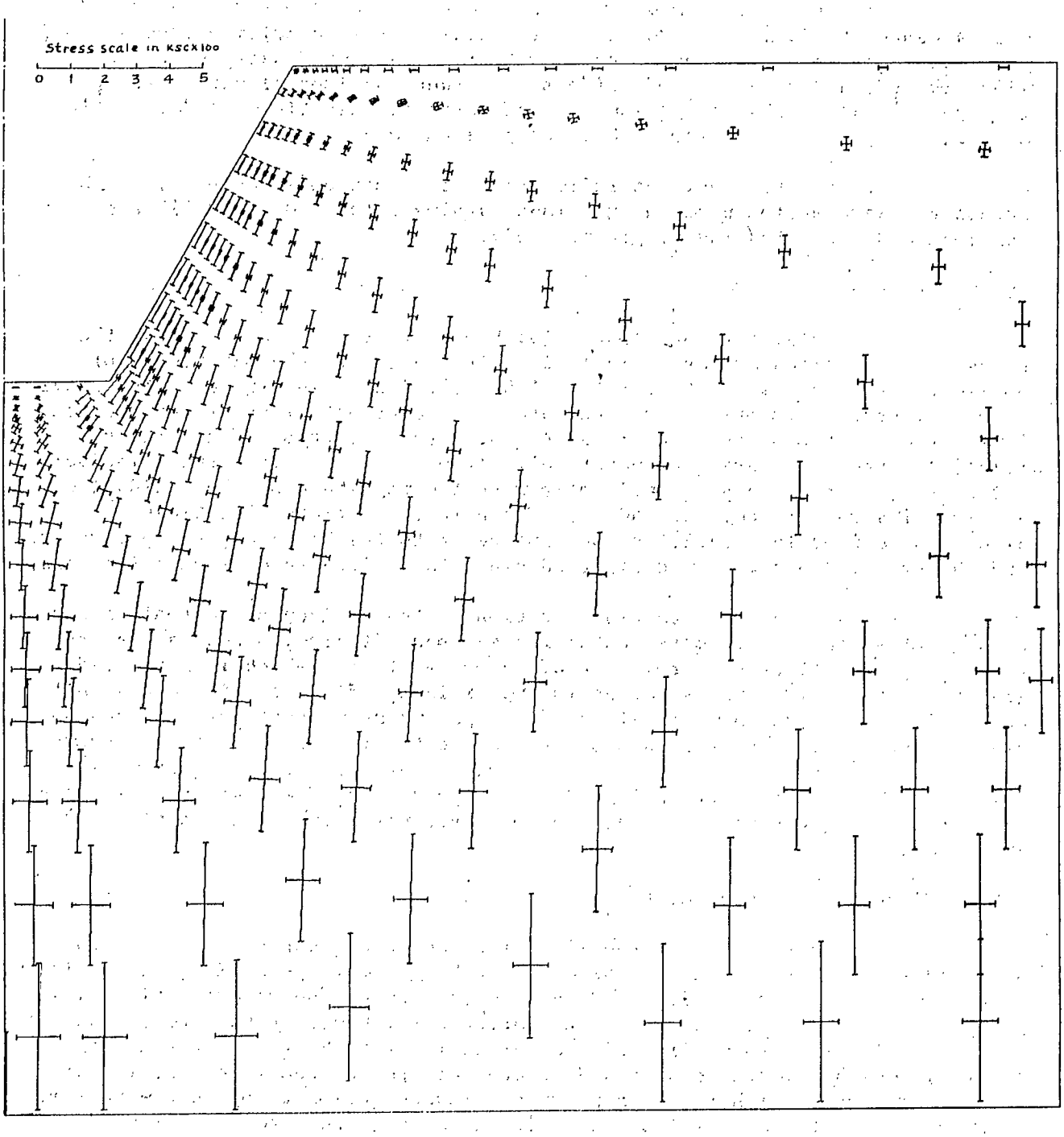

Figure 5. Direction and magnitude of principal stresses in a 60^{o} slope model; plane strain, K = 1/3.

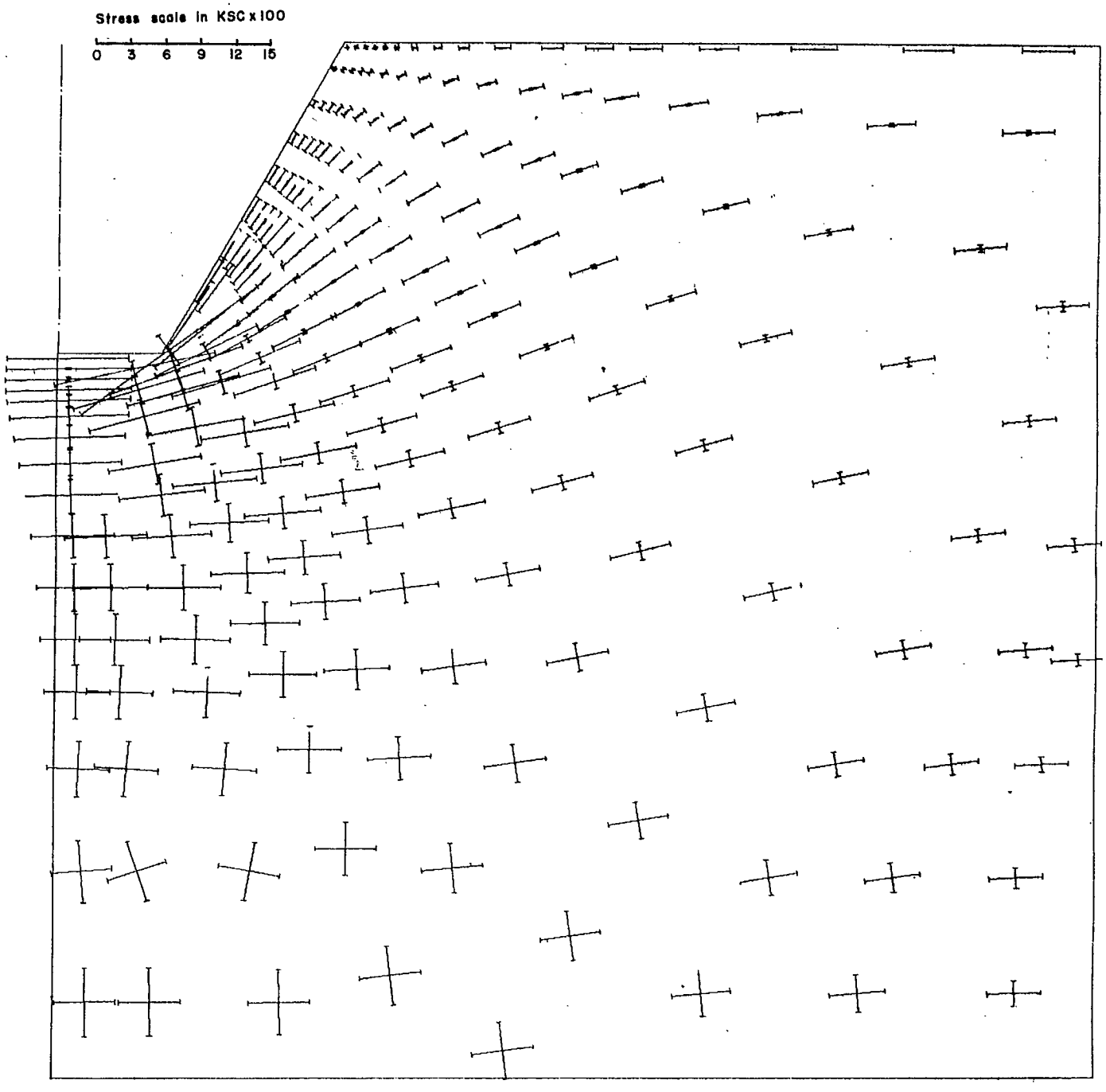

Figure 6. Direction and magnitude of principal stresses in a 60° slope model; plane strain, K = 3.

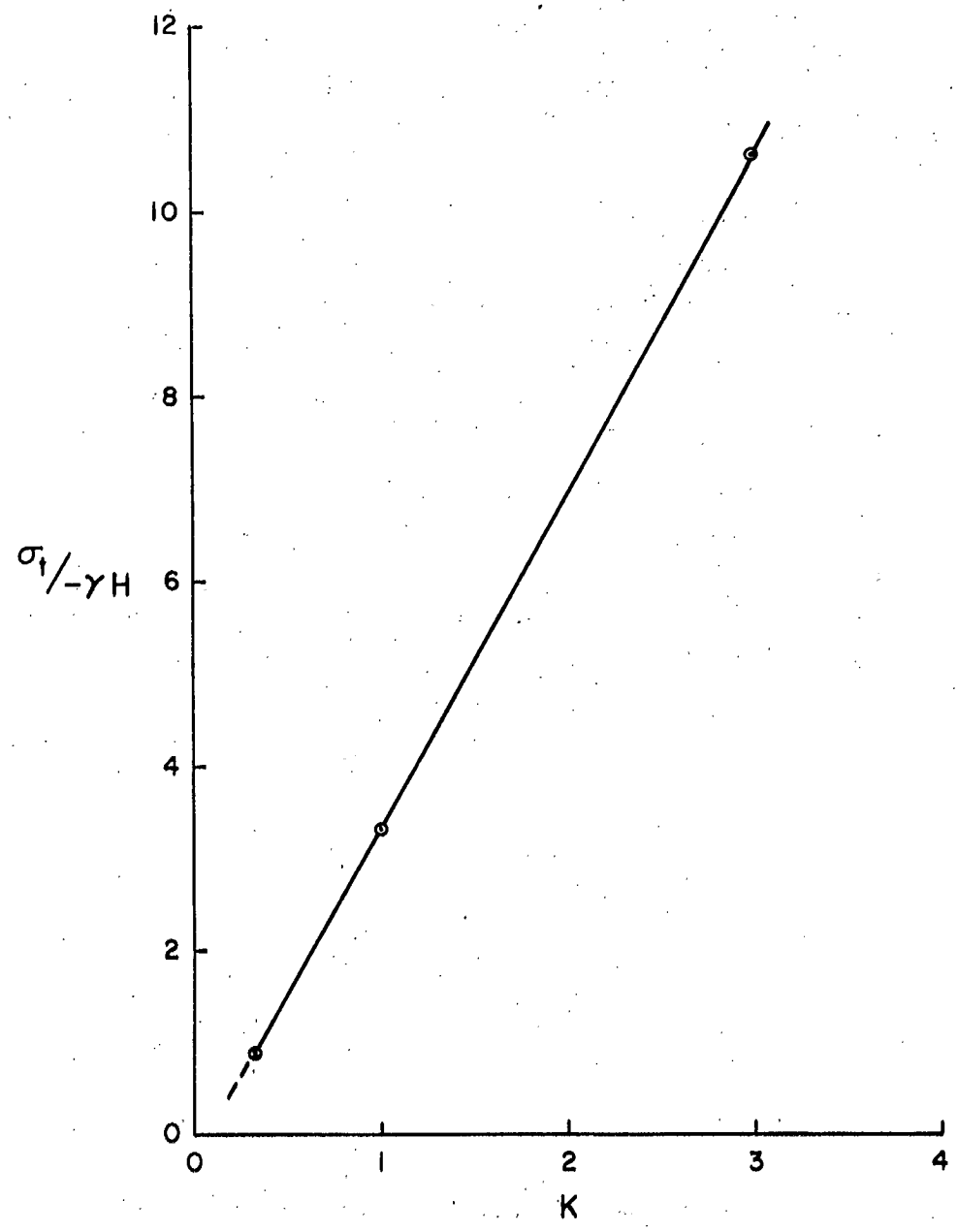

Figure 7. Tangential stress near the toe of a 60° slope as a function of the parameter K.

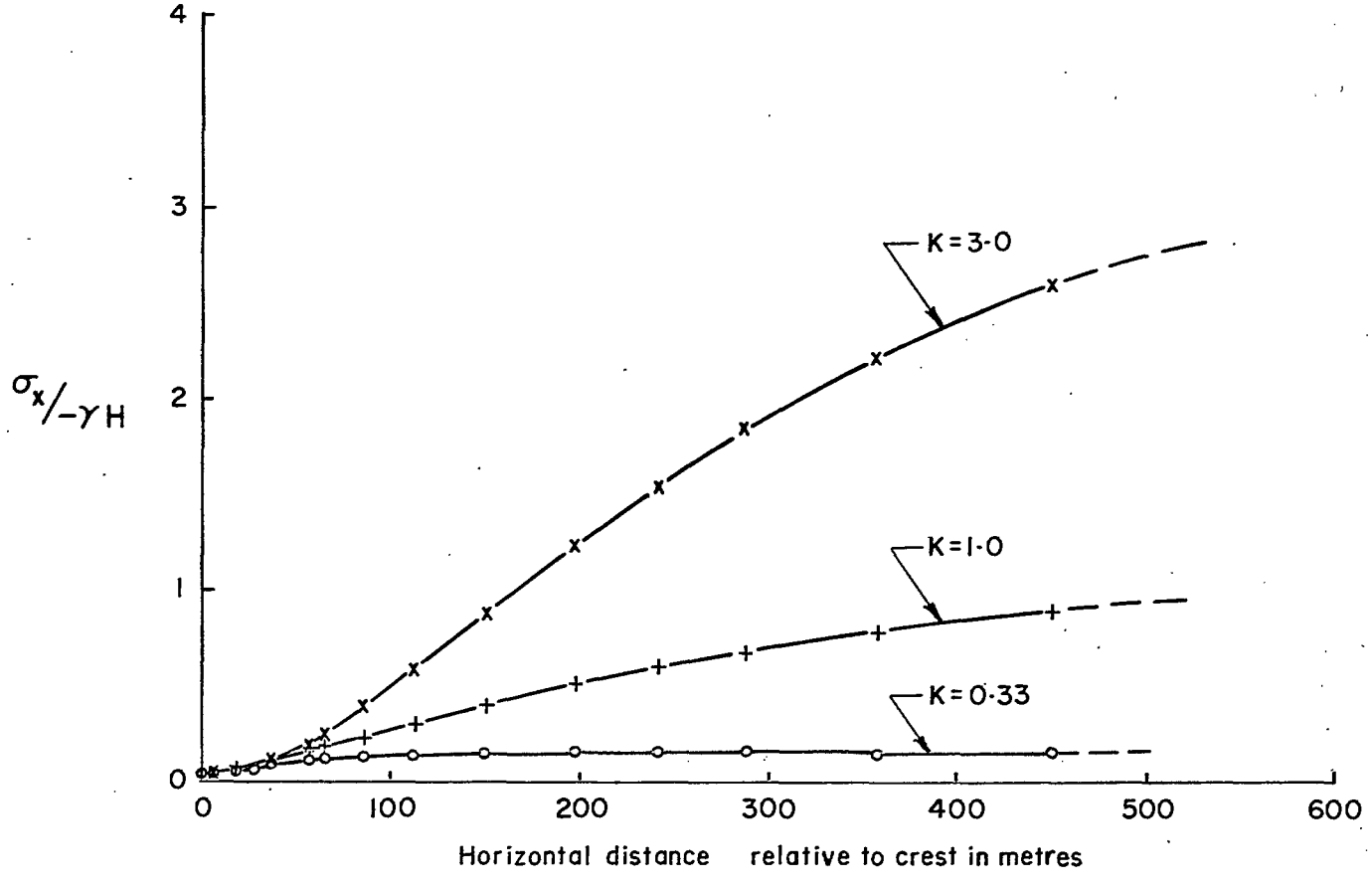

Figure 8. Horizontal stress distributions behind the crest.

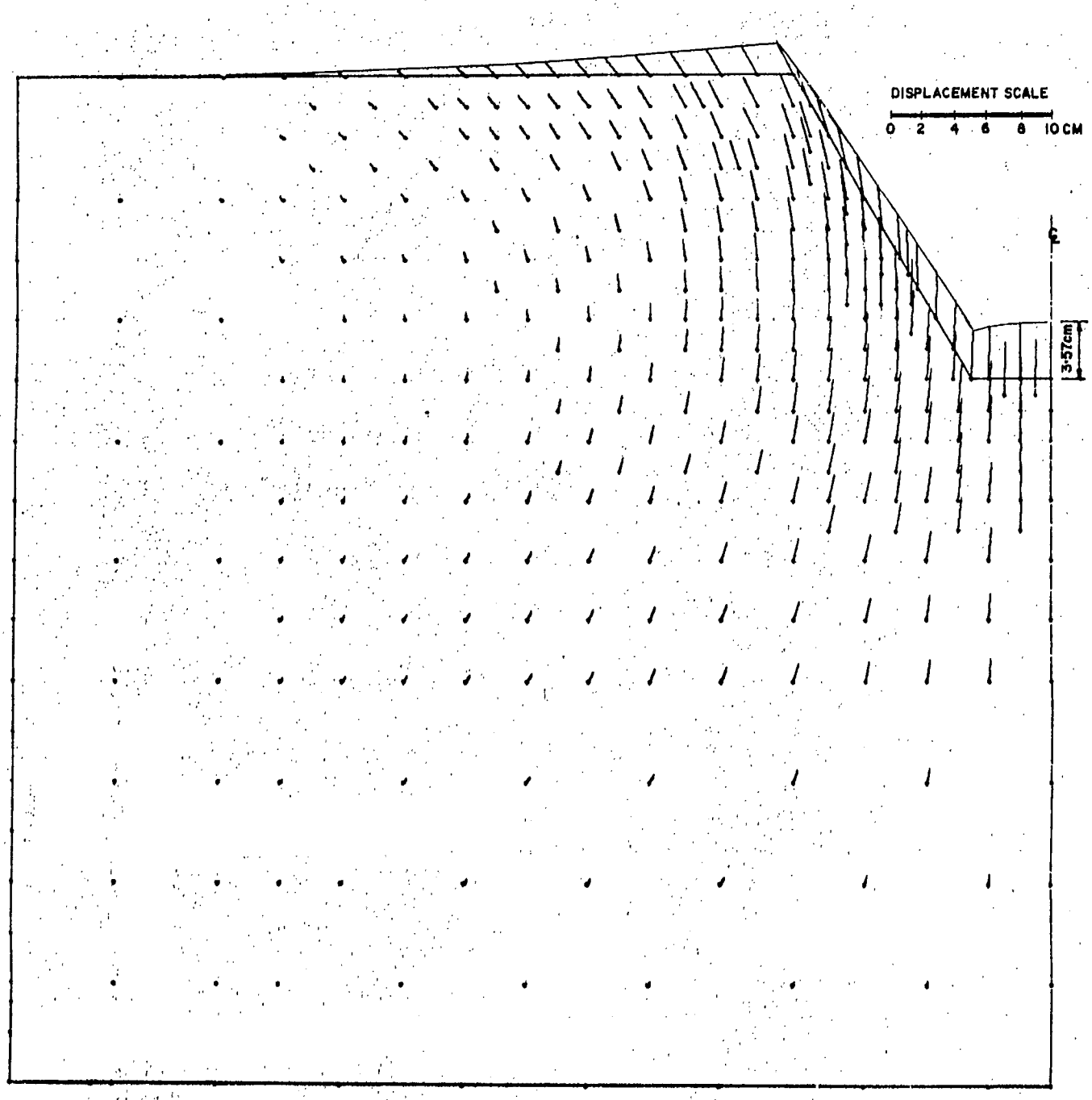

Figure 9. Excavation displacements in a 60° slope model; plane strain, K = 1/3.

Figure 10 shows that the excavation displacement of the slope crest for a 60° slope increases proportionally with increase in K or the magnitude of the horizontal stress. The magnitude of displacements developed along the slope face, particularly near the crest, should be measurable with an appropriate type of instrument. These measurements might be a valuable guide to the reactions occurring in the ground.

3.3 The Influence of Slope Angle on Stress and Displacement Distributions

Four finite element models were constructed to simulate open-pit mines with slope angles of 30°, 45°, 60° and 90° respectively. All models had a slope height of 300 m (900 ft) and approximately the same width of excavation, except the vertical slope (90°) which was wider. All models satisfied the boundary criteria that the distance to the boundary be approximately four times the height of the opening.

The field stress conditions consisted of gravitational stresses arising from an average density of 2.7 gm/cm^3 (168 lb/ft^3) and uniform horizontal stresses S_h of 81 kg/cm^2 (K = 1) for one case and 243 kg/cm^2 (K = 3) for a second case. The ore and wall rocks were the same as assumed previously, i.e., perfectly elastic with deformation properties of 7.03×10^5 kg/cm^2 (10×10^6 psi) and $\mu = 0.2$.

Stresses and deformations were determined in the models for plane strain conditions.

3.3.1 Stresses

Figure 11 is a composite graph of the variations of the tangential stress acting along the slope faces for various slope angles and under a variety of loading conditions. The tangential stresses are normalized by dividing the stresses by $(-\gamma H)$. Since the sign convention adopted in this report is that compressive stress is negative, all the positive values in this figure and some of the subsequent figures will indicate compression. It is seen that there is little change of tangential stress over approximately the upper third of the slope height under gravity loading (Figure 11c). However, large variations occur near the toes; the tangential stress concentration factors are 0.15, 0.40, 0.90 and 2.05, respectively, for the slope angles of 30°, 45°, 60° and 90°.

As the residual horizontal stress increases, the tangential stresses are also increased along the slope face. With a moderate horizontal stress, say K = 1, the tangential stress near the toe still increases with slope angle. As K increases to 3, the difference between the tangential stresses for the various slope angles become relatively small.

Under high residual horizontal stress field, the tangential stresses seemed to be larger for the upper portion of slope faces with lower slope angles as compared to those of steeper slopes, as shown in Figures 11a and 11b.

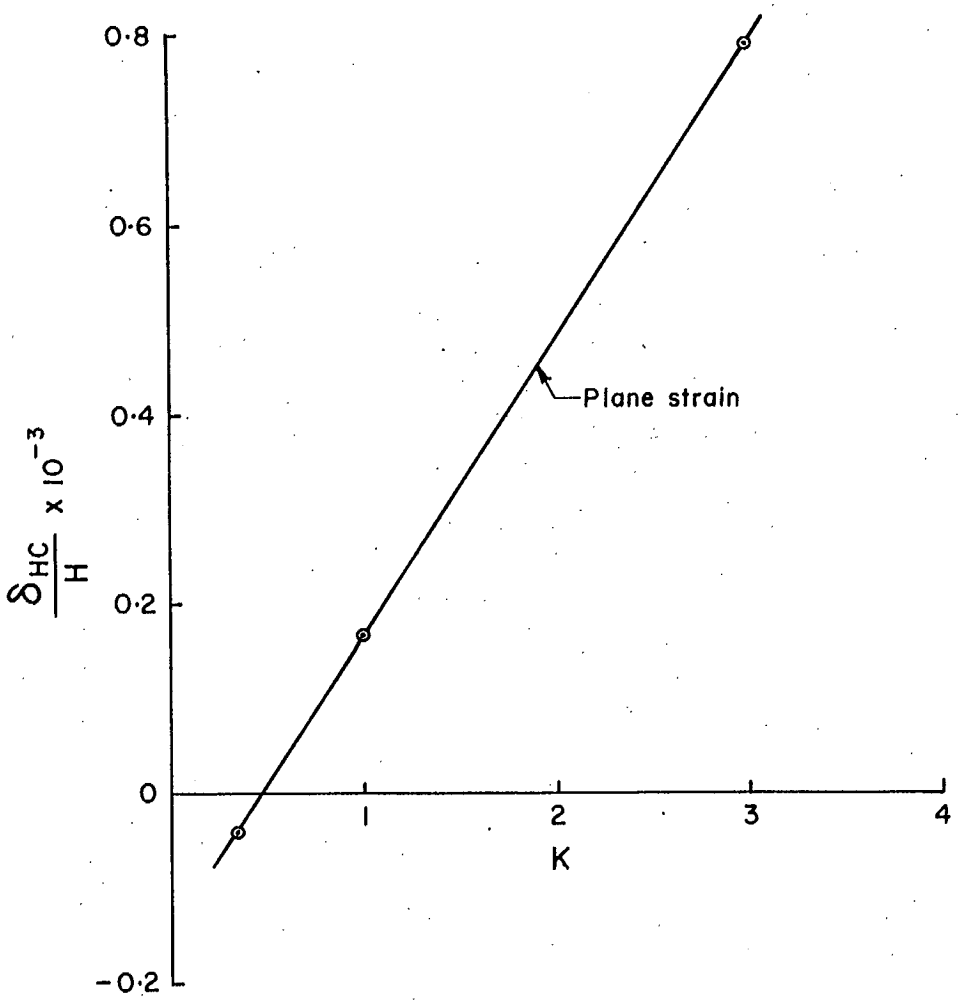

Figure 10. Excavation displacements in a 60° slope model; plane strain, K = 3.

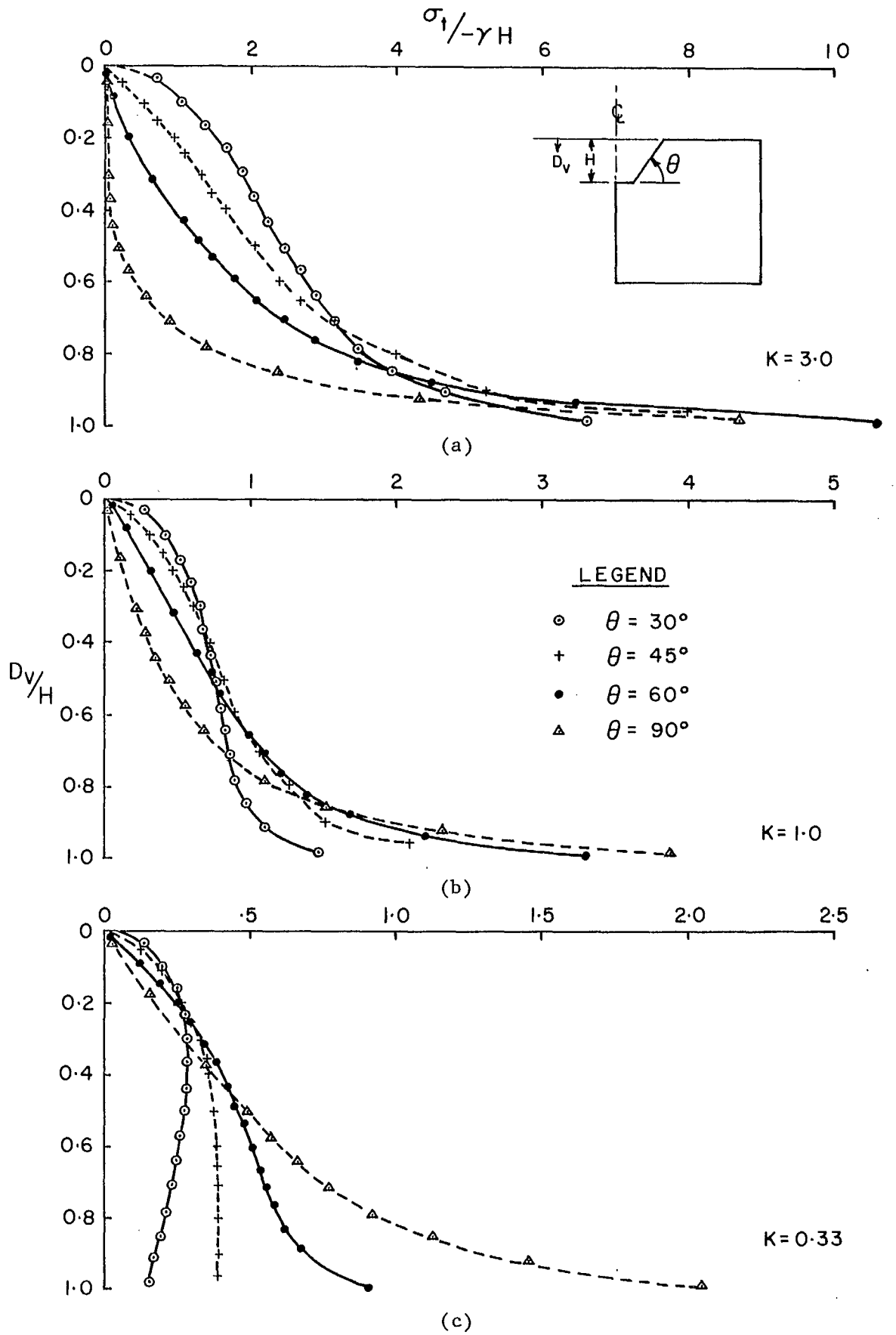

Figure 11. Tangential stress distributions along slope walls for various slope angles and a variety of loading conditions.

Figures 12, 13 and 14 are plots of horizontal stress, σ_x, along a horizontal section below the toe for the loading of K = 1/3, 1, and 3 respectively. For the case of K = 1/3, the stresses are substantially the same with only a small variation under the toe for all slope angles, i.e. 30^o, 45^o, 60^o, and 90^o. Tensile stresses occurred near the bottom of the pit for the slope angles of 60^o and 90^o. The relief of the vertical stress by removing the pit material causes upward displacements; this upward displacement could be associated with tensile stresses.

The horizontal stresses, σ_x, along the same section under the toe, follow the same pattern for all the slopes investigated. That is, it increases from the centre section of the model to a maximum directly under the toe and then decreases rapidly to the field stress at a distance approximately equal to the slope height, as shown in Figures 13 and 14. For K = 3, the tangential stress components under the toe can be as much as 8.1, 10.8, 12.3, and 12.6 times the gravity stress at the toe respectively for the slope angles of 30^o, 45^o, 60^o, and 90^o.

Figures 15, 16 and 17 are plots of horizontal stresses along a vertical section behind the crest. The variations of the horizontal stresses for the different slope angles under the same loading are small except for the vertical slope where the horizontal stresses immediately behind the slope face (vertical) are and should be equal to zero; it increases in the toe area as shown in these three figures. These horizontal stresses decrease to the field stress value at a depth equal to approximately the pit depth.

As mentioned previously, the sign convention adopted in this report is that tension is positive; therefore the minor principal stress, σ_3, will be the largest compression. Figure 18 shows the variations of the minor principal stress near the toe with slope angle and K. The minor principal stress, σ_3, is normalized by dividing by the factor $(-\gamma H)$. The compressive stress near the toe increases rapidly with increase of the horizontal stress. Under the same loading, the rate of increase of the minor principal stress near the toe is almost linear for the slope angles between 30^o and 60^o; the rate of increase decreases as angle increases from 60^o to 90^o except for gravity loading as shown in Figure 18.

3.3.2 Excavation Displacement vs Slope Angle

Figure 19 is a plot of horizontal excavation displacement at the slope crest versus slope angles for a variety of the loading conditions, i.e. K = 1/3, 1, and 3. The horizontal excavation displacement, δ_{hc}, is also non-dimensionalized by dividing by the slope height, H. As it is shown in Figure 19, the horizontal displacement at the crest is almost proportional to the slope angle. Also, a linear relationship exists between δ_{hc} and the parameter K.

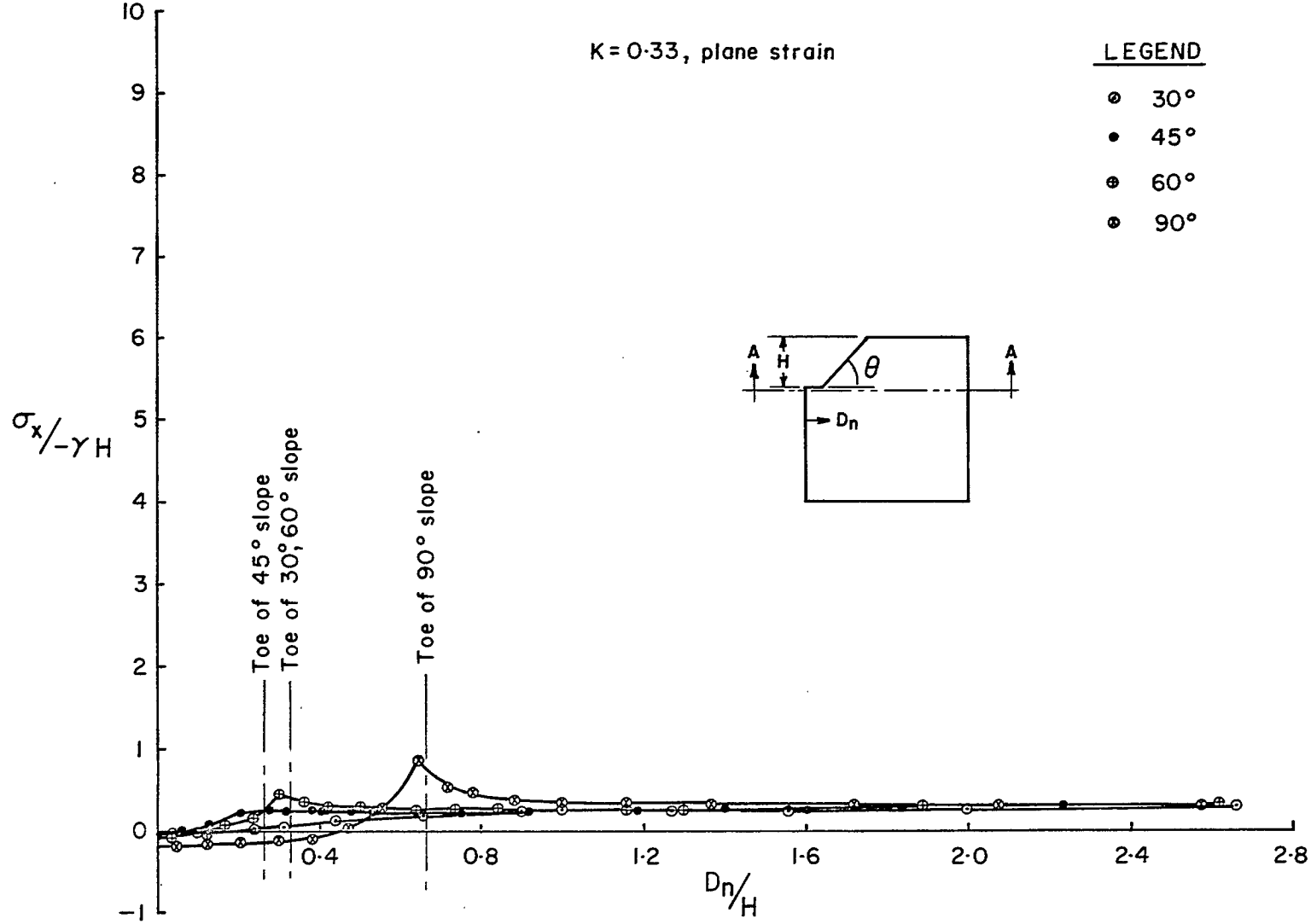

Figure 12. Comparison of horizontal stresses along a horizontal section below the toe for various slope angles; plane strain, K = 1/3.

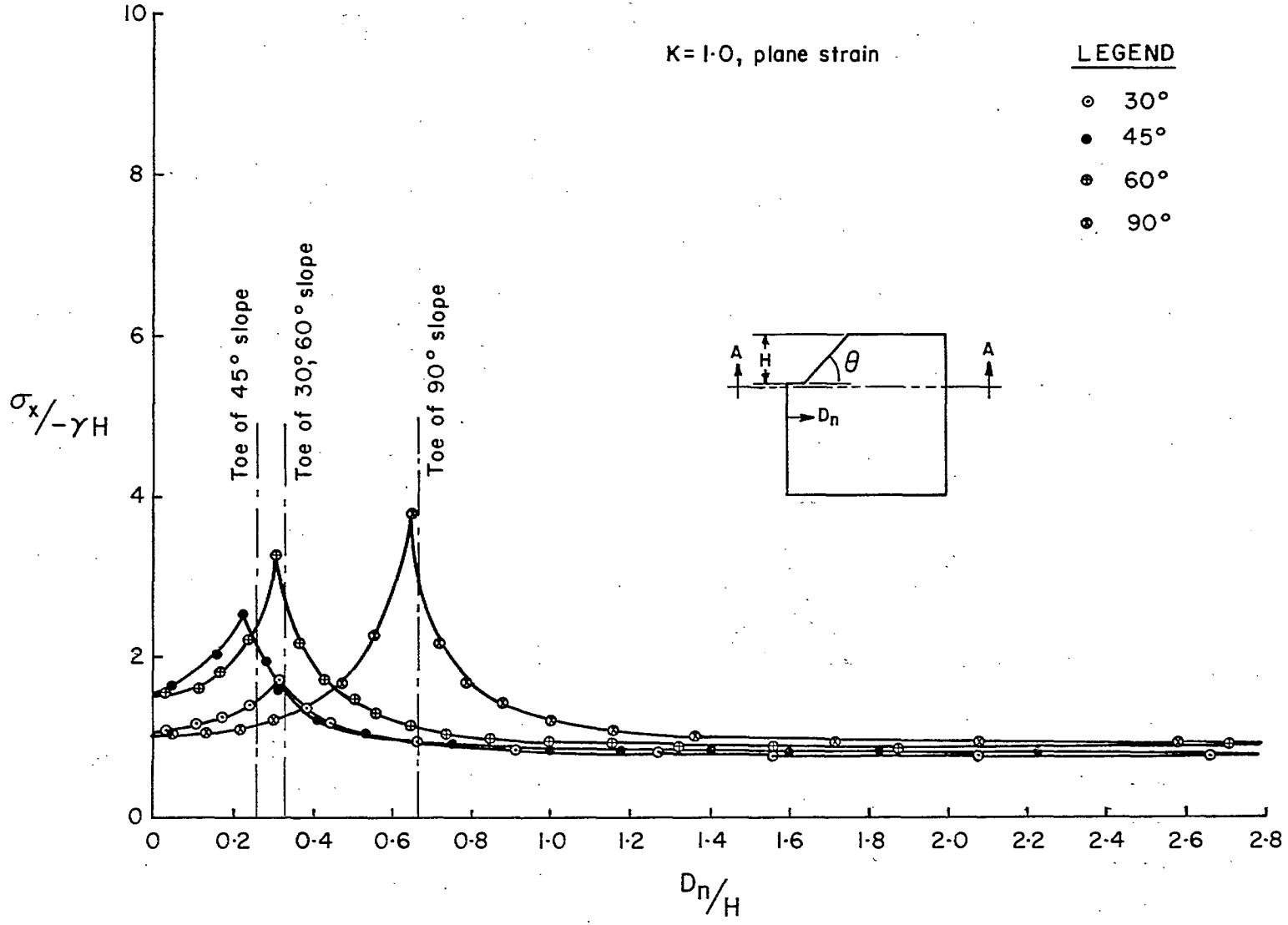

Figure 13. Comparison of horizontal stresses along a horizontal section below the toe for various slope angles; plane strain, K = 1.

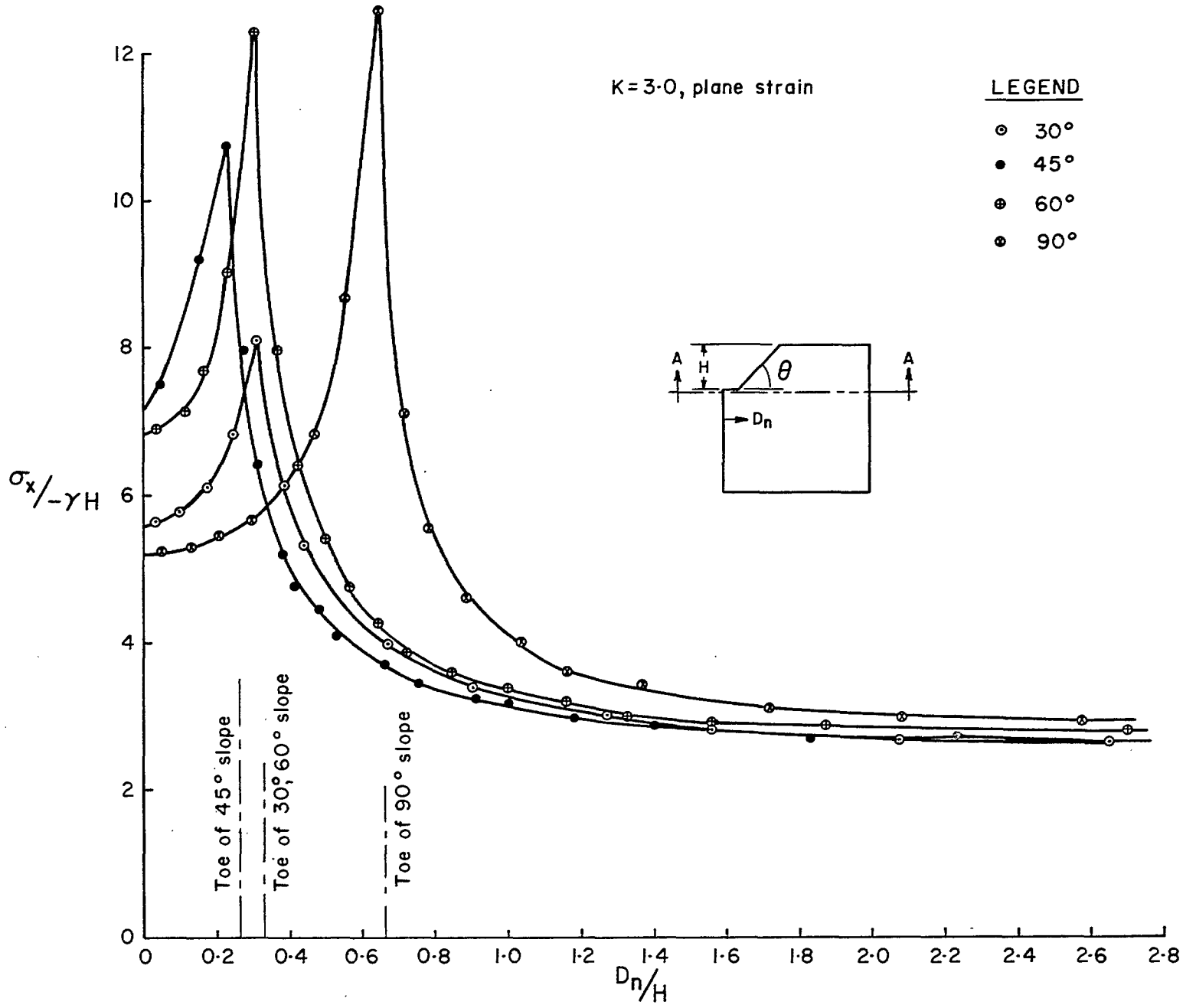

Figure 14. Comparison of horizontal stresses along a horizontal section below the toe for various slope angles; plane strain, K = 3.

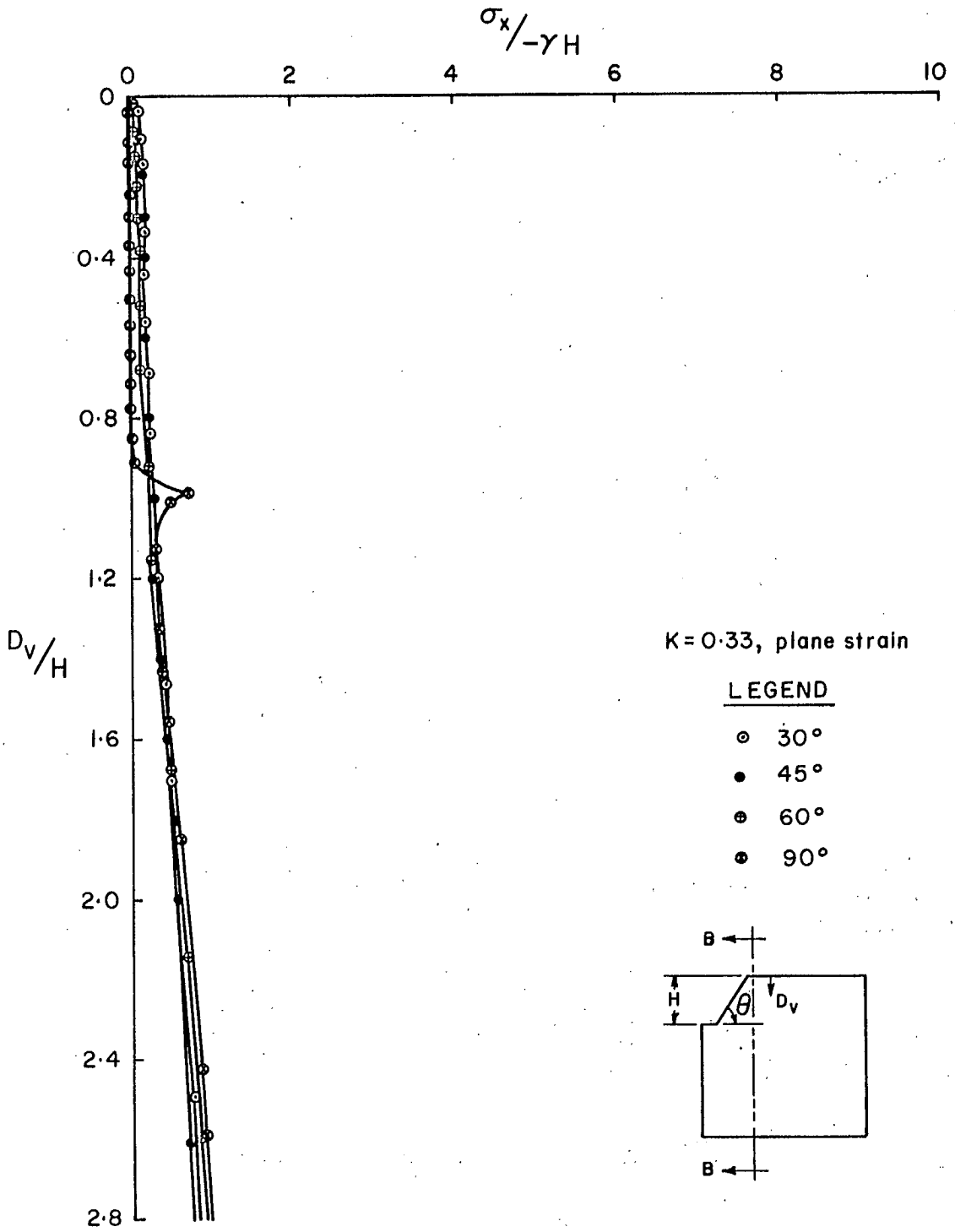

Figure 15. Comparison of horizontal stresses along a vertical section behind the crest for various slope angles; plane strain, K = 1/3.

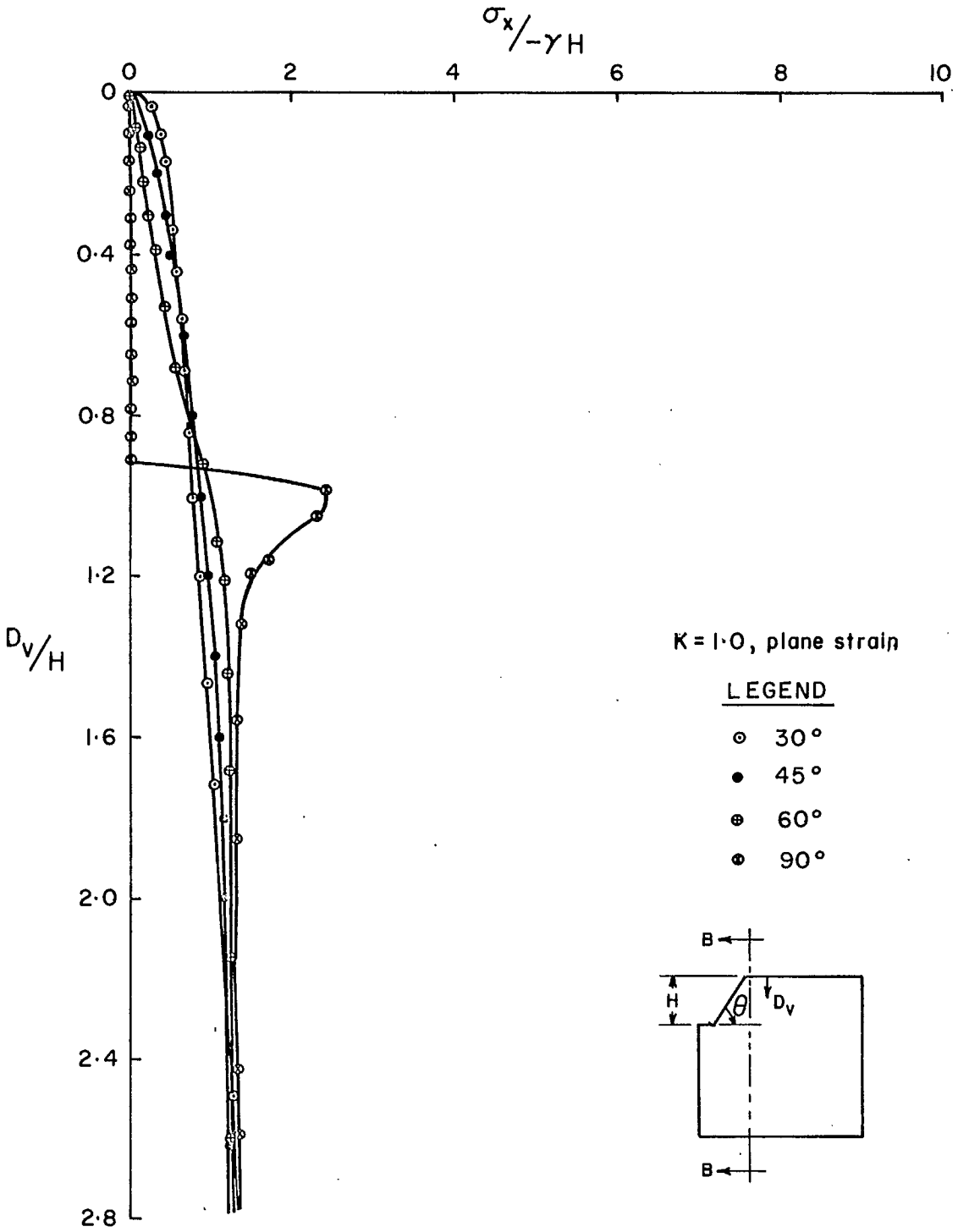

Figure 16. Comparison of horizontal stresses along a vertical section behind the crest for various slope angles; plane strain, K = 1.

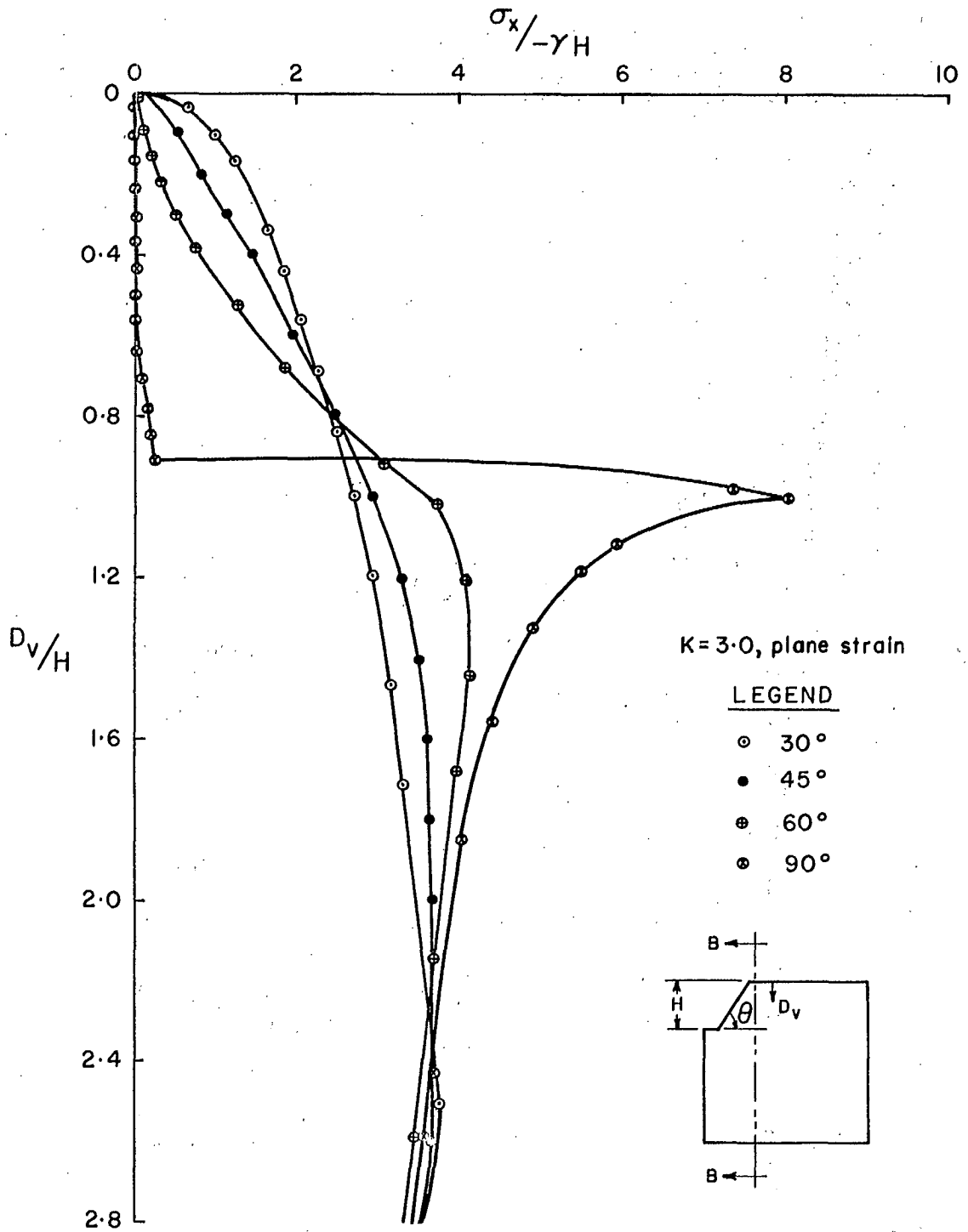

Figure 17. Comparison of horizontal stresses along a vertical section behind the crest for various slope angles; plane strain, K = 3.

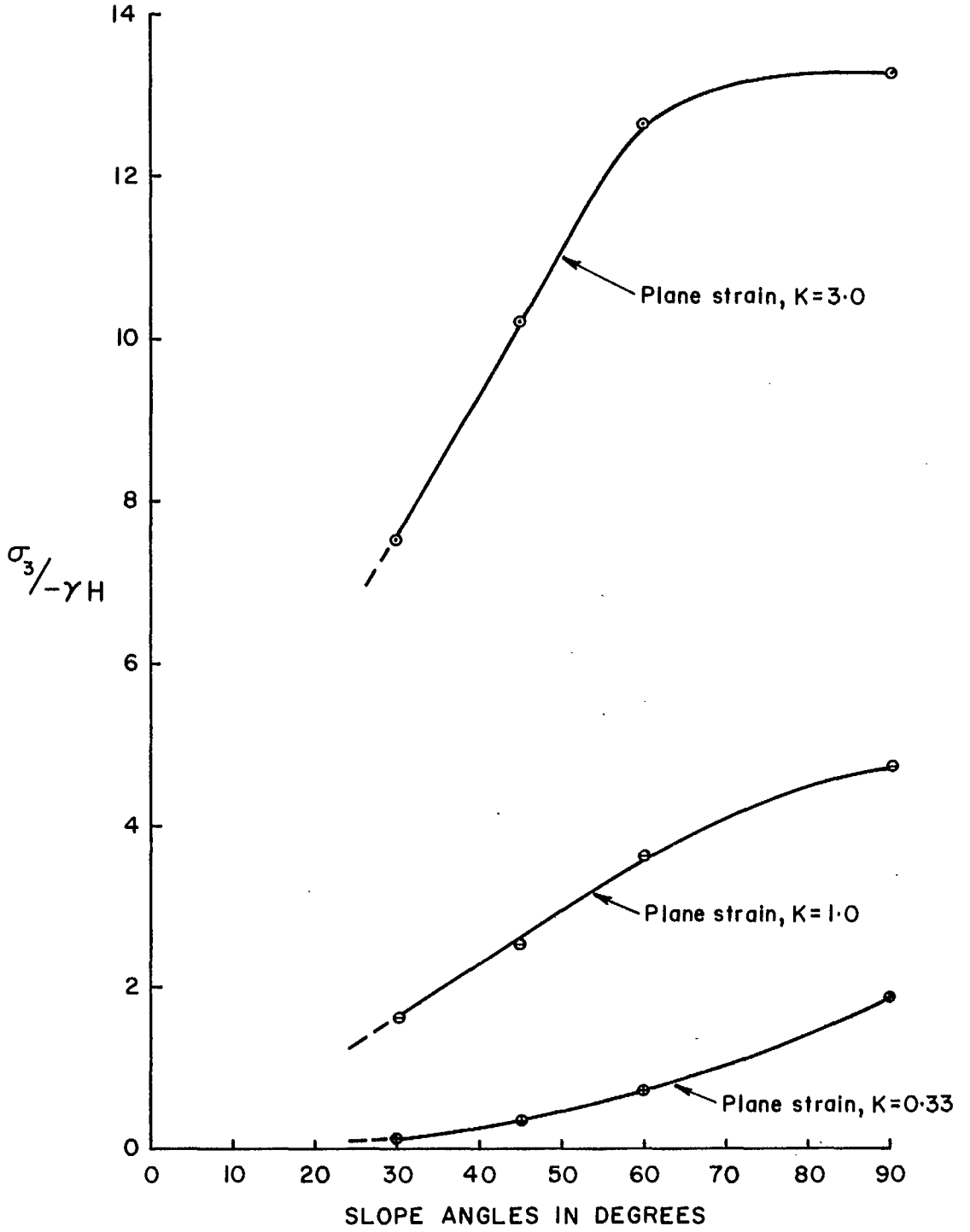

Figure 18. Minor principal (largest compressive) stresses near the toe as a function of slope angle.

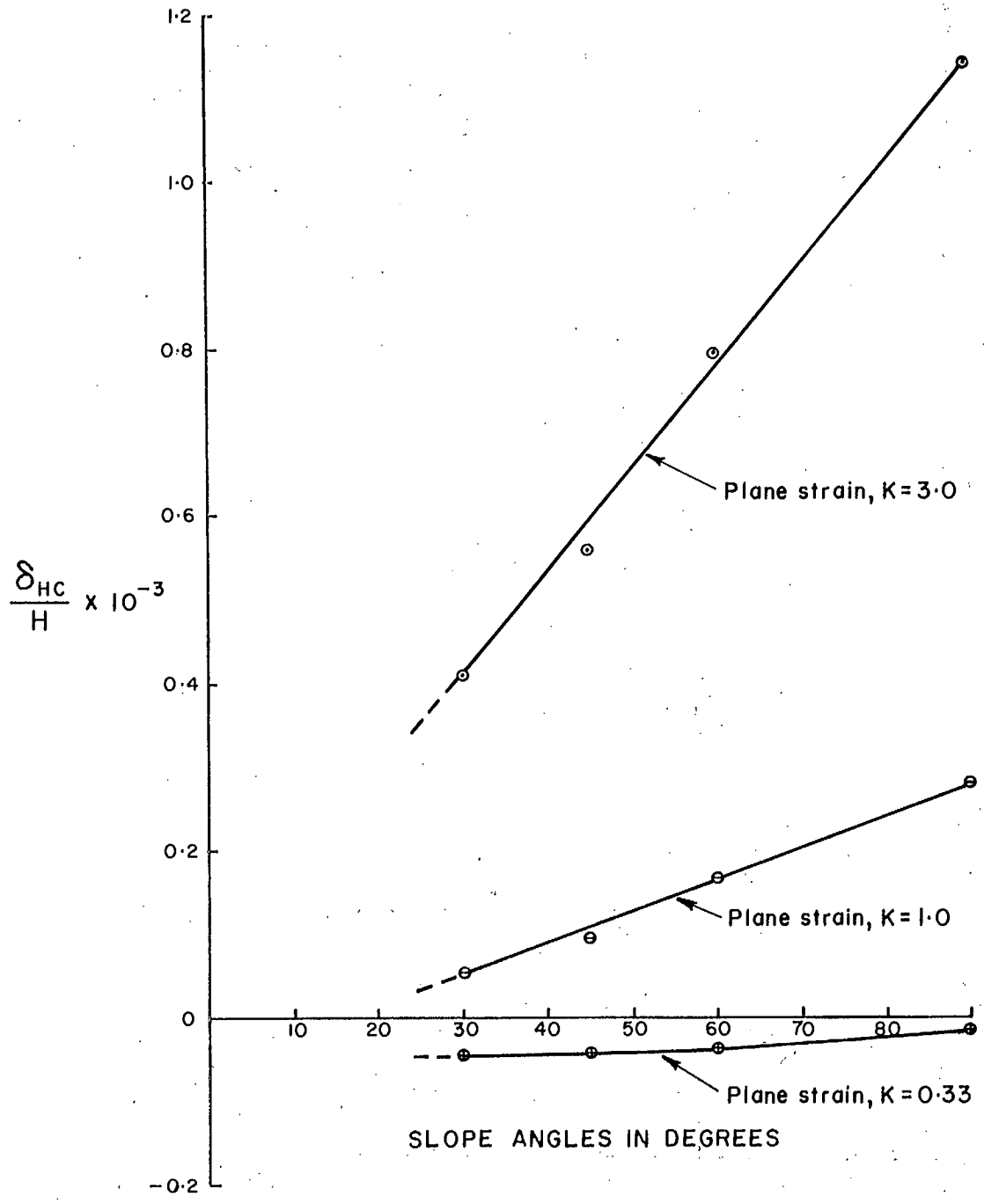

Figure 19. Excavation displacements at the crest as a function of the slope angle.

Under gravity loading, the horizontal displacements, δ_{hc}, for all slope angles, were directed into the walls; with the addition of the horizontal tectonic stress, the displacements were directed toward the opening. The following equations can be used to approximate the horizontal displacement, δ_{hc}:

$$\frac{\delta_{hc}}{H} = -0.03029 - 0.00071_{\theta} + 0.00001\theta^2 \quad \ldots \text{ for } K = 1/3$$

$$\frac{\delta_{hc}}{H} = -0.03293 + 0.00267\theta \quad \ldots \text{ for } K = 1$$

$$\frac{\delta_{hc}}{H} = -0.00435 + 0.01360\theta \quad \ldots \text{ for } K = 3$$

where H is the pit depth in centimetres and θ is the slope angle in degrees, and δ_{hc} is the horizontal excavation displacement in centimetres x 10^{-3}.

3.4 Slope Configurations in Relation to its Economy of Operation and Its Stability

It was thought that the volume of waste excavation might be reduced by changing the slope configuration. Therefore, the stress distributions were examined in a series of models with parabola outlines in contrast to the conventional constant slope. Results were compared with that of a typical 45° slope.

3.4.1 Slope Configurations

A series of six two-dimensional mathematical models were prepared: three were concave and three were convex. The details of the slopes are shown in Figure 20. The distance between the crest of the modified slopes and that of the original 45° slope is 30, 60, and 90 m either to the right or to the left of crest of the original 45° slope, depending upon whether it is concave or convex. These modified slopes can be considered as slopes with varying angles at different depths of the pit. The dips of the chords, or equivalent slope angles, at several depths are shown in Table 2.

3.4.2 Excavation Volume

For simplicity, the orebody is assumed to be vertical; the width of orebody is assumed to be 150 metres. At a pit depth of 300 metres (900 ft), the total volumes of excavation for a 45° slope and for the modified slopes were calculated. The differences of the volumes excavated between the 45° slope and the modified slopes are shown in Table 3. A reduction of approximately 70,600, 52,900, 35,300, and 17,600 tons of waste rock per linear metre on 392,000 tons would occur from the four modified slopes No. 1, No. 2, No. 3 and No. 6, and there are increases in waste excavations with slopes No. 4 and No. 5.

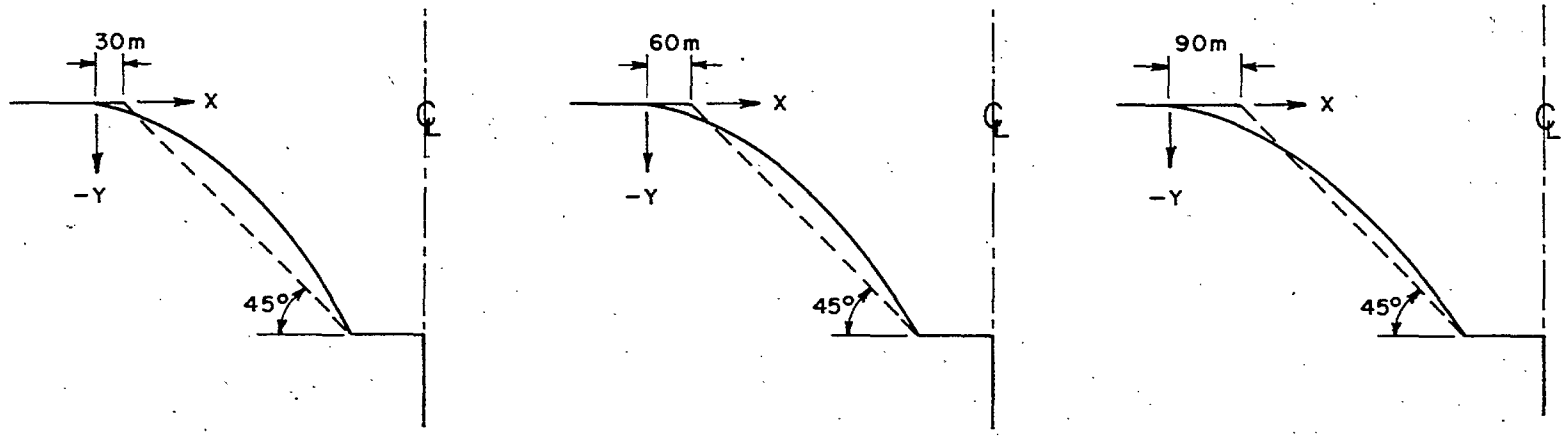

(1) $X^2 = 4(-90.75)Y$ (2) $X^2 = 4(-108.0)Y$ (3) $X^2 = 4(-126.75)Y$

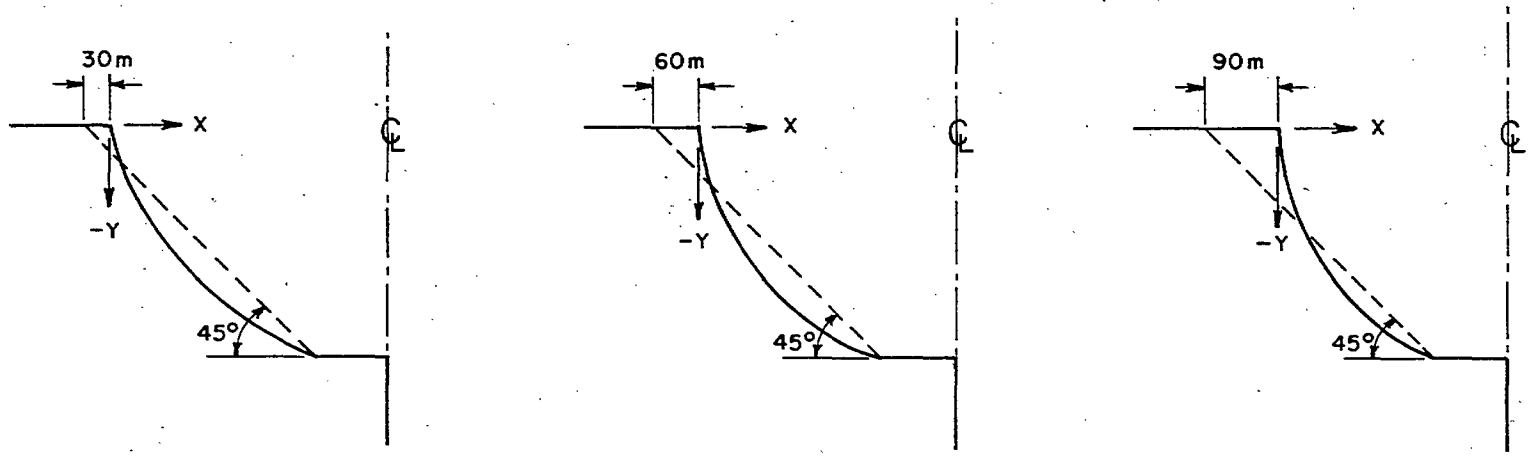

(4) $Y^2 = 4(83.33)X$ (5) $Y^2 = 4(93.75)X$ (6) $Y^2 = 4(107.14)X$

Figure 20. Definition of the modified slopes.

TABLE 2

Dips of the Chords, or Equivalent Slope Angles, at Various Depths

Modified Slope	Equivalent Slope Angle*	
	Depth - Metres	Slope Angle - Degrees
No. 1	0- 35	25
	35- 75	35
	75-140	46
	140-300	56
No. 2	0- 40	23
	40- 75	35
	75-140	45
	140-300	54
No. 3	0- 38	22
	35- 70	32
	70-140	42
	140-300	51
No. 4	0- 75	75
	75-120	59
	120-175	47
	175-230	40
	230-300	32
No. 5	0- 75	75
	75-130	62
	130-181	48
	180-230	43
	230-300	37
No. 6	0- 80	75
	80-130	66
	130-185	52
	185-230	47
	230-300	40

* Dip of the chord.

TABLE 3

Differences of the Volumes Excavated between the 45° and Modified Slopes

Excavations / Cases	Total Volumes to be Excavated per Linear Metre	Difference Between Volumes Compared with 45° Slope
45° Slope	(133,500) ((392,647))	--
No. 1	(109,500) ((322,058))	(-24,600) ((70,588))
No. 2	(115,500) ((357,352))	(-18,000) ((35,294))
No. 3	(121,500) ((445,588))	(-12,000) ((52,941))
No. 4	(151,500) ((410,290))	(+12,000) ((17,647))
No. 5	(139,500) ((375,000))	(+ 6,000) ((17,647))
No. 6	(127,500)	(- 6,000)

( ) Volumes in cubic metres

(( )) Volume in short tons

"-" means less excavation as compared with the 45° slope

"+" means extra excavation as compared with the 45° slope

1 ton = 0.34 m^3 (12 ft^3)

3.4.3 Experimental Results

Three different loadings were examined for each slope model, i.e., with simple gravity ($K = 1/3$) and with residual horizontal stress of 81 kg/cm^2 ($K = 1$) and 243 kg/cm^2 ($K = 3$). The increases of stresses are approximately proportional to the parameter K. Displacements are directed more in the horizontal direction and toward the openings with increases in K.

3.4.3.1 Compressive Principal Stress along Slope Faces

Figures 21, 22 and 23 are the plots of the minor (compressive) principal stresses acting along the slope face of a 45^o slope and those of the modified slopes for the loading conditions $K = 1/3$, 1 and 3 respectively. The differences of stress distributions between the 45^o slope and the six modified slopes are clearly indicated in these figures.

Under gravity stress field, the stresses developed in modified slopes Nos. 1, 2 and 3 are smaller than those of the 45^o slope, except near the toe where they are larger. The minor principal stresses developed along the slope faces for the modified models Nos. 4, 5 and 6 are considerably larger at the middle height of the pit walls, as shown in Figure 21, although at the toe they are less than those for the 45^o slope.

With residual horizontal stresses, the minor principal stresses along the slope faces for the modified slopes Nos. 1, 2 and 3 are also smaller than those of the 45^o slope except near the toe. For the case of $K = 1$, the minor principal stress near the toe of No. 1 slope is only 10% higher than that of the 45^o slope and this difference becomes smaller with the increase of K. The stresses developed in the models Nos. 4, 5 and 6 are somewhat larger, as shown in Figures 22 and 23, than for the 45^o slope except in the toe.

3.4.3.2 Stresses along a Horizontal Section under the Toe

A horizontal section under the toe was chosen as close to the pit bottom as possible. The horizontal stress components, σ_x, along that section are plotted as shown in Figures 24, 25 and 26 respectively for $K = 1/3$, 1, and 3. As can be seen, the stress variations are small.

3.4.3.3 Excavation Displacement vs Excavation Volume

The term "excavation displacement" at the slope crest has frequently been used as a measure of slope stability. The idea is that the larger the displacement at the crest the greater the probability of the instability. However, the limiting value of displacement which would cause instability cannot yet be determined. Figure 27 shows the horizontal excavation displacement at the crest of each slope versus the volume of excavation per linear metre. Since the orebody is assumed to be vertical, the larger the excavation volume, the more the waste rock will be excavated. It can be seen that the excavation displacements at the crests of the modified slopes Nos. 1, 2 and 3 are approximately 18% lower than that of the 45^o slope and that the crest displacement does not seem to be much different for the three cases although the reduction would be quite different, i.e., 70,600, 52,900 and 35,300 tons of waste rock per linear metre respectively for slopes Nos. 1, 2 and 3. For the convex slopes

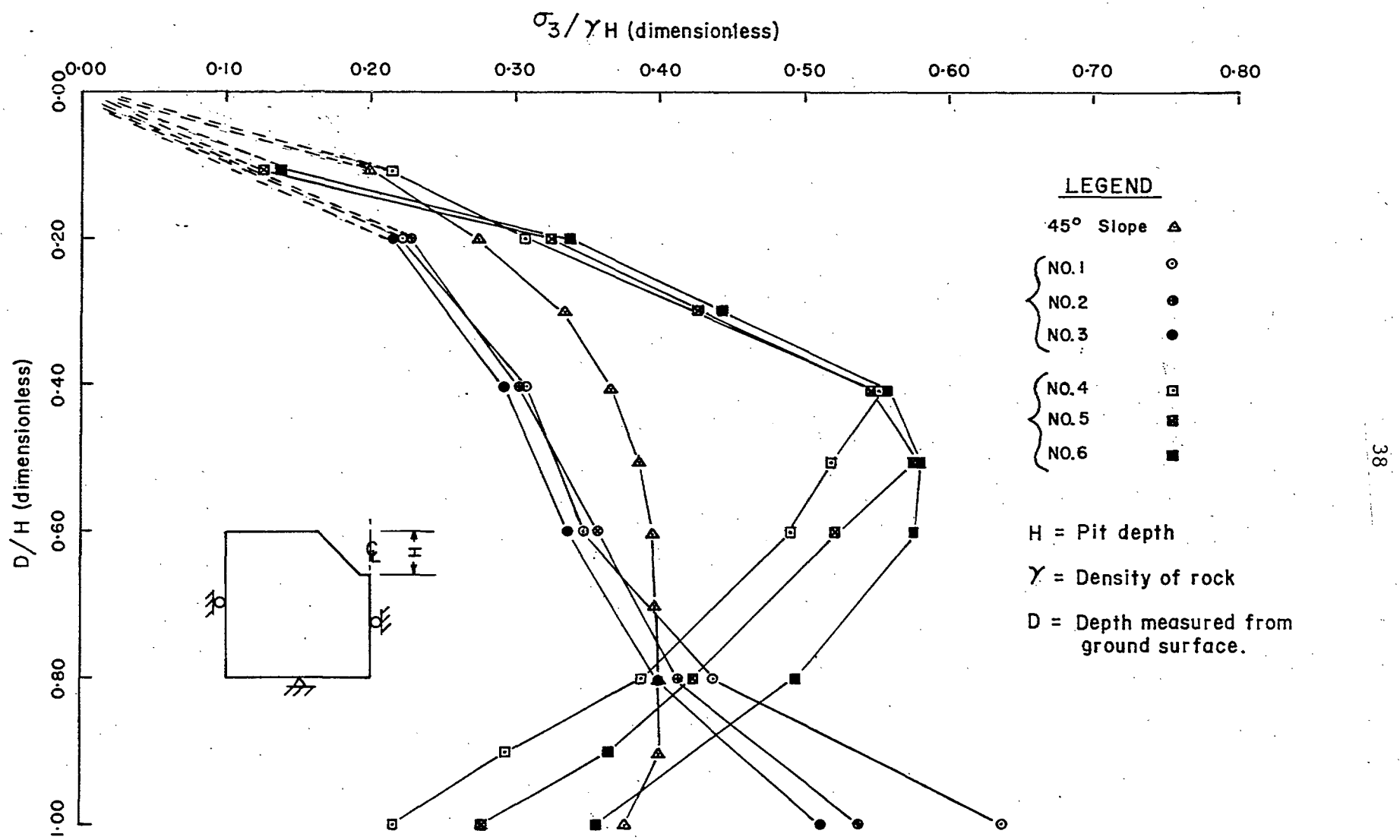

Figure 21. Comparison of compressive principal stresses along the slope walls between a typical 45° slope and the modified slopes; plane strain, K = 1/3.

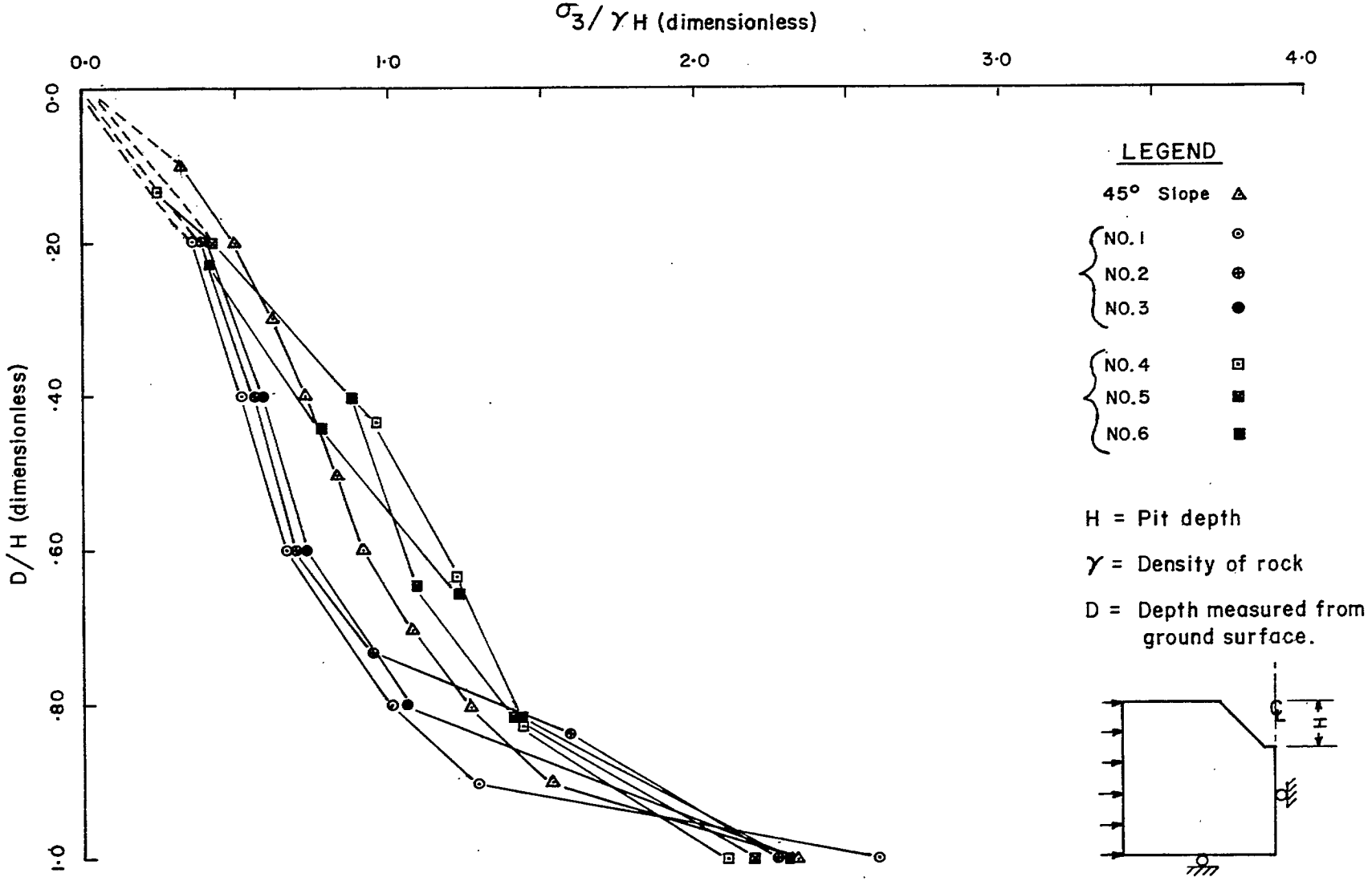

Figure 22. Comparison of compressive principal stresses along the slope wall between a typical 45° slope and the modified slopes; plane strain, K = 1.

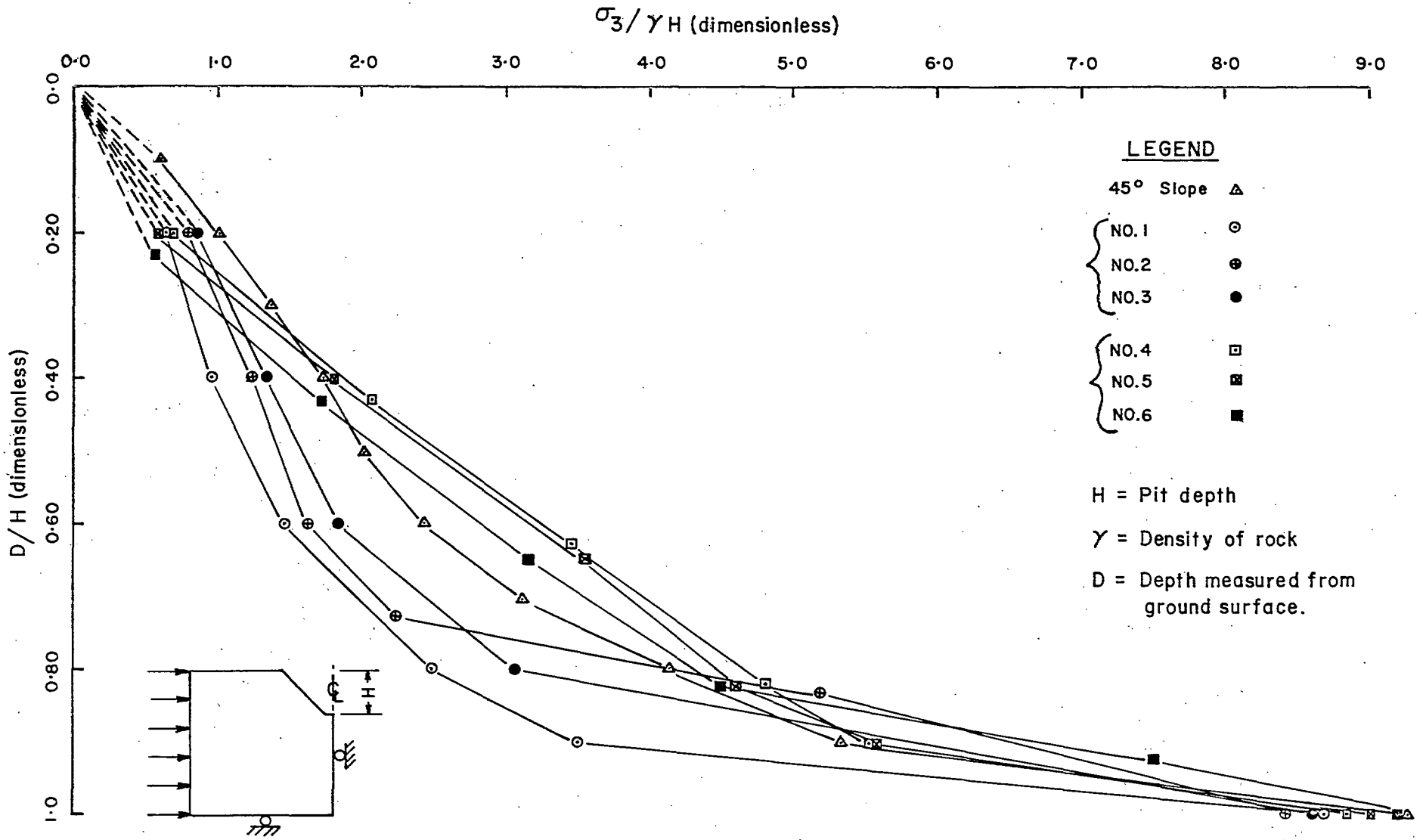

Figure 23. Comparison of compressive principal stresses along the slope walls between a typical 45° slope and the modified slopes; plane strain, K = 3.

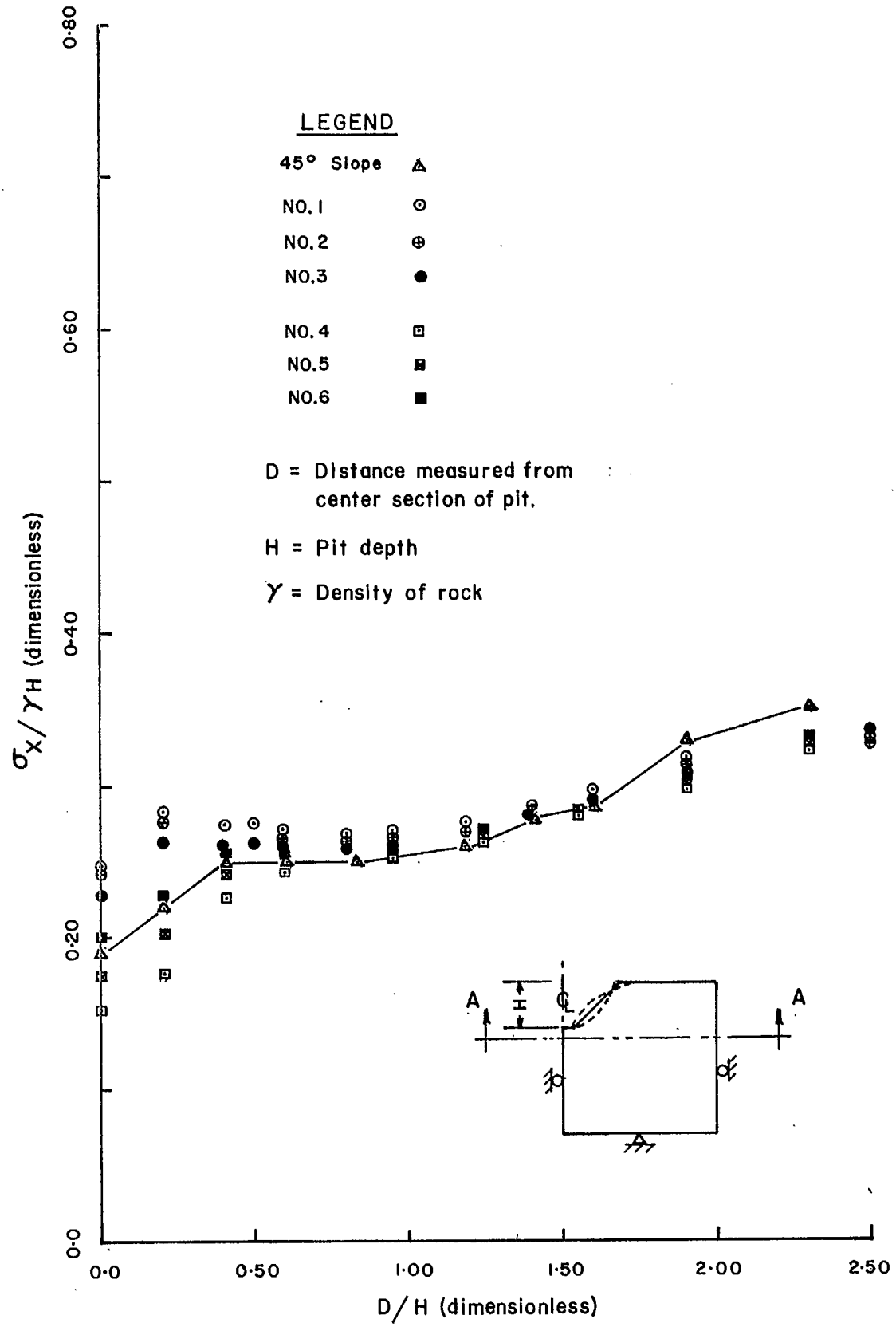

Figure 24. Comparison of horizontal stresses along a section A-A between a typical 45° slope and the modified slope; plane strain, K = 1/3.

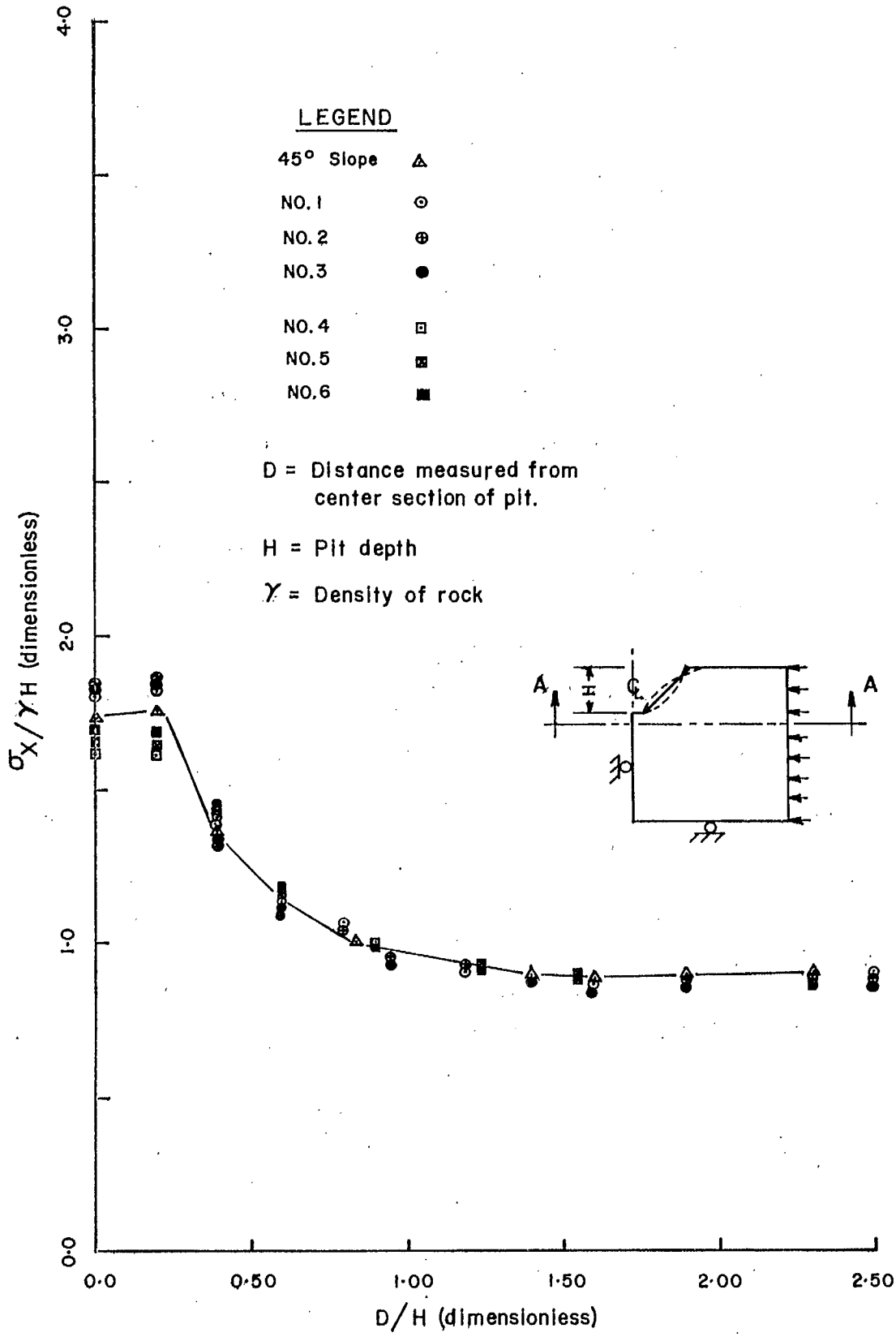

Figure 25. Comparison of horizontal stresses along a section A-A between a typical 45° slope and the modified slopes; plane strain, K = 1.

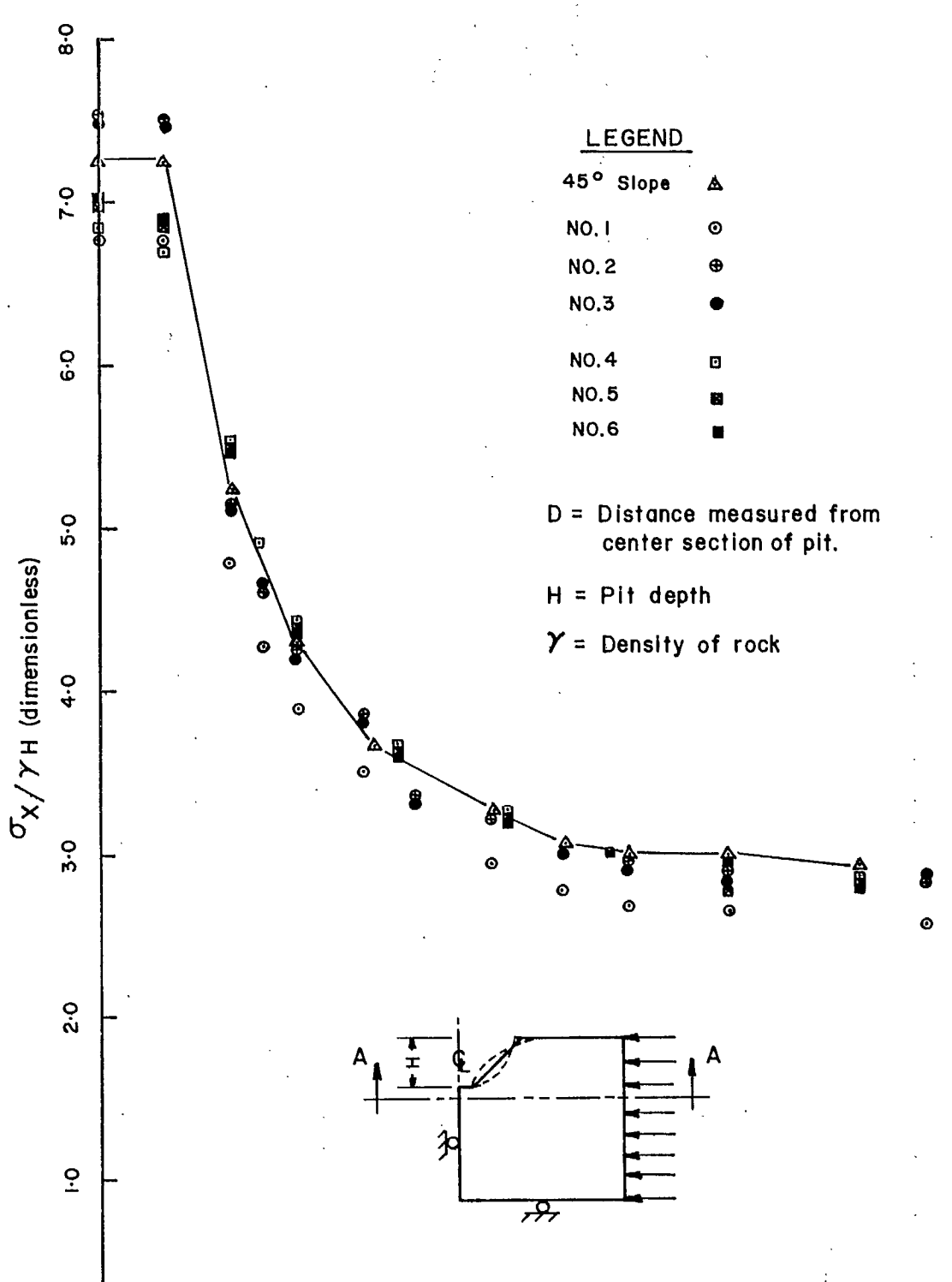

Figure 26. Comparison of horizontal stresses along a section A-A between a typical 45° slope and the modified slopes; plane strain, K = 3.

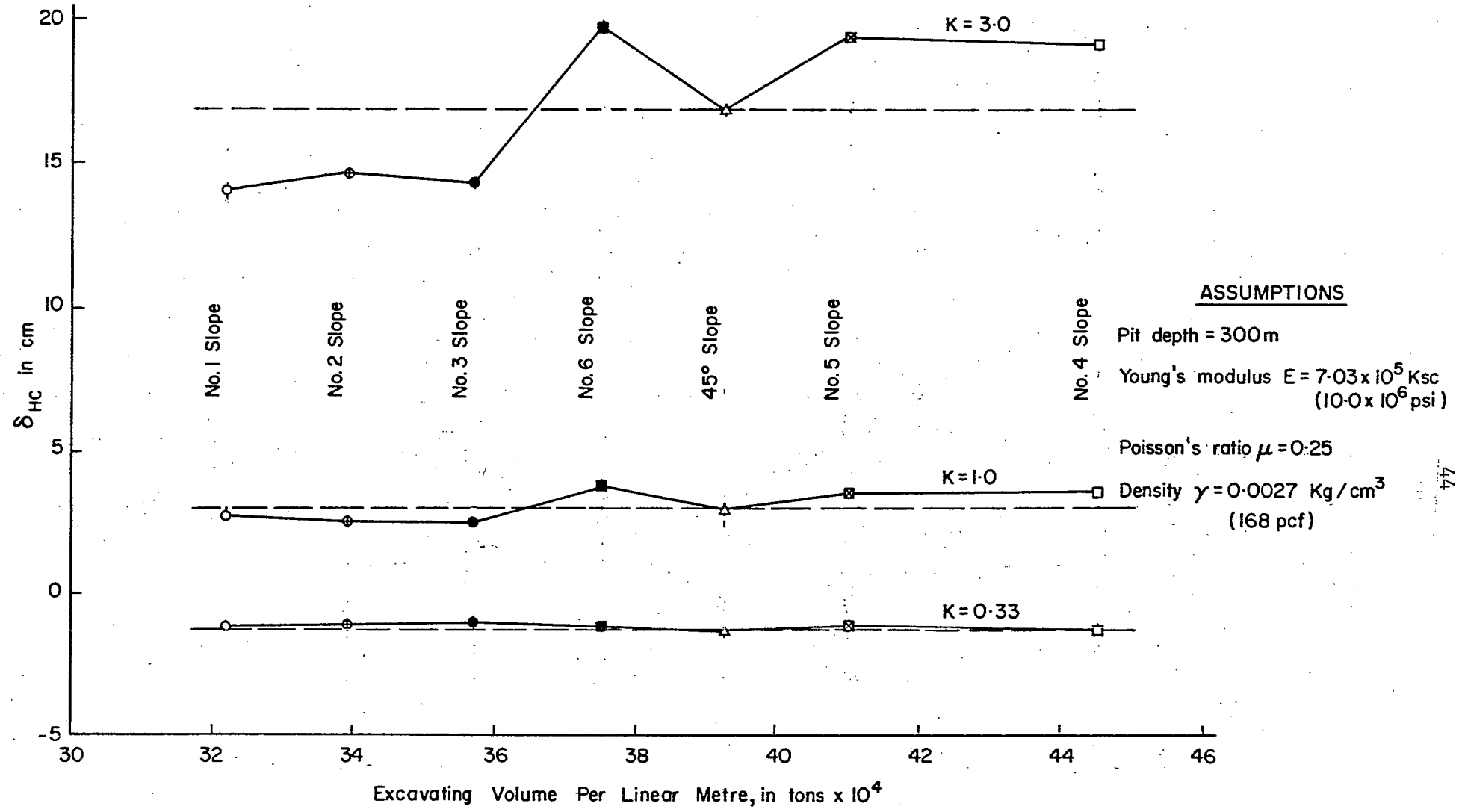

Figure 27. Excavation displacements at the crest as a function of excavating volume.

Nos. 4, 5 and 6 the excavation displacements are about 12% higher than that of the 45° slope and the volumes of waste rock were increased except for the model No. 6.

3.4.3.4 Minor Principal Stress near the Toe vs Excavating Volume

The minor principal stresses or maximum compressions, near the toe, show very little difference for these modified models as compared to that of the 45° slope (Figure 28). Owing to the difficulty in reproducing the mesh details adjacent to the toes of each model, these values are less significant than the patterns of stress differences throughout the faces of the various models. However, the conclusions follow those based on crest displacement. Generally speaking, the toe stresses are smaller for models Nos. 1, 2 and 3, and larger for the models Nos. 4, 5 and 6, compared to that of the 45° slope. Thus, there are some indications that economic benefit might be obtained from using the shape of the modified models Nos. 1, 2, and 3.

3.5 The Investigation of Axisymmetric Geometry with Axisymmetric or Arbitrary Loading

To supplement the result from two-dimensional study, the finite element method as applied to axisymmetric geometry has been used (4, 5). The solutions of plane strain and of axisymmetric geometry with axisymmetric and arbitrary loadings are compared.

Three models with slope angles of 30°, 60°, and 90° were used for the axisymmetric study. The two-dimensional finite element model shown in Figure 1(b) becomes a section through a cylinder when the axisymmetric programs are used. The stress distributions around the slopes were determined, for $\mu = 0.25$ and $E = 7.03 \times 10^5 kg/cm^2 (10 \times 10^6$ psi) unless mentioned otherwise. The loading conditions were: first, with a gravitational stress only; second, in addition to gravity stress, axisymmetric horizontal boundary pressure, i.e., $p_r = p_t$; third, with only uniaxial radial (p_r) or tangential pressure (p_t). The details regarding the loading conditions are included in Table 1. The magnitudes of p_r and p_t were also varied from 27 to 243 kg/cm^2, i.e., one-third to three times the gravity stress S_v at the toe of the slope.

3.5.1 Horizontal Stresses along Sections under the Toe and behind the Crest

The horizontal stresses along two sections, one under the toe and the other behind the crest, were examined.

Figures 29, 30 and 31 are the plots of horizontal stresses along a horizontal section under the toe for axisymmetric loading of K = 1/3, 1 and 3. Figures 32, 33 and 34 are similar plots but for the vertical section behind the toe. Comparing Figures 29 and 32 with Figures 12 and 15, the stress patterns are seen to be almost identical for plane strain and axisymmetric solutions in a gravity stress field. With the addition of residual horizontal stresses, as expected the horizontal stresses under the toe are increased; but the magnitudes of these horizontal stresses are smaller than those of the plane strain solutions. For K = 1, the stress concentration factors under the toe are approximately 1.2, 1.9 and 2.0, respectively, for slope models of 30°, 60° and 90°, as compared with factors of 1.7, 3.2, and 3.8 for the same

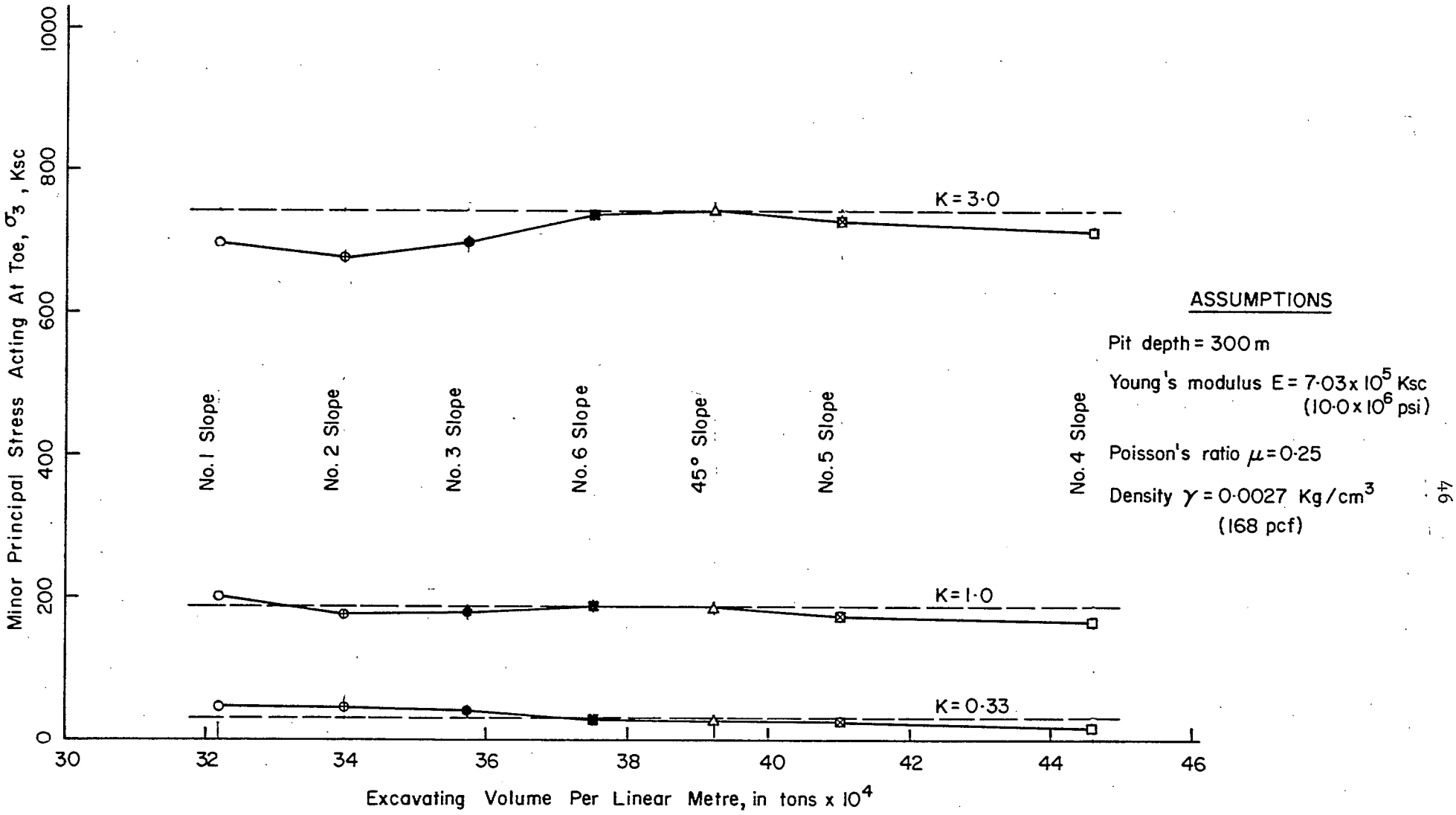

Figure 28. Compressive principal stresses near the toe as a function of excavating volume.

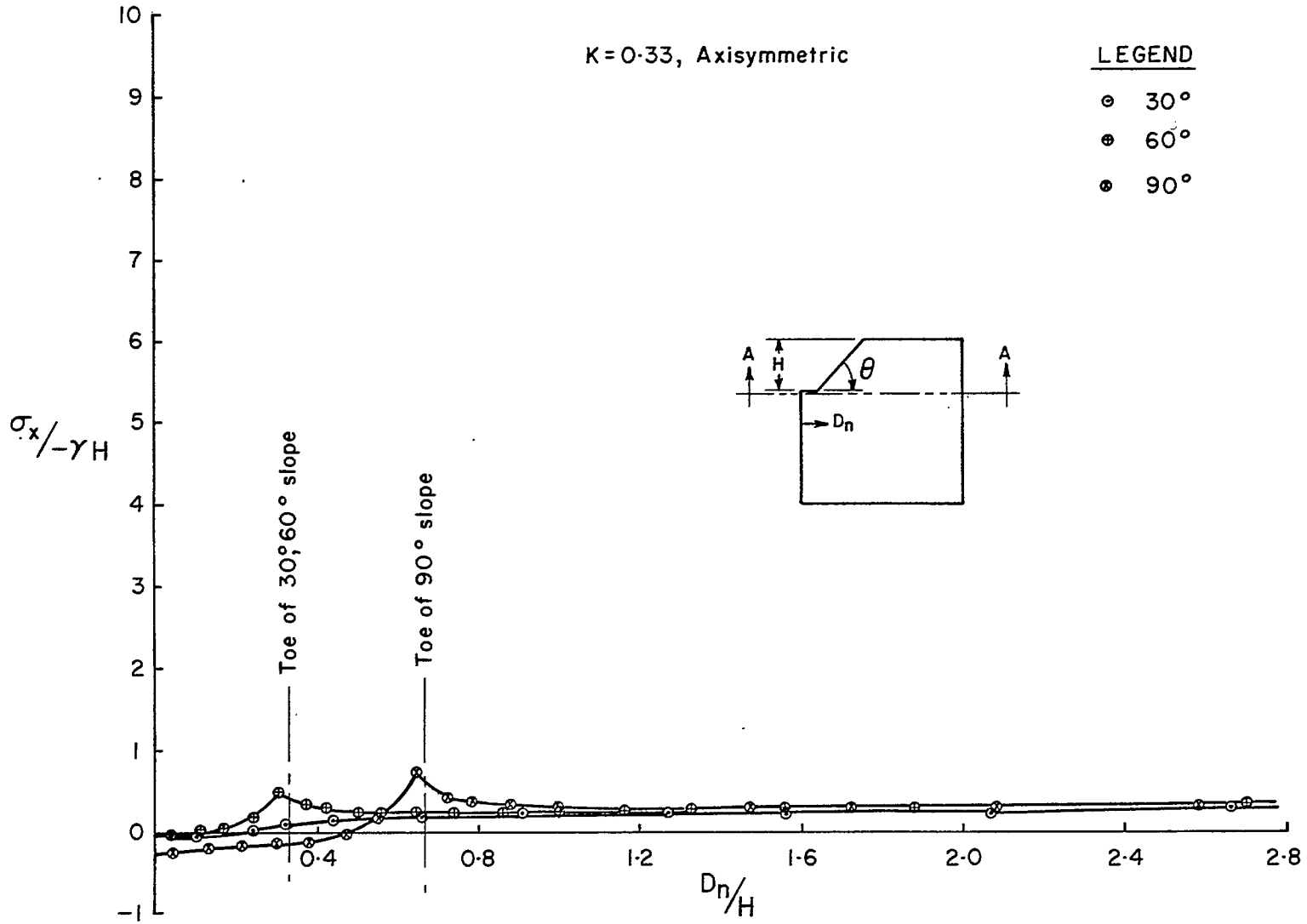

Figure 29. Comparison of horizontal stresses along a horizontal section below the toe for various slope angles; axisymmetric geometry and loading, K = 1/3.

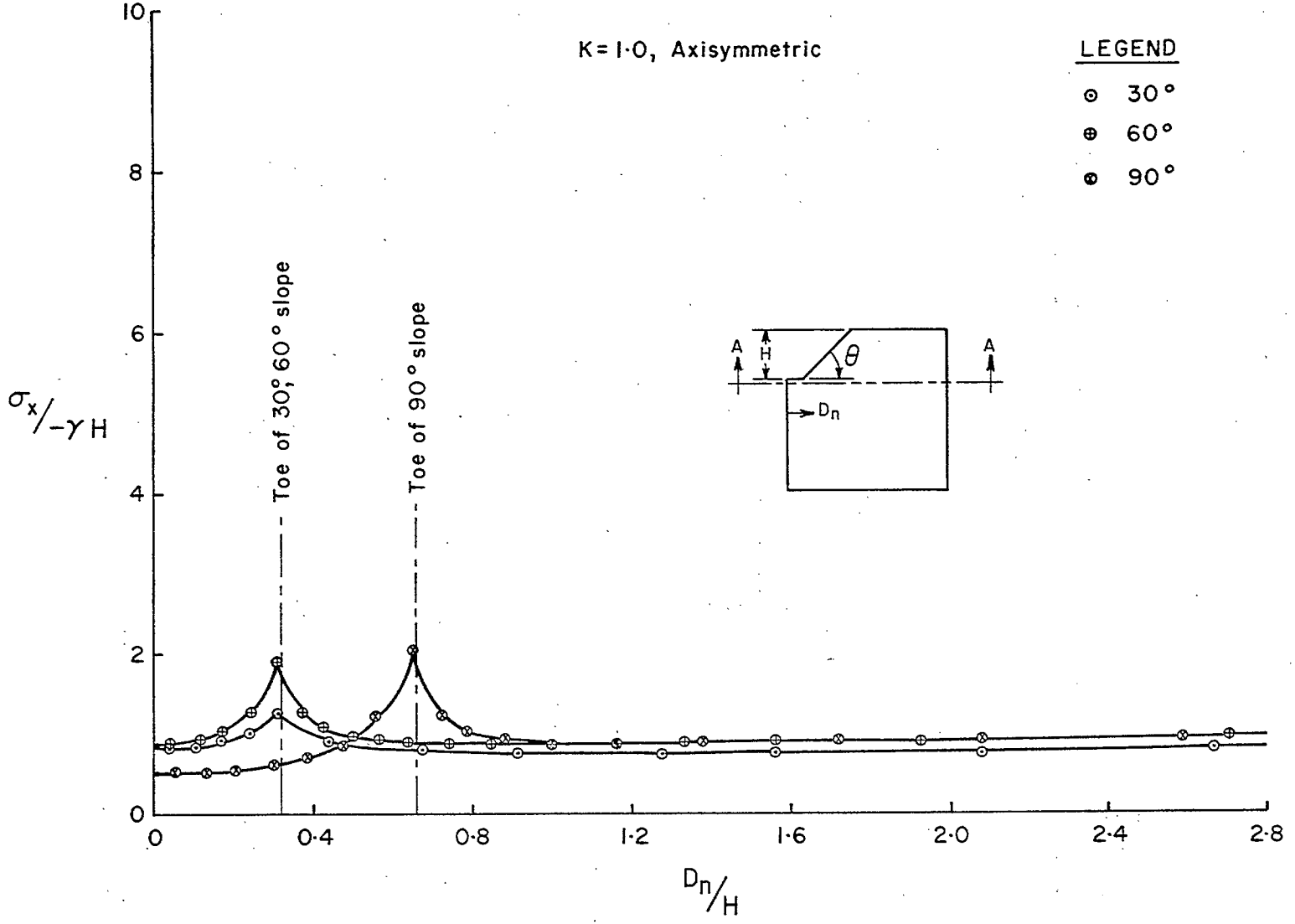

Figure 30. Comparison of horizontal stresses along a horizontal section below the toe for various slope angles; axisymmetric geometry and loading, K = 1.

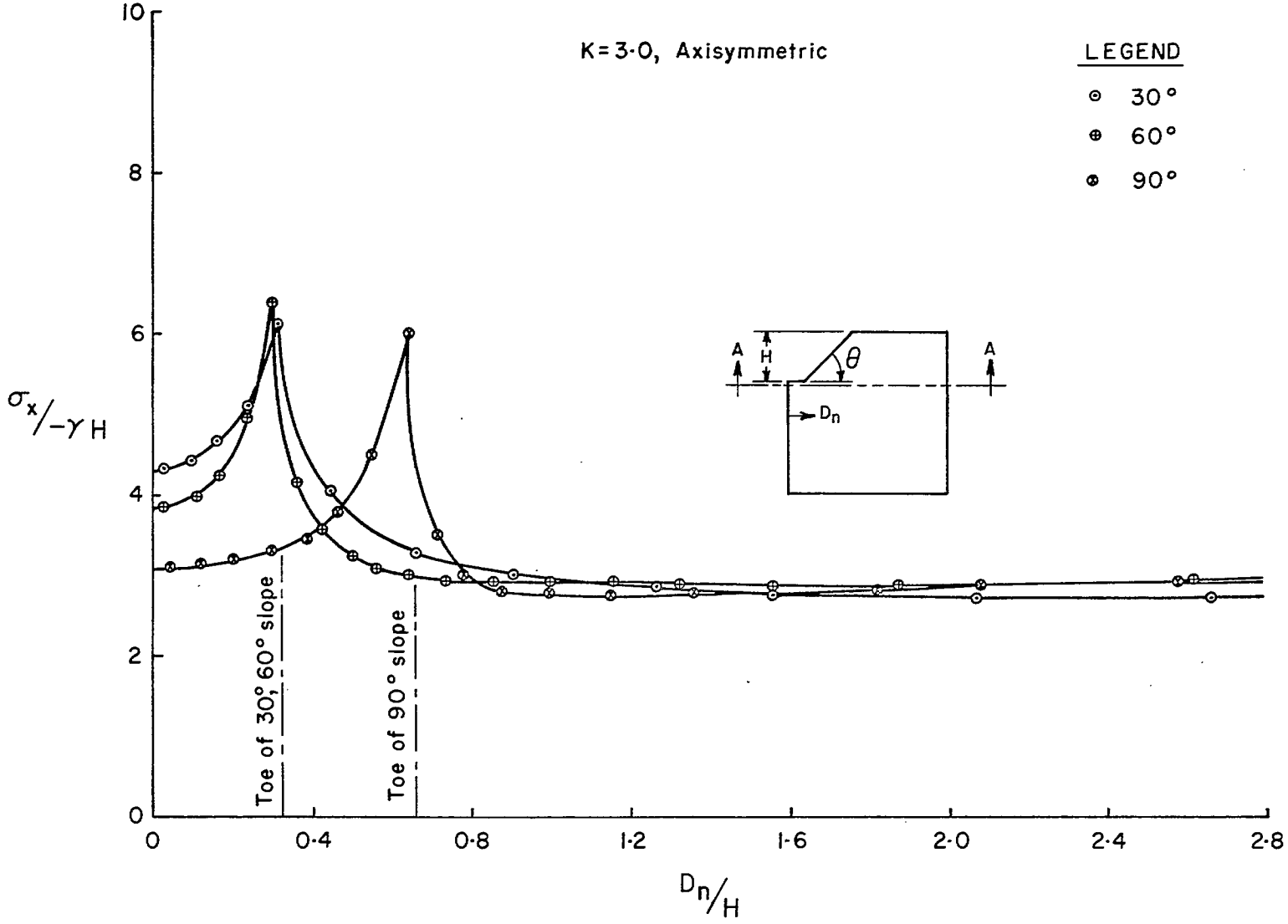

Figure 31. Comparison of horizontal stresses along a horizontal section below the toe for various slope angles; axisymmetric geometry and loading, K = 3.

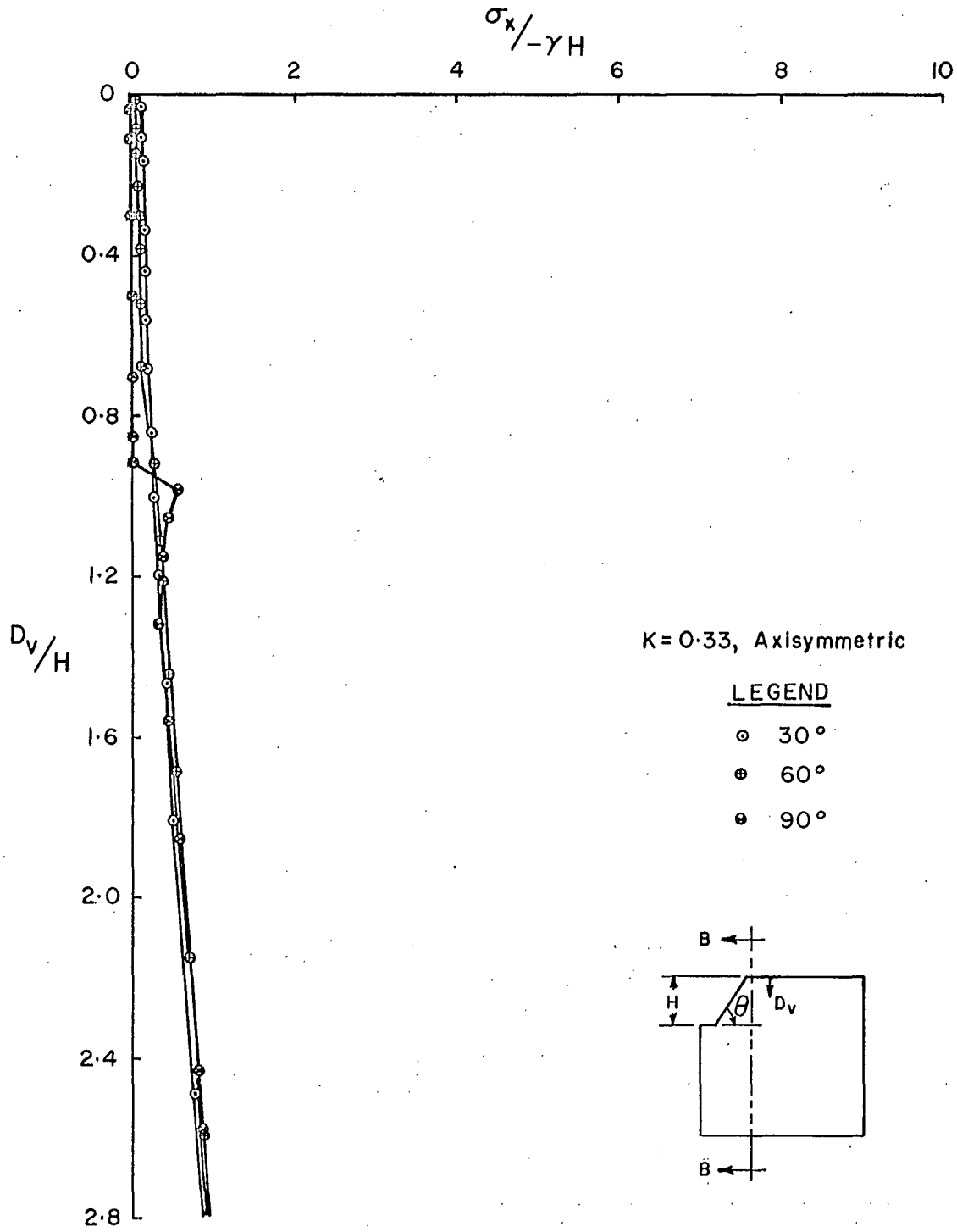

Figure 32. Comparison of horizontal stresses along a vertical section behind the crest for various slope angles; axisymmetric geometry and loading, K = 1/3.

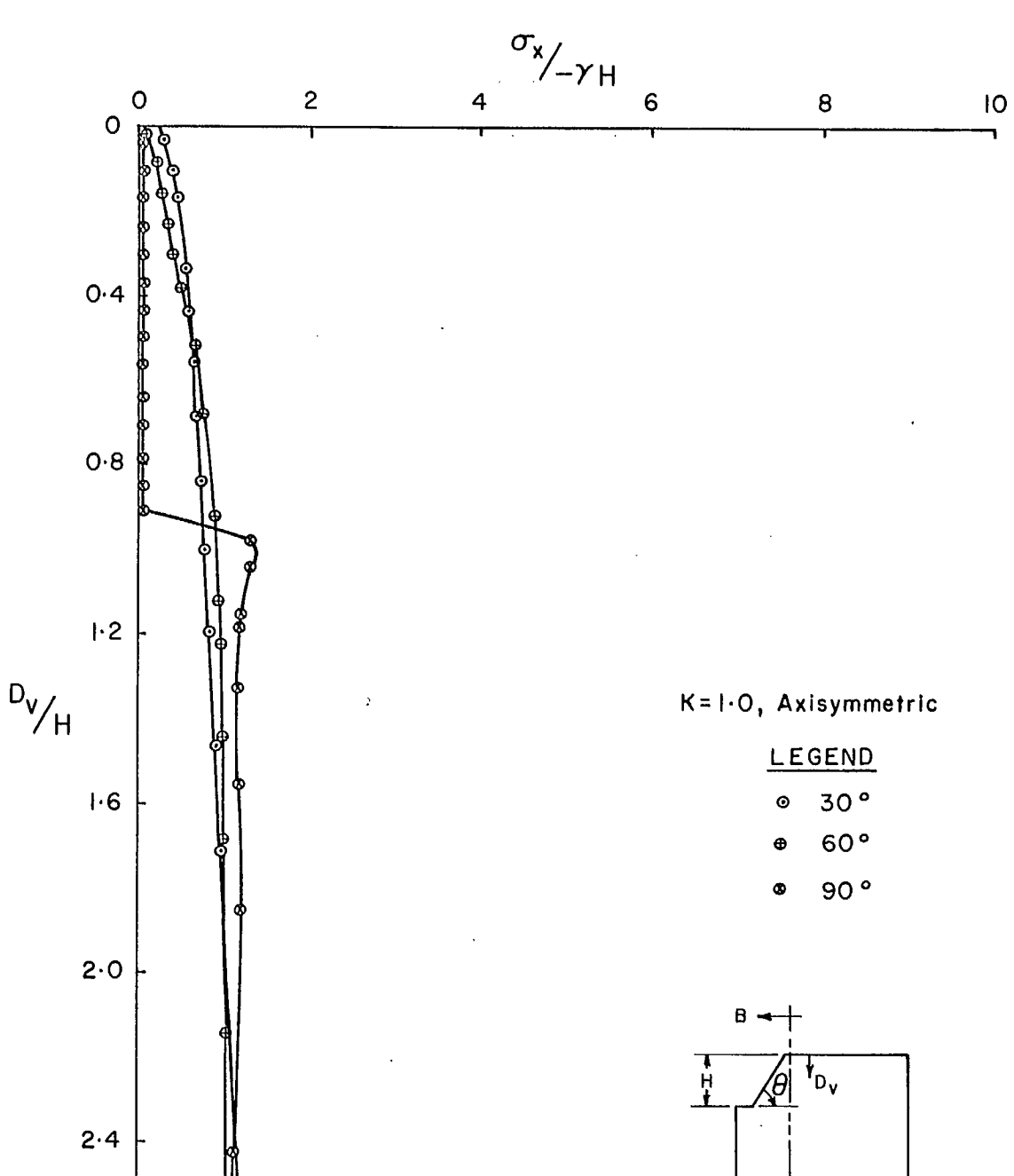

Figure 33. Comparison of horizontal stresses along a vertical section behind the crest for various slope angles; axisymmetric geometry and loading, K = 1.

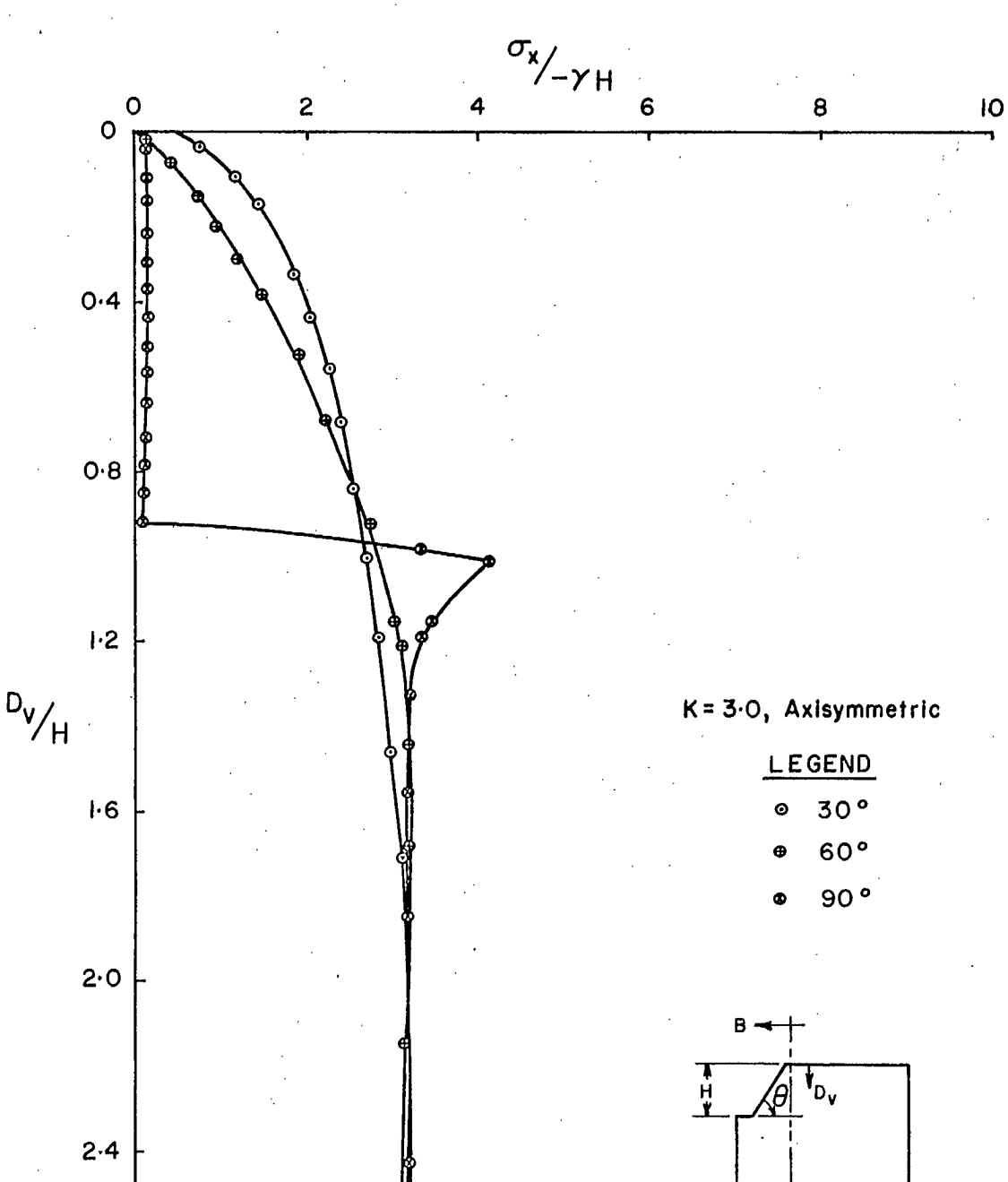

Figure 34. Comparison of horizontal stresses along a vertical section behind the crest for various slope angles; axisymmetric geometry and loading, K = 3.

models with plane strain solutions. Similar results were observed for K = 3: the stress concentrations are approximately 6.1, 6.4, and 6.0 for axisymmetric solution as compared to that of 8.1, 12.2, and 12.6 for plane strain respectively for slope angles of 30^{o}, 60^{o} and 90^{o}. The results of two-dimensional and three-dimensional solutions can thus deviate by as much as 100% or more near the toe areas. In both cases, in a high horizontal stress field the horizontal stresses immediately under the toe are not affected much by the increase of slope angle.

Similar conclusions can be made for the horizontal stresses along the vertical section behind the toe for both plane strain and axisymmetric geometry as shown in Figures 32, 33 and 34.

3.5.2 Tangential Stresses along the Slope Walls

Figures 35 and 36 are the plots of tangential stress concentrations versus depth along the slope walls (actually the stresses are acting at a depth of 0.026H into the slope wall) respectively for 30^{o} and 90^{o} slopes. Plane strain solutions were replotted on the same graphs for comparison. Once again, it is clear that the solutions of plane strain and of axisymmetric geometry, under a gravity field, are almost identical (Figures 35(c) and 36(c)). The maximum tangential stress concentrations near the toe of the 30^{o} slope are 0.3 and 0.4 respectively for the plane strain and for the axisymmetric loading. For the vertical slope, it is 1.85 for axisymmetric loading versus 2.05 for plane strain.

With the introduction of tectonic stress, the tangential stresses along the slope wall of the 30^{o} slope, for both solutions, do not deviate much over a large portion of the slope face, as shown in Figure 35. Near the toe, differences occur; the stress concentrations are 1.2 and 4.9 for axisymmetric analysis as compared to those of 1.5 and 6.6 for plane strain respectively for loadings of K = 1 and 3.

For the vertical slope, the tangential stresses for plane strain are higher than those from the axisymmetric solution over approximately the lower third of the slope. Near the toe, the tangential stress concentrations are 2.5 and 3.5 for the axisymmetric analysis, and 3.9 and 8.8 for plane strain for K = 1 and 3 respectively.

Only the 60^{o} slope model was used to examine the effect of non-axisymmetric loading on the stress and displacement distributions around excavations. The residual horizontal stress was applied either in the radial direction (r) or in the tangential direction (t) with magnitudes of: 27 kg/cm^2 (K = 1/3), 81 kg/cm^2 (K = 1), and 243 kg/cm^2 (K = 3).

Figure 37 is a composite plot of tangential stresses along the wall of a 60^{o} slope for a variety of loading conditions (refer to Table 1, Cases 37 to 42). Plane strain and axisymmetric solutions with either axisymmetric or arbitrary loadings were compared. Under non-axisymmetric loading, for the Cases 37 (K = 1/3, P_r = 27 kg/cm^2, P_t = 0) and 38 (K = 1/3, P_r = 0, P_t = 27 kg/cm^2), there is only a slight variation in tangential stress concentrations along a large portion of the slope wall when a low horizontal stress is applied, with the exceptions that the stress concentrations near the toe are 11% higher and 39% lower respectively for Case 37 and Case 38 as compared to that of the

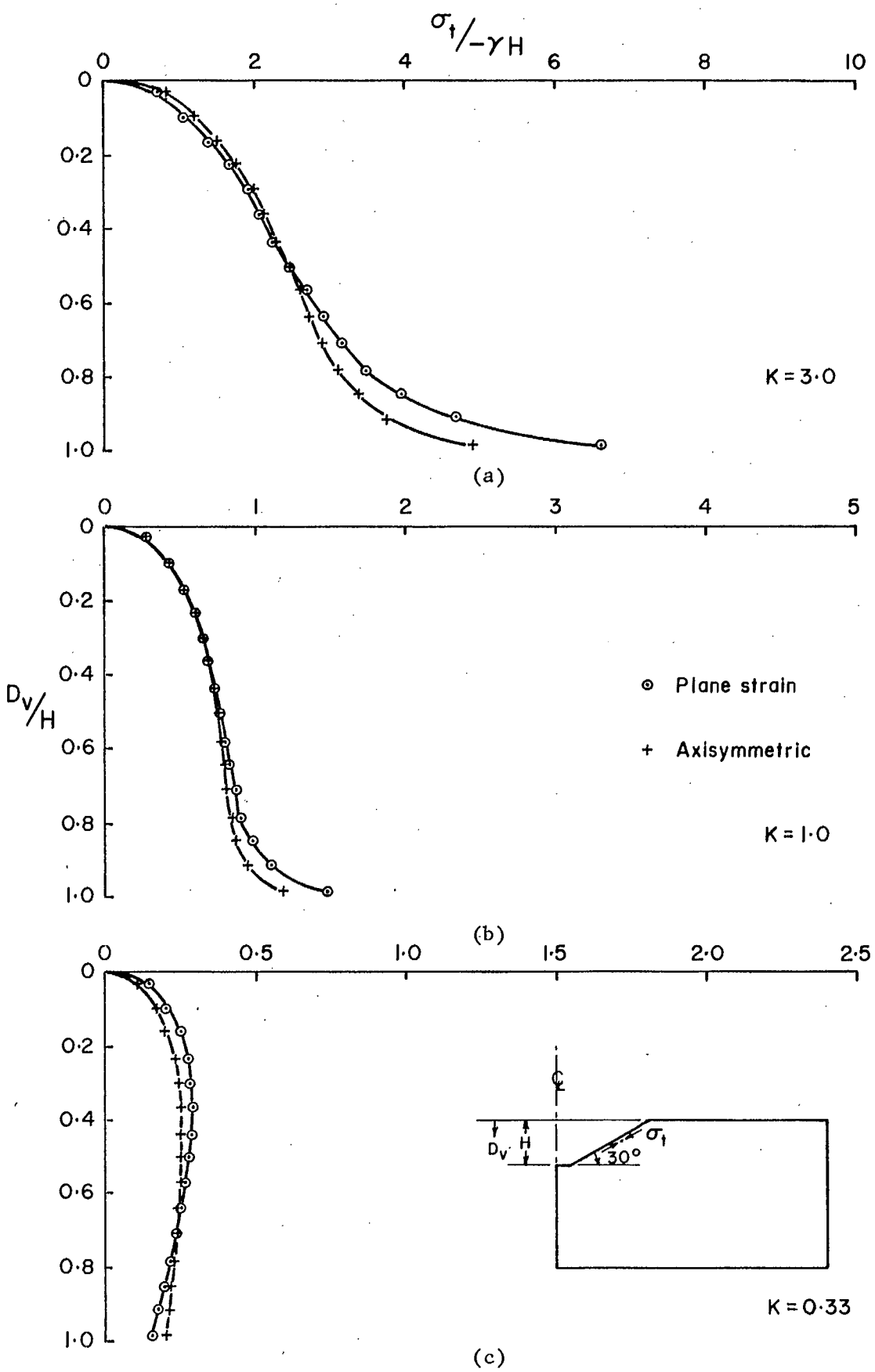

Figure 35. Comparison of tangential stresses along the slope wall of a 30° slope between solutions of plane strain and of axisymmetric geometry and loading.

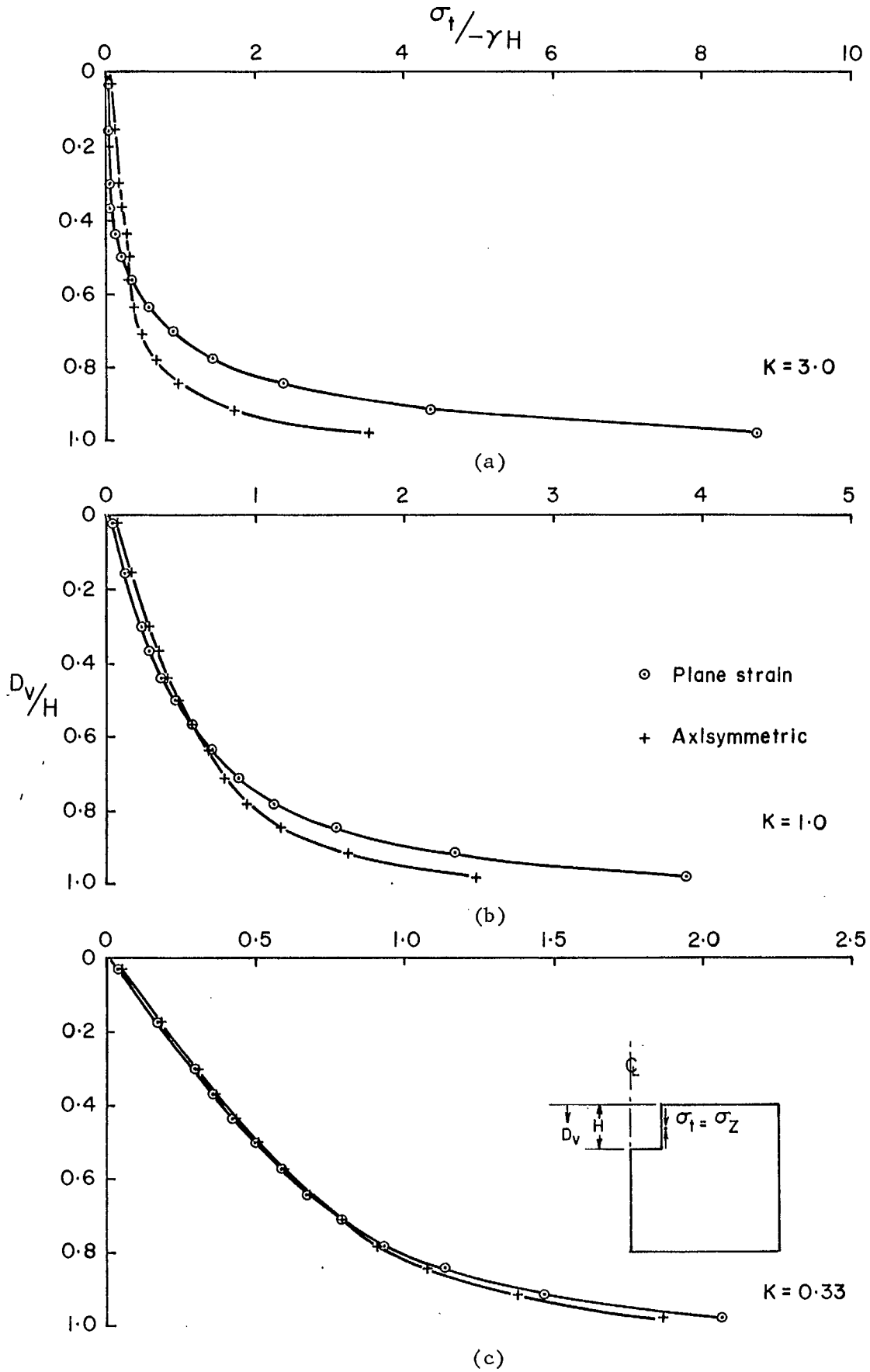

Figure 36. Comparison of tangential stresses along the slope wall of a vertical slope between solutions of plane strain and of axisymmetric geometry and loading.

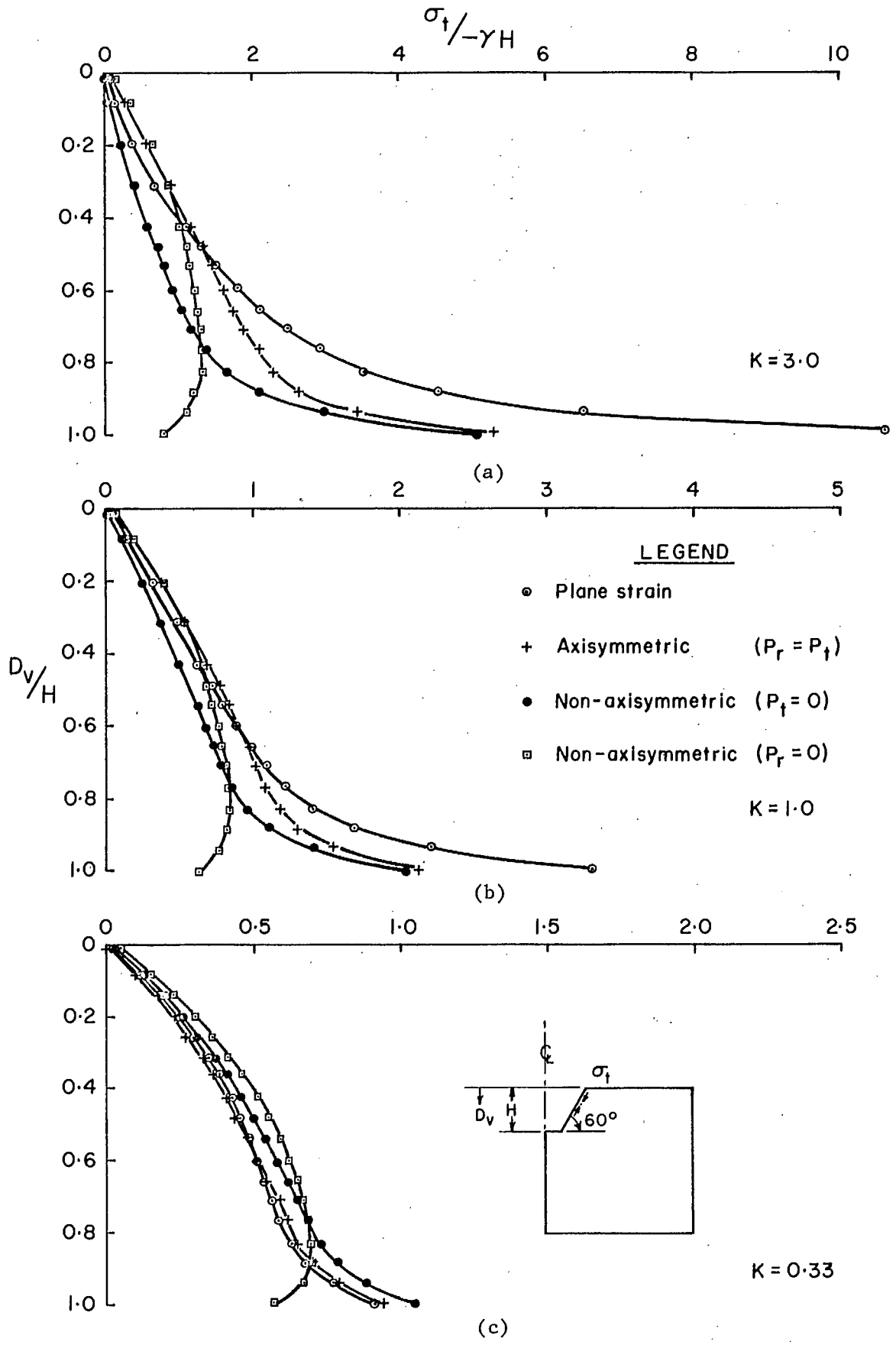

Figure 37. Comparison of tangential stresses along the slope wall of a 60° slope between solutions of plane strain and of axisymmetric geometry with arbitrary loading.

axisymmetric loading (Case 34), as shown in Figure 37(c). Again the plane strain solution (Case 1) is identical to that of the axisymmetric solution (Case 34).

From Figure 37 it is clear that the deviations between the different solutions become more pronounced with increases in the residual horizontal stress. For instance, the stress concentration near the toe for plane strain can be approximately 50% and 100% higher respectively for K = 1 and K = 3 compared to that of the corresponding axisymmetric loading (Cases 35 and 36). But under non-axisymmetric loading, the stresses at the toe are 72% and 85% lower respectively for the Cases 40 ($K = 1$, $P_r = 0$, $P_t = 81$ kg/cm^2) and 42 ($K = 3$, $P_r = 0$, $P_t = 243$ kg/cm^2), compared to that of the corresponding axisymmetric loading (Cases 35 and 36). For the Cases 39 ($K = 1$, $P_r = 81$ kg/cm^2, $P_t = 0$) and 41 ($K = 3$, $P_r = 243$ kg/cm^2, $P_t = 0$), the differences in stresses near the toe are very small compared to that of the corresponding axisymmetric loading cases. In other words, when an open-pit mine is under a uniaxial horizontal stress field, the stress concentrations near the toe area in a cross section perpendicular to the direction of the residual horizontal stress would be much lower than would be expected for the cross section parallel to the direction of the residual stress.

3.5.3 Minor Principal (Largest Compressive) Stresses near the Toe

Figure 38 shows the stress concentrations of the minor principal stress near the toe as a function of the parameter K. It is clear that the stress concentration of the minor principal stress under any assumptions, i.e. plane strain, axisymmetric or non-axisymmetric loading, is approximately proportional to K.

Again, the stress concentrations of the minor principal stress deviate little between the plane strain and axisymmetric solution in a gravity stress field. However, the stress concentration can be 100% higher or more for plane strain compared to axisymmetric geometry when a high horizontal stress field is encountered, e.g., K = 3. The stress concentration for axisymmetric geometry depends on the orientation of the compressive principal horizontal stress. For instance, when the compressive principal stress is acting at a direction of 90° to the rz-plane ($P_r = 0$, $P_t \neq 0$), the stress concentration increases very slightly as K increases as shown by curve 4 in Figure 38; under K = 3, the stress concentration is only 1/12 of that for plane strain.

Figure 39 shows a plot of minor principal (largest compressive) stresses near the toe as a function of slope angle for both plane strain and axisymmetric solutions. The results for plane strain have been already discussed in a previous section. Once again, the axisymmetric solution is identical to that of the plane strain under only gravity stress. As shown in Figure 39, the deviations between the two solutions become wider as K increases. Generally speaking, the stress concentrations near the toe increase with the increase of slope angles, except for the case of K = 3, for which the stresses remain approximately equal when the slope angle is increased from 60° to 90°.

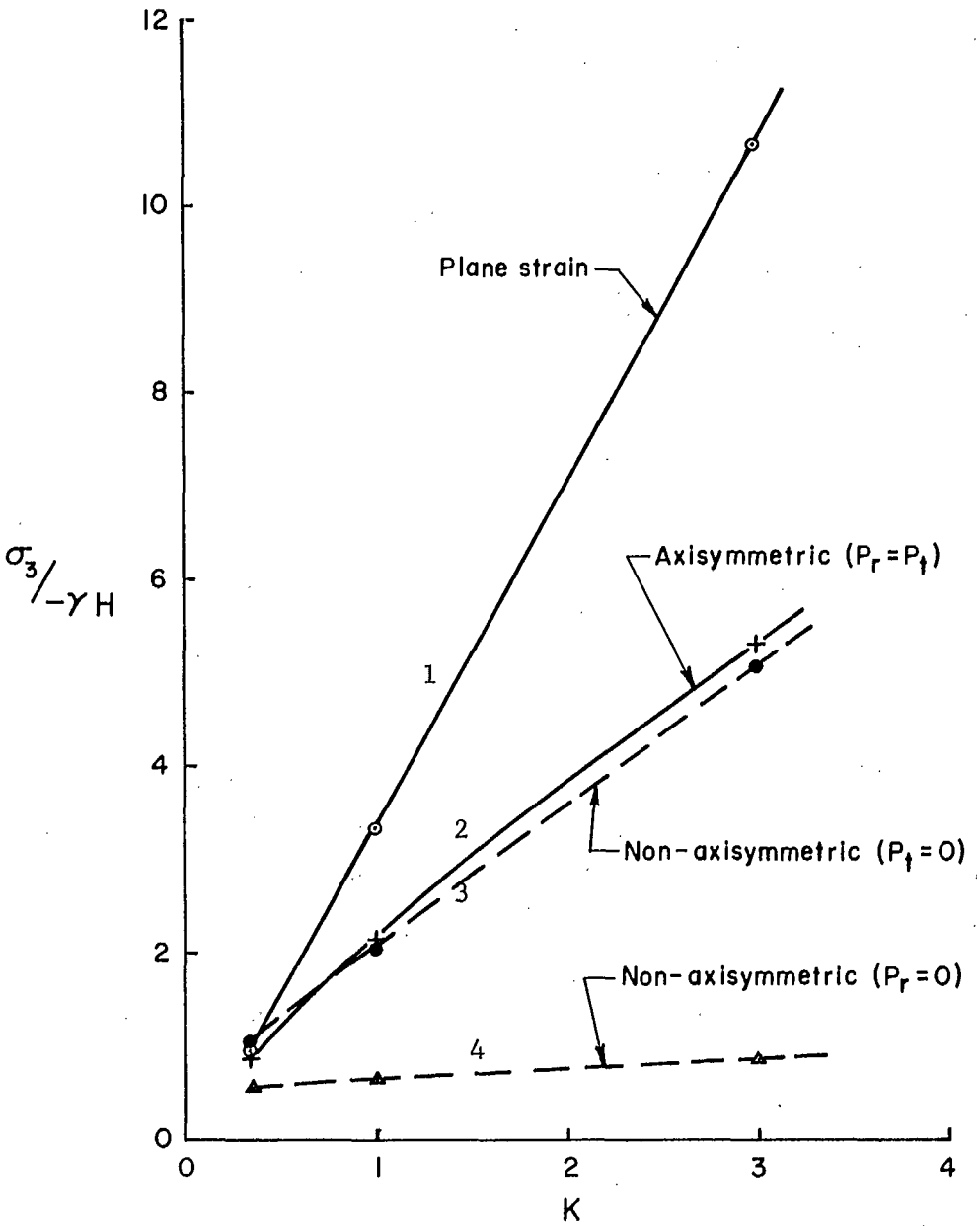

Figure 38. Comparison of minor principal (largest compressive) stresses near the toe of a 60^{o} slope between the solutions of plane strain and of axisymmetric geometry with arbitrary loading.

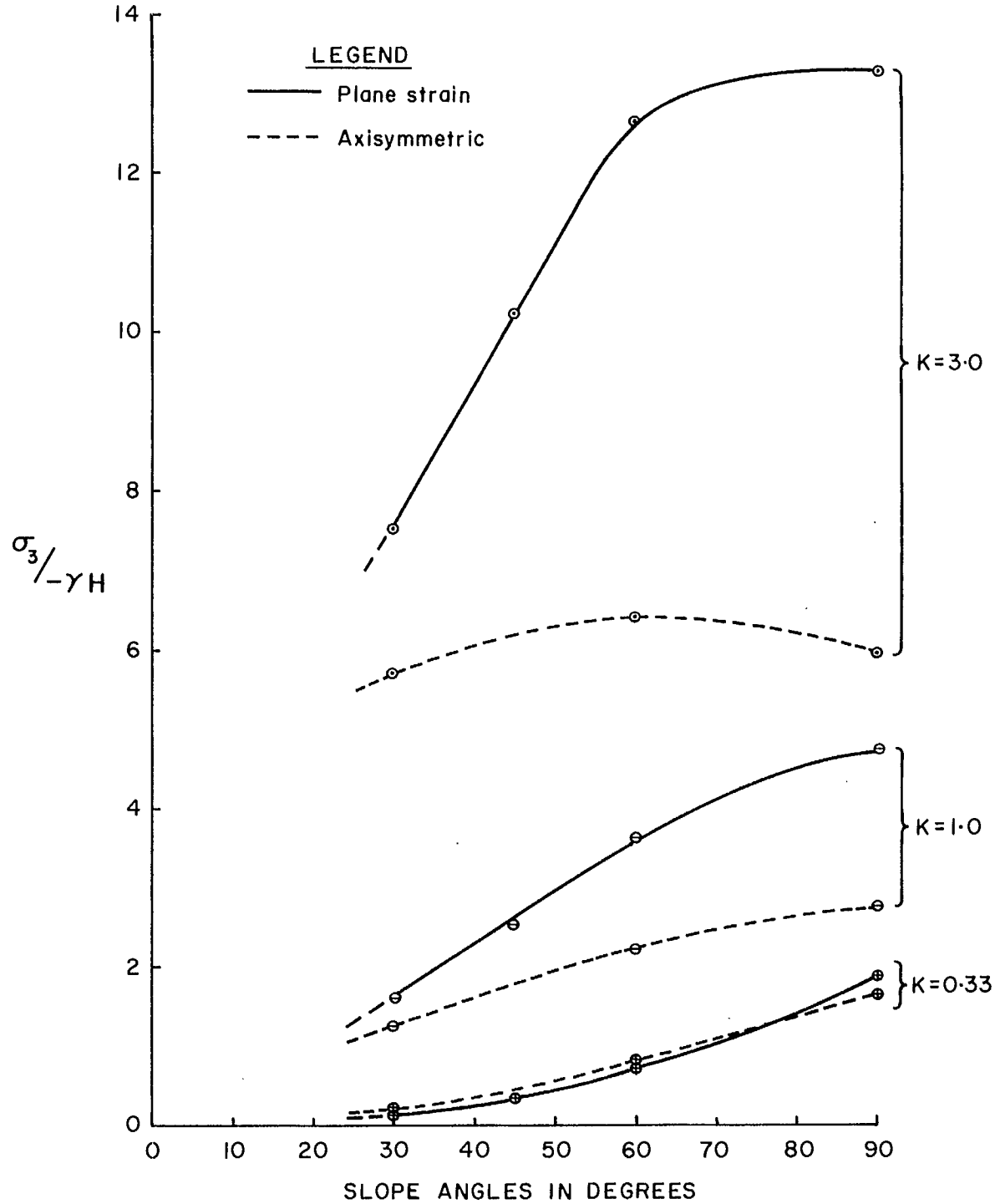

Figure 39. Comparison of minor principal stresses near the toe of various slope angles between the solutions of plane strain and of axisymmetric geometry and loading.

3.5.4 Circumferential Stress Along the Slope Face

Figures 40 and 41 show the circumferential stresses acting at the toe and at the crest as a function of K respectively. For both cases, the circumferential stresses are proportional to K. All stresses are compressive under the axisymmetric loading $P_r = P_t$ (Cases 34, 35, 36) and in the selected plane under non-axisymmetric loading $P_r = 0$ (Cases 38, 40, and 42), but the circumferential stresses become tensile in the selected plane for the non-axisymmetric loading $P_t = 0$ (Cases 37, 39, and 41).

Figure 42 is a composite plot of circumferential stresses for a variety of loadings, which indicates that the largest magnitudes either tension or compression occur at about one-third of the slope height up from the toe. The stresses are tension for the Cases 37, 39, and 41, which are under non-axisymmetric loading with $P_t = 0$ and $P_r = 27$, 81, and 243 respectively. Relaxation of surface rock, either by tension fractures or other means, was simulated by reducing the modulus of deformation of the layer of elements adjacent to the slope face; this reduced the maximum stresses as shown in Figure 42. The effect of circumferential stress on the stability is not well known, but it can be stated that compressive stress would be favourable for stability and tensile stresses would be unfavourable.

3.5.5 Excavation Displacement at the Crest

Figure 43 is a plot of the horizontal excavation displacement normalized by dividing the displacement by the slope height (H) at the crest of a 60° slope as a function of the parameter K. The results indicate that the displacement for plane strain is greater than the axisymmetric cases except under gravity stress. For instance, the excavation displacement at the crest for plane strain is 3.03 and 3.44 times higher than that of the axisymmetric loading solution respectively for K = 1 and K = 3. Under a gravity stress field, the displacement at the crest in plane strain is directed toward the wall; the movement is negligible for the axisymmetric geometry. Under non-axisymmetric loading, the displacement at the crest in the direction of the residual horizontal stress did not deviate much from that of the axisymmetric loading as shown by the curves 2 and 3; but the horizontal movement in the direction at 90° to the residual horizontal stress is directed into the wall instead of toward the opening as curve 4 indicates.

Figure 44 is a plot of excavation displacement at the slope crest as a function of slope angle for a variety of loadings. Only solutions of plane strain and axisymmetric loading are compared. When an open-pit mine is cut under gravity stress only, the displacement at the crest is generally directed into the walls, and the magnitudes of the movement (into the wall) decrease as the slope angle increases. With the addition of horizontal stress, the displacements are toward the opening and the magnitude of movement is approximately proportional to the slope angle. Also, in plane strain the displacements are greater than those for axisymmetric solutions for K = 1 and 3.

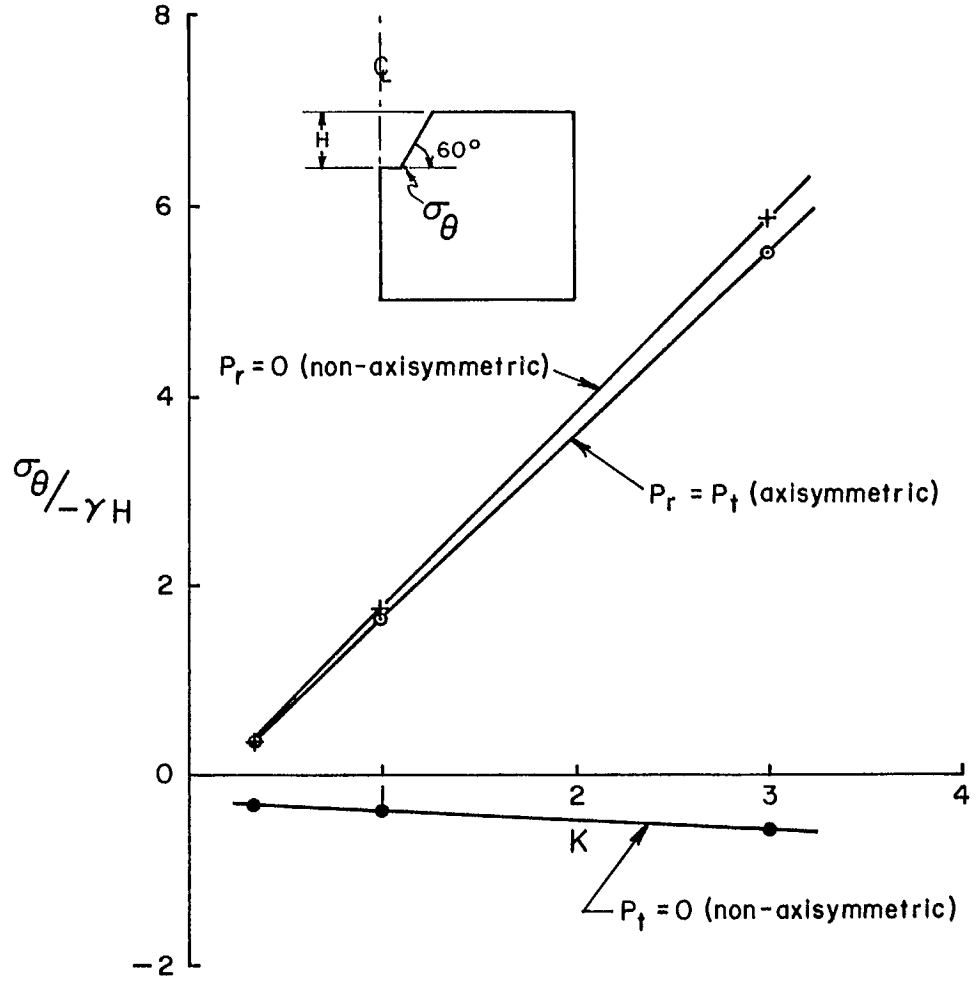

Figure 40. Circumferential stresses near the toe of a 60° slope for the solution of axisymmetric geometry with arbitrary loading.

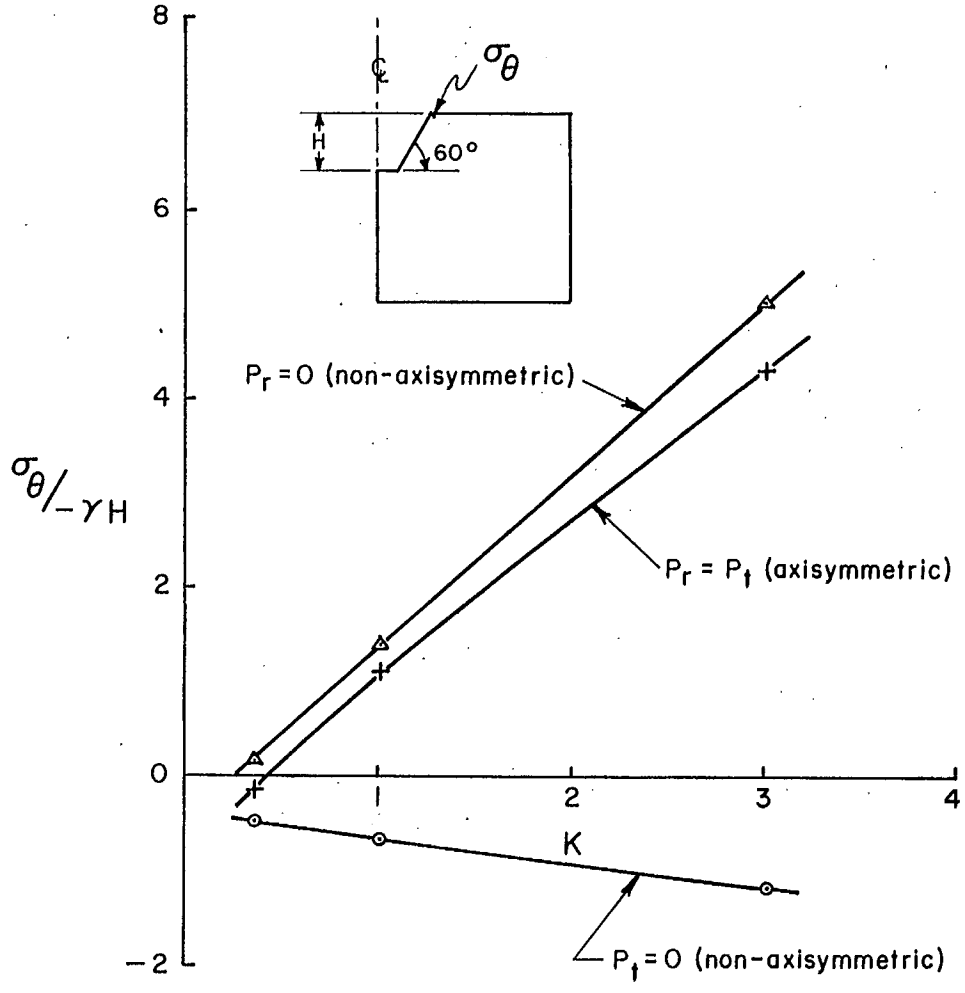

Figure 41. Circumferential stresses near the crest of a 60° slope for the solution of axisymmetric geometry with arbitrary loading.

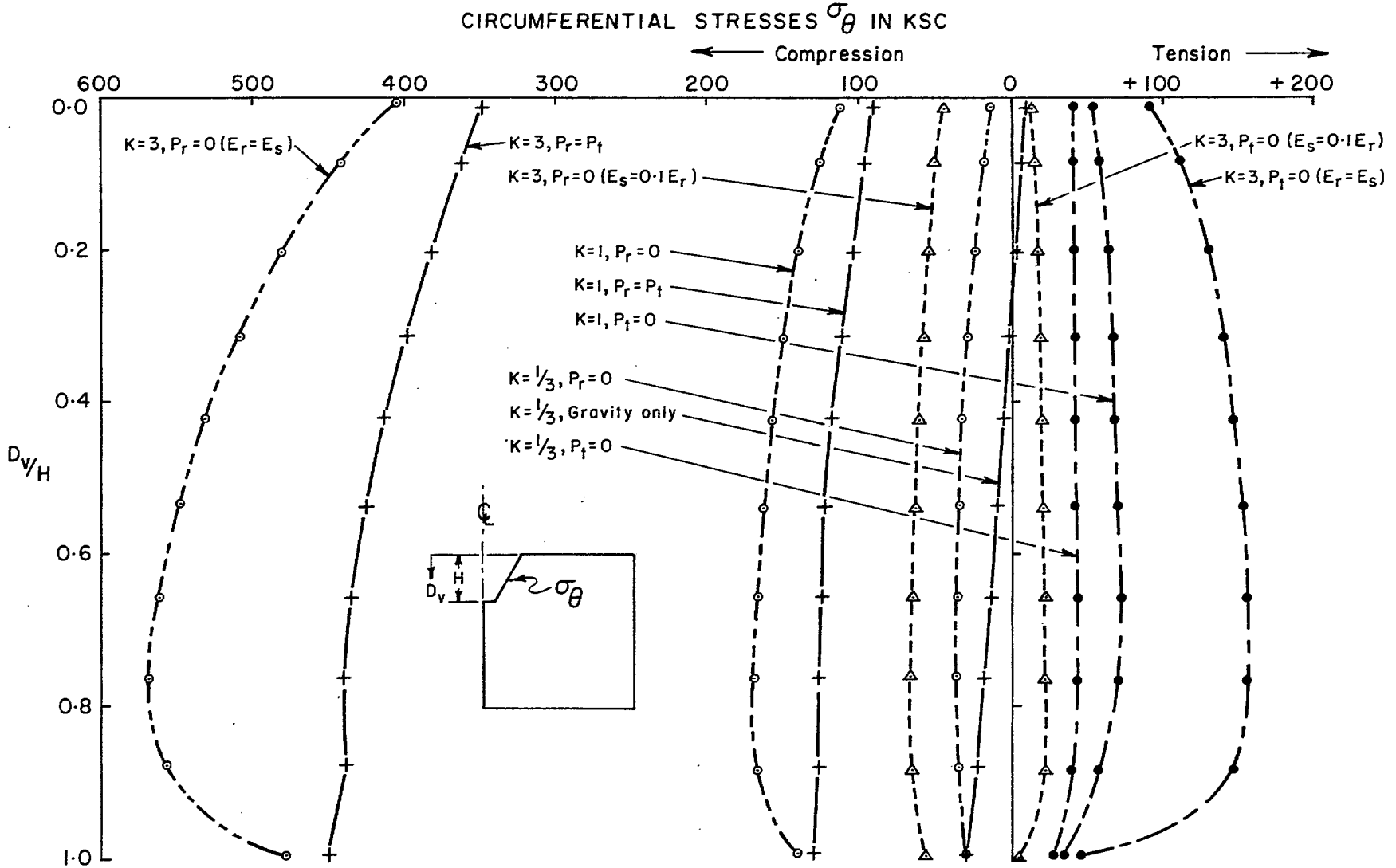

Figure 42. Circumferential stresses along the slope wall of a 60° slope for a variety of loading conditions.

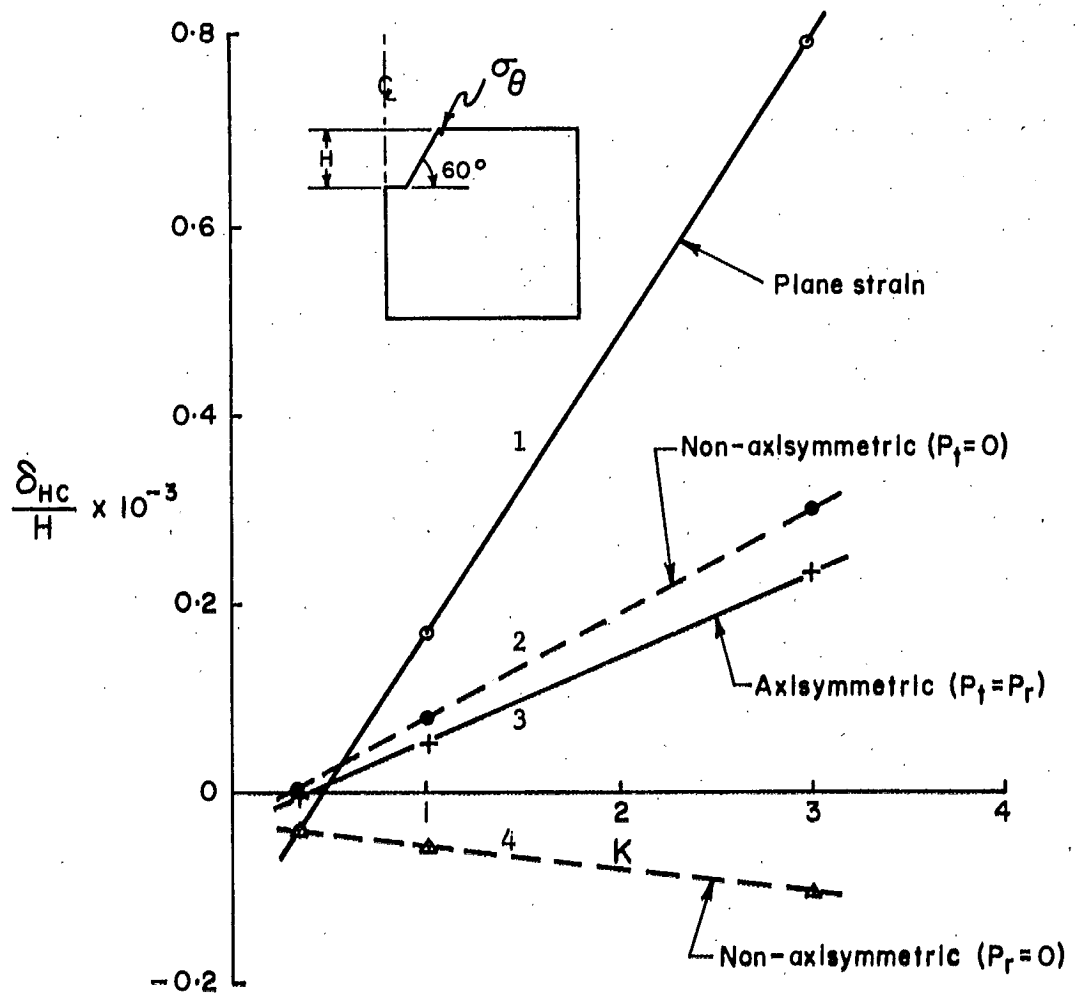

Figure 43. Comparison of excavation displacements of a 60° slope as a function of the parameter K between the solutions of plane strain and of the axisymmetric geometry with arbitrary loading.

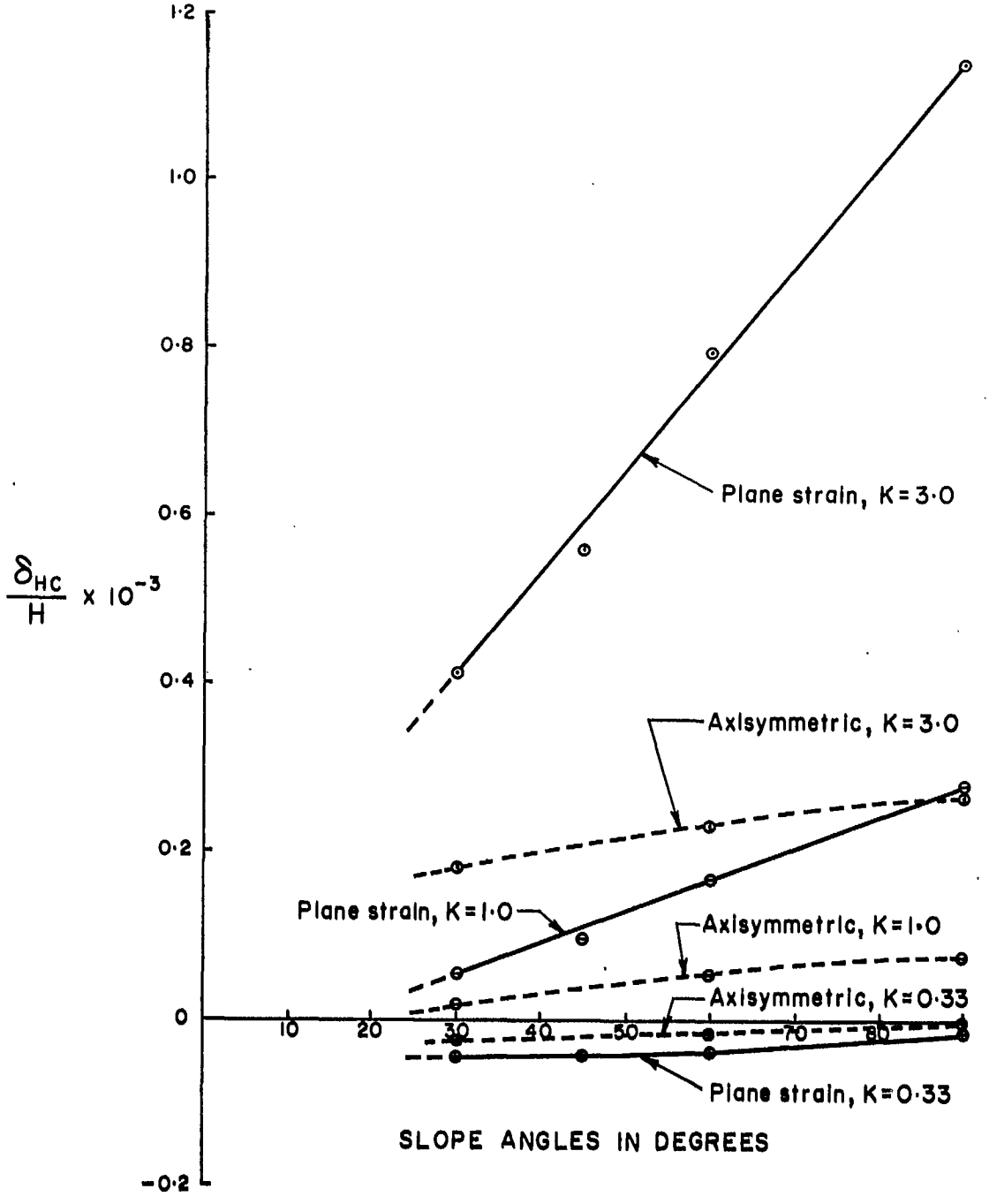

Figure 44. Comparison of excavation displacement as a function of slope angle between the solutions of plane strain and of the axisymmetric geometry with arbitrary loading.

3.6 The Development of Tensile Zones

It might be significant that tensile zones seem to be developed near the face of the pit walls in the section parallel to the direction of the maximum compressive horizontal field stress. This tensile zone was shown to penetrate into the wall about 70 metres (200 ft) at approximately the middle portion of the slope wall for K = 3. With K = 1, the tensile zone would penetrate approximately 30 metres (90 ft) into the walls. As shown in Figure 45, the penetration of this tensile zone into the pit wall seems to be proportional to the factor K.

The development of tensile zones in the t-direction (perpendicular to the uniaxial horizontal stress) is quite different. A large area of this cross-section around the toe and extended downward is in a state of tension with the highest concentrations near the boundary, as shown in Figure 46. This phenomenon seems to occur even under low uniaxial horizontal field stress (i.e. K = 1/3). By resorting to the classical solution for a sphere, it seems that tensile stresses could be developed but that they are very dependent on Poisson's ratio.

4. FRACTURE CRITERIA

The failure of materials differs according to their physical properties and the stress field to which they are subjected. It is not unreasonable to use the maximum principal stress theory for predicting tension fracture and Mohr's strength theory for predicting shear failure.

Tension fracturing of rock would occur on planes where the principal stress reaches the tensile strength of rock; however, with the presence of numerous joints and fissures, most rock masses are probably incapable of sustaining tensile stress.

The stress conditions at points around the 60° slope under several loading conditions were analysed for sliding conditions. In order to handle the numerous calculations of Mohr's circle, a computer program was developed; the output is in a form of numerical plot. If any Mohr's circle touches or cuts the assumed failure envelope, the symbol of a filled square (■) is plotted at that point along with the numerical value of the maximum shear stress. If a stress circle does not touch the envelope, a cross (+) is plotted, and the maximum shear stress is also printed.

By assuming the rock under investigation has values of 50 kg/cm^2 and 40° respectively for c and ϕ, the analysis based on the Mohr's strength theory indicated that a large area around the toe and near the pit bottom would be in a state of plastic equilibrium, as shown in Figure 47 for Cases 41 and 42. There is a slight difference in the zones of plastic equilibrium for the plane parallel to uniaxial horizontal stress, as shown by the dashed lines, and for the plane perpendicular to the uniaxial horizontal stress, as shown by the dotted line.

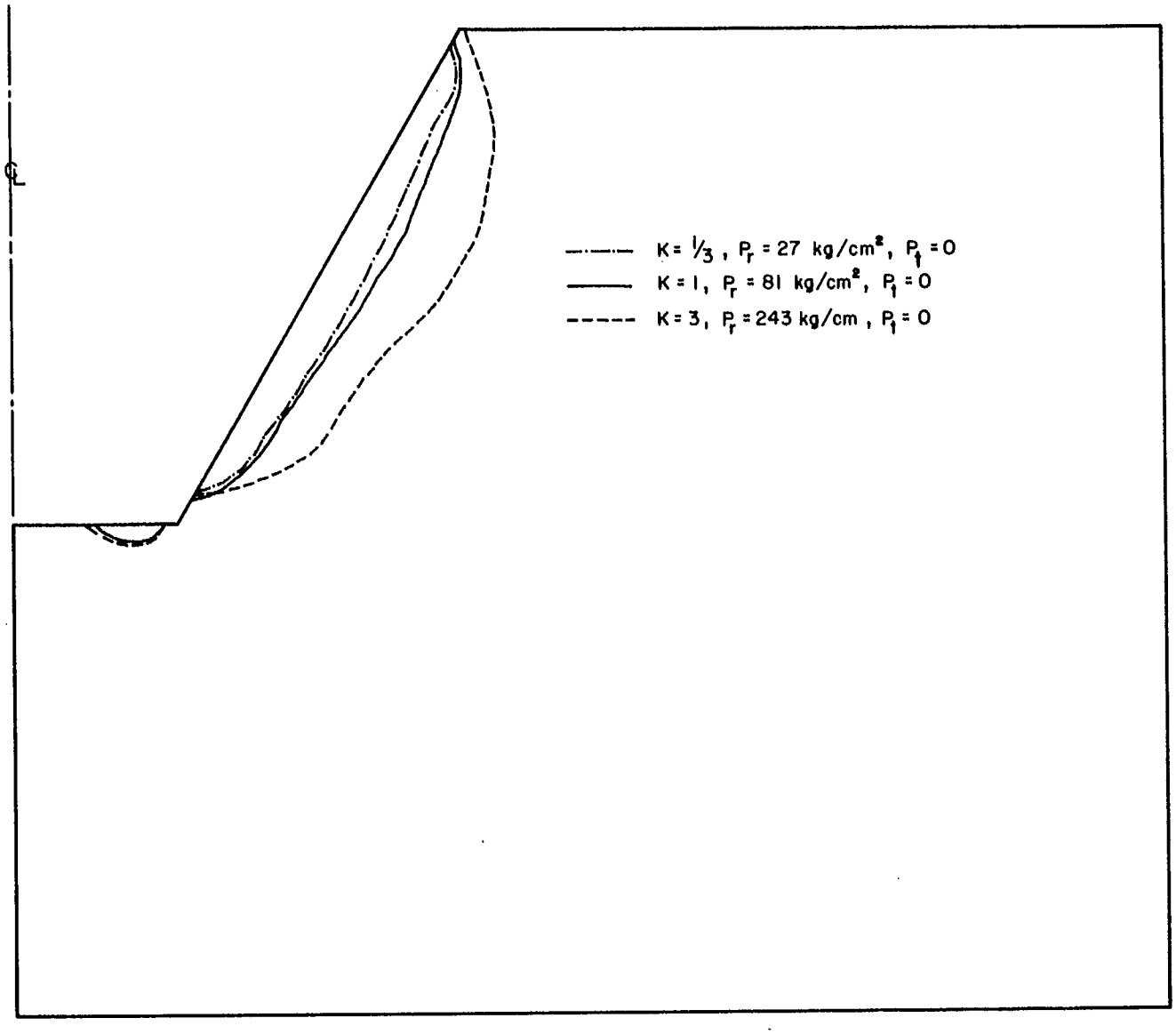

Figure 45. Development of tensile zones around a 60° slope under compressive horizontal field stress (P_r || to the rz plane, $P_t = 0$).

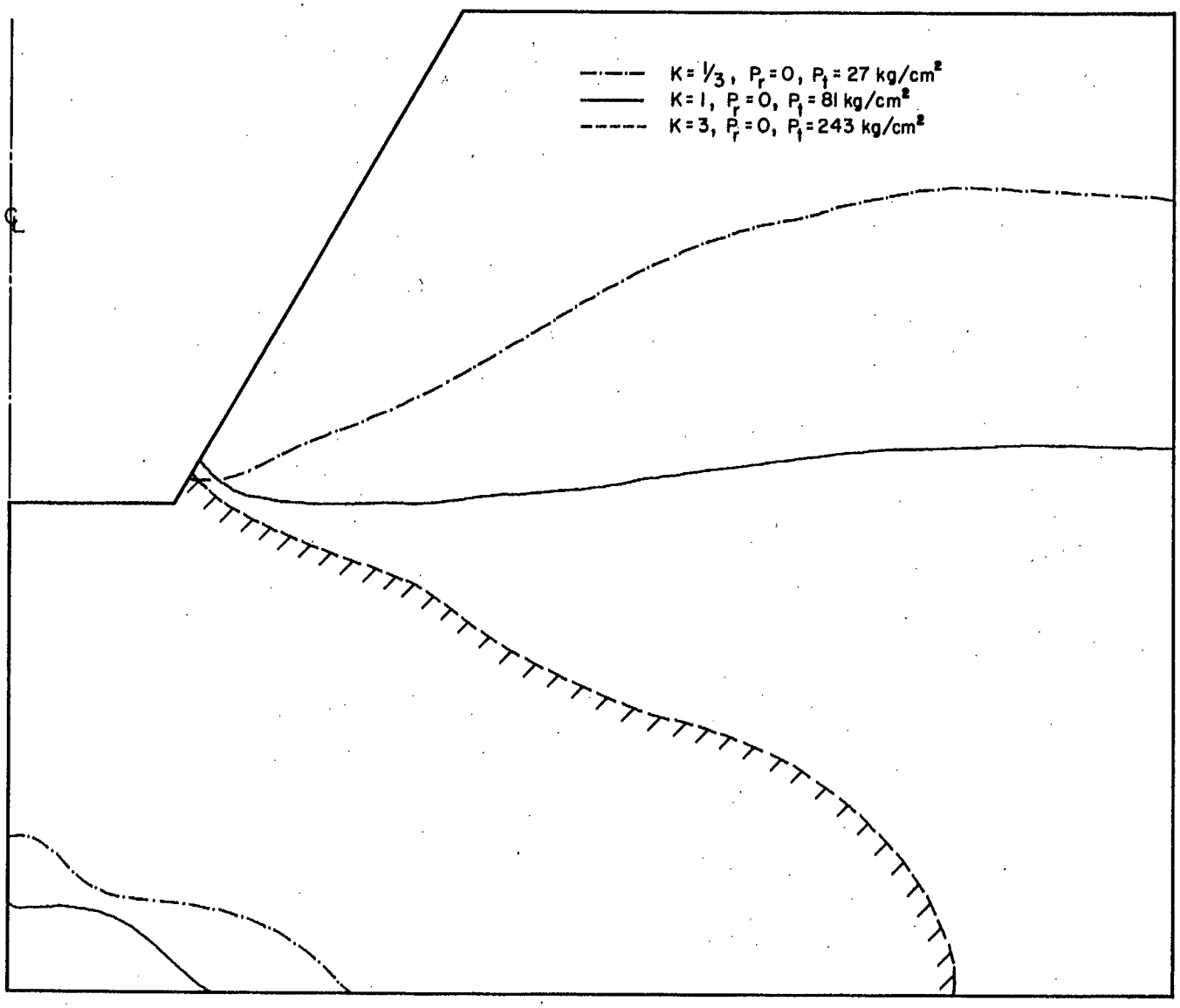

Figure 46. Development of tensile zones around a 60° slope under compressive horizontal field stress ($P_t \perp$ to the rz plane, $P_r = 0$).

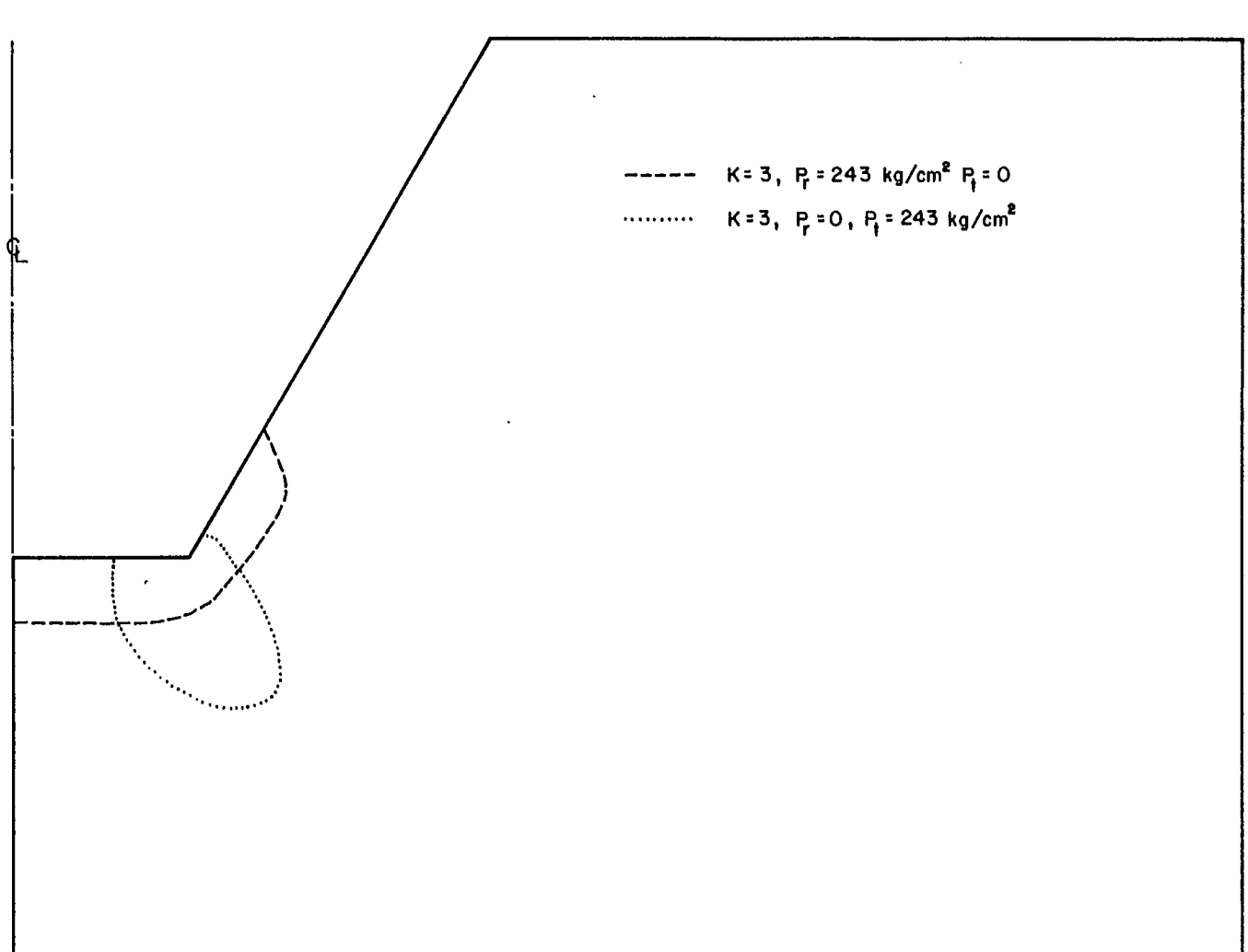

Figure 47. Potential failure zones around the toe of a 60^{o} slope under compressive horizontal field stress (based on Mohr's strength theory, c = 50 kg/cm^2, $\phi = 40^{o}$, E = 7.03 x 10^5 kg/cm^2, $\mu = 0.2$).

An alternate analysis was made to plot the contours of the ratio τ_{max}/σ_n, where τ_{max} is the maximum shear stress and σ_n is normal stress acting on the maximum shear plane. The contour lines of τ_{max}/σ_n might provide some information regarding potential zones of failure. These potential zones of failure are located around the toe, in the pit bottom, and along the pit walls. Figures 48 and 49 show that the zones with high ratios of τ_{max}/σ_n are also the areas where Mohr's circle touches or cuts the assumed failure envelope.

5. CONCLUSIONS

On the basis of the results presented herein, the following conclusions, concerning analysis of stresses and displacements around open-pit mines using the finite element method, have been drawn:

1. The finite element technique seems to be a very flexible and economical tool compared to any conventional model work for stress analysis with the complex geometry of open-pit mines. With this method, the inclusion of anisotropic properties does not unduly complicate the problem. In addition, arbitrary loadings can be readily analyzed.

2. If in an elastic, competent, and gravity-loaded rock mass, the mining of an open pit with slope angles up to 60° and a depth of 300 metres (900 ft) would not be expected to create large stresses around the opening. The presence of horizontal tectonic stresses could increase the expected stresses and displacements greatly.

3. The stresses and displacements depend to an important degree upon the initial state of stress. In a gravity stress field, the displacement along the slope face will be directed into the walls but, with the addition of residual horizontal stress, the displacement will be directed toward the opening. The movement at the pit floor can be either upward or downward depending on the initial stress field and Poisson's ratio of the rock mass. Furthermore, the stress and displacement patterns are affected by the orientation of the residual horizontal stresses. Therefore, a knowledge of the premining stress field is required to predict stresses and deformations.

4. The excavation displacements at the slope crest are approximately proportional to the factor K and to the slope angle. With an appropriate type of instrument, the magnitude of these movements or change in movement at or near the crest and along the slope face should be detectable. These measurements might be a valuable guide to the reactions occurring in the ground.

5. The initial result of geometry studies has been encouraging, since economic benefit could result by changing the slope configuration from conventional constant slope into a parabola-shaped slope, because there is no significant increase of stress in some of the modified slopes compared to the stresses in a typical 45° slope. On the contrary, the stresses developed in these modified slopes in some cases are even smaller. Therefore, these modified configurations of slopes seem to be favorable for the design of open-pit mines.

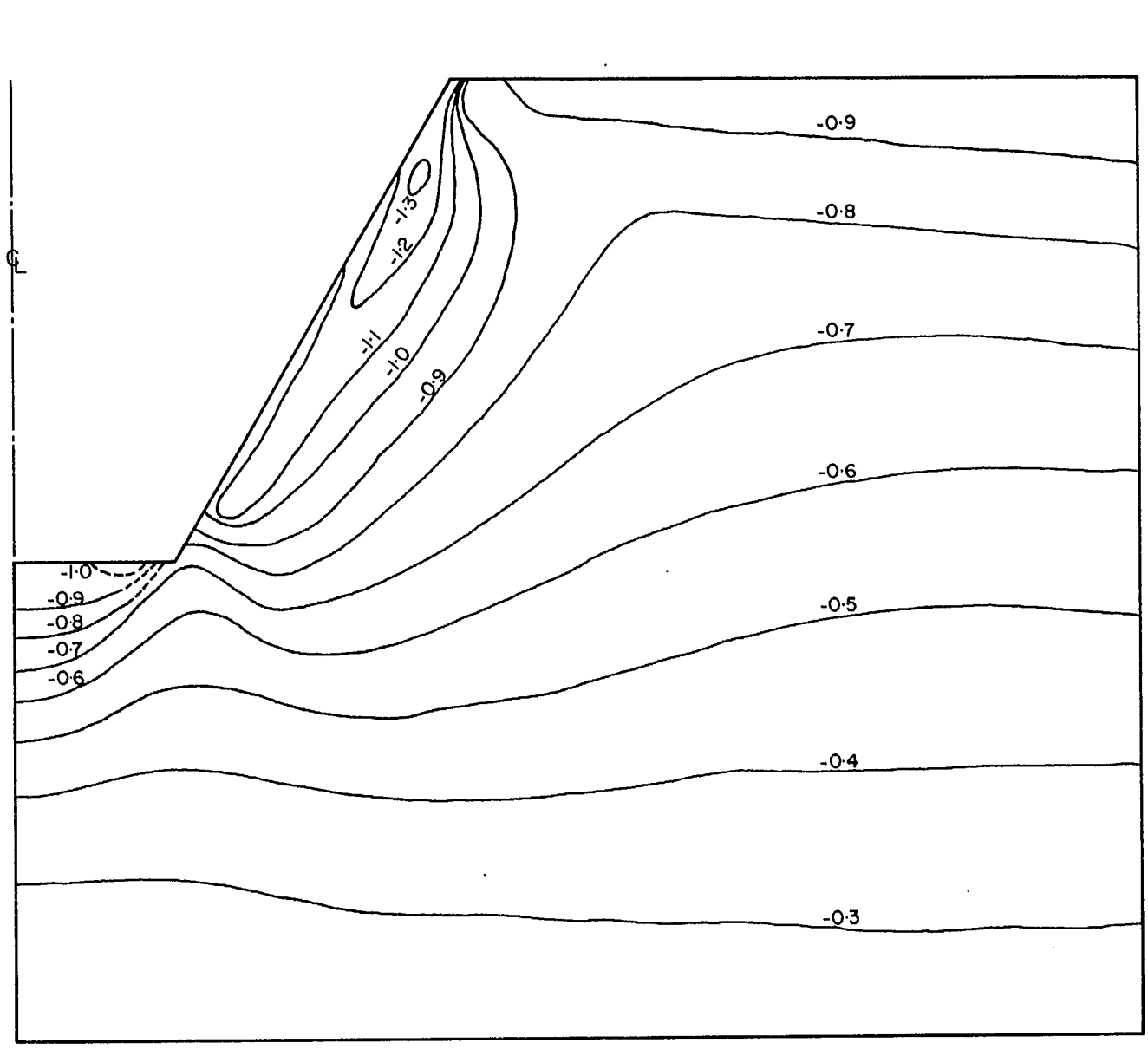

Figure 48. Contours of τ_{max}/σ_n around a 60° slope under unidirectional horizontal field stress. K = 3, P_r = 243 kg/cm^2, P_t = 0.

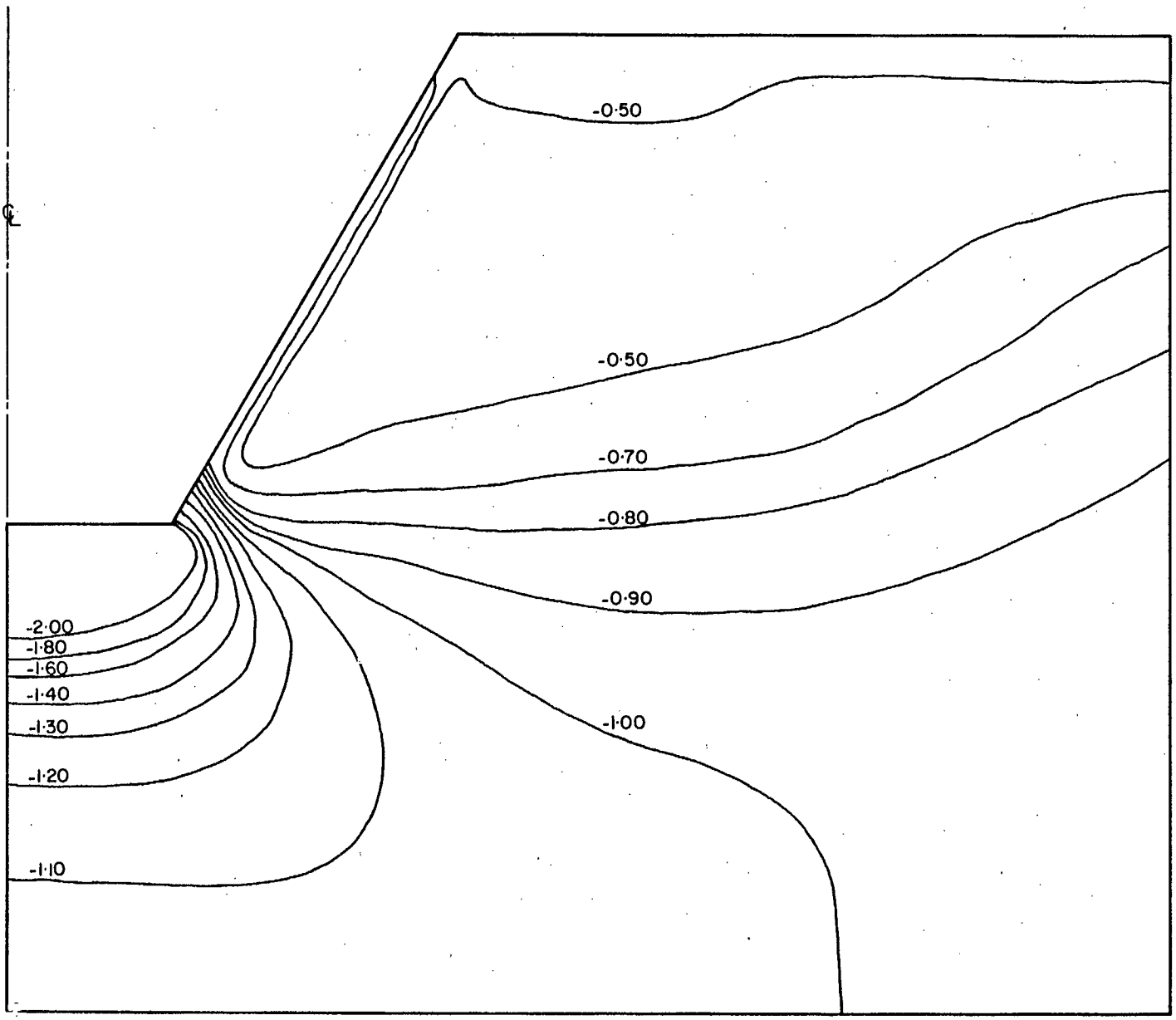

Figure 49. Contours of τ_{max}/σ_n around a 60^o slope under unidirectional horizontal field stress. K = 3, P_r = 0, P_t = 243 kg/cm^2.

6. Tensions seem to occur along the slope face under some loading conditions, particularly in axisymmetric models when loaded with uniaxial horizontal stresses. Evidence of tectonic stresses several times greater than the gravity stress, at depth, has been verified by measurements in several instances. Therefore, the development of such tension or expansion zones may actually occur and this would influence the slope stability as well as the use of artificial supports which is supposed to stabilize and to increase slope angles. Hence, the anchors of such an artificial support system, should be located beyond these tension zones.

7. In the presence of residual horizontal stresses, it is important to select either a plane strain or axisymmetric solution to simulate the actual geometry, because these cases can deviate by as much as 100% or more near the toe areas.

8. The tensile circumferential stresses that might be developed in axisymmetric models under non-axisymmetric loading would be unfavorable for stability.

9. The areas of critical stresses and deformations may be located in the pit bottom, around the toe of slope, and in the slope face, depending on the orientation of the residual horizontal stresses.

6. ACKNOWLEDGEMENTS

This work has been based on the programs developed in the Department of Civil Engineering, University of California (Berkeley). The generosity of Professors R. Clough, B. Goodman, R. Taylor, E. Wilson and Dr. R. Dunham is much appreciated. Mr. N. A. Toews provided great assistance in modifying the programs and in examining various mathematical aspects of these problems.

7. REFERENCES

1. Wilson, E.L., "Finite Element Analysis of Two-Dimensional Structures", Dept. of Civil Engineering Report No. 63-2, University of California (1963).

2. Clough, R.W., "The Finite Element Method in Plane Stress Analysis", Proceedings, 2nd Conference on Electronic Computation, A.S.C.E., Struct. Div., Pittsburgh, Pa., Sept. 1960, pp. 345-378.

3. Yu, Y.S., Gyenge, M., and Coates, D.F., "Comparison of Stress and Displacement in a Gravity-Loaded 60° Slope by Photoelasticity and Finite Element Analysis", Report MR 68/24-ID, Mines Branch, Dept. of Energy, Mines and Resources, Ottawa (March 1968).

4. Wilson, E.L., "Structural Analysis of Axisymmetric Solids", Journal of American Institute of Aeronautics and Astronautics, Vol. 3, No. 12 (1967).

5. Dunham, R., and Nickell, R., "Finite Element Analysis of Axisymmetric Solids with Arbitrary Loadings", Structural Engineering Laboratory Report No. 67-6, University of California, Berkeley (1967).

6. Zienkiwicz, O.C., and Cheung, Y.K., "The Finite Element Method in Structural and Continuum Mechanics", McGraw-Hill, London (1967).

7. Coates, D.F., "Pillar Loading. Part III: Field Measurement", Research Report R180, Mines Branch, Dept. of Energy, Mines and Resources, Ottawa (1968).

8. Gyenge, M., and Coates, D.F., "Development of Stress Analysis by Photoelasticity for Slopes", Report FMP 67/8-MRL, Mines Branch, Ottawa (1967).

9. Yu, Y.S., and Coates, D.F., "A Comparative Study of Slope Configurations in Relation to its Economy of Operation and its Stability", Report MR 68/117-LD, Mines Branch, Ottawa (1968).

10. Coates, D.F., and Yu, Y.S., "Three-Dimensional Stress Distributions Around a Cylindrical Hole and Anchor", Report MR 69/57-LD, Mines Branch, Ottawa (1969).

= = = =

YSY:DFC:br